An Isotope Study of the Felsic Units of the Bushveld Large Igneous Province, South Africa

Duane Fourie

2010

Roadside outcrop of Nebo Granite looking west along the R518 near Mokopane.

Submitted in fulfilment of the requirements for the degree of Master of Science.

The Department of Geological Sciences,

University of Cape Town,

Rondebosch 7700,

South Africa

Acknowledgements

I would like to thank all the technical staff at UCT for assisting with the Laboratory work throughout the project with special thanks to Farooza Rawoot for help with the oxygen isotope work and Dr. Kirsten Drosdt for assistance with the zircon separation. Thanks to Jarryd Finkelstein and Andre Fourie for accompanying and assisting me with my sample collection and my supervisor Prof. Chris Harris for reading and editing of the thesis. Special thanks to Kate Naude for reading and re reading my drafts and suggesting changes.

Abstract

An O, H, Sr and Nd isotope study was carried out on the ~ 2059 Ma Bushveld granites and granophyres. A small number of Rooiberg Group felsites were also studied. Quartz was separated from 41 samples and zircon was separated from 6 samples and analyzed using a combination of conventional and laser fluorination. Average values of $\delta^{18}O$ for quartz and zircon were 7.78 ‰ ± 1.05 (n = 56) and 5.19 ‰ ± 1.17 (n = 11) respectively. Alkali feldspar samples showed variable $\delta^{18}O$ values from 7.4 ‰ to 10.2 ‰, averaging 8.64 ‰ ± 1.01 (n = 10). Separated biotite and amphibole gave average $\delta^{18}O$ values of 2.94 ‰ ± 2.42 (n = 9) and 3.91 ‰ ± 1.01 (n = 19) respectively.

High-temperature equilibrium oxygen-isotope fractionations are preserved between quartz and zircon from the granite and granophyre units but not between quartz and the other minerals analysed. However quartz separated from five samples, showed no significant difference in core and rim $\delta^{18}O$ values. The δD values of amphibole and biotite were –99 ‰ ± 17 (n = 13) and –84 ‰ ± 16 (n = 3) respectively. These data suggest a combination of magmatic degassing and alteration by fluid having low δD values. Taken as a whole, the oxygen and hydrogen-isotope data suggest that the $\delta^{18}O$ values of quartz and zircon provide a reliable proxy for the $\delta^{18}O$ values of the Bushveld granite and granophyre magma. Using fractionation factors of 1.5 ‰ for quartz-magma and –0.6 for zircon-magma, the $\delta^{18}O$ value of the granite/granophyre magmas calculated, ranged from 5.8 ‰ to 6.8 ‰, averaging 6.0 ‰ (using actual $\delta^{18}O$ values; n = 64, 56 Qtz & 8 Zr). Radiogenic isotope data (Sr and Nd) was gathered from a subset of 12 samples and gave an initial Sr value ranging from – 1.99 to 0.86, indicating significant disturbance to the Rb-Sr system after emplacement, presumably by fluids. The initial Nd value ranged from 0.506110 to 0.510498 with an average value of 0.509490 (n = 12). ε_{Nd} values ranged from –74.9 to 11.2 with average values for the granites/granophyres and felsites, with the two outlying values omitted, of –3.9 ± 1.4 (n = 8) and –4.1 ‰ ±1.2 (n = 2) respectively.

Previously published data for the ultramafic/mafic RLS (Rustenberg Layered Suite) shows average $\delta^{18}O$ and ε_{Nd} values of 7.1 ‰ (n = 101) and –6.8 (n = 22) respectively. The $\delta^{18}O$ values of the Bushveld Granite and granophyre units are on average 1.2 ‰ lower than those reported for the RLS. Average reported ε_{Nd} values for the RLS are also ~ 2 units more

negative than the average felsic unit ε_{Nd} values.

So-called A-Type granites from Brazil, Namibia, Turkey and Eastern China have average $\delta^{18}O$ values of 8.08 ‰ ± 0.7 (n = 9), 11.23 ‰ ± (n = 17), 11.07 ‰ ± 0.94 (n = 6) and 6.87 ‰ ± 1.53 (n = 63) respectively. The majority of the A-Type granites have $\delta^{18}O$ values higher than that of the Bushveld granite and granophyre units, and taken at face value, this suggests a smaller crustal input in the case of the Bushveld granite and granophyre.

The $\delta^{18}O$ values of the granite and granophyre magmas are lower than the RLS and some are lower than expected for a mantle-derived magma. Yet at the same time the ε_{Nd} values suggest a substantial crustal component. The low $\delta^{18}O$ values and the negative ε_{Nd} values can be explained if the granites and granophyres were derived from a crustal source that has had its $\delta^{18}O$ values lowered by high-temperature interaction with meteoric water. This source could be compositionally similar to the RLS, although, as yet, no RLS samples have been identified with low $\delta^{18}O$ values.

The granite and granophyre units appear to be petrogenetically closely related based on their isotope characteristics, whereas the Rooiberg Felsite Suite could not be well characterised in terms of its isotope composition because of small grain size and extensive post-emplacement alteration that prevented mineal seperation for analysis. A single zircon $\delta^{18}O$ value of 7.3 ‰ was obtained for the felsite and indicates a crustal parental magma. This is interpreted to suggest that the felsite is not petrogenetically related to the granite and granophyre units.

Table of Contents

1 INTRODUCTION 1

1.1 Previous Work 7

1.1.1 Review of Major and Trace Element Data for the Bushveld Complex 8

1.1.2 Rooiberg Felsite 8

1.1.3 Rashoop Granophyre 9

1.1.4 Nebo Granite 10

2 GEOLOGICAL SETTING 13

2.1 Rock Types 17

2.1.1 Rooiberg Felsite 17

2.1.2 Rustenburg Layered Suite (RLS) 18

2.1.3 Rashoop Granophyre 20

2.1.4 Lebowa Granite Suite 22

3 PETROGRAPHY AND SAMPLE DESCRIPTION 24

3.1 Rooiberg Felsite 33

3.2 Rashoop Granophyre 35

3.3 Nebo Granite 37

4 METHODOLOGY 39

4.1 Mineral Separation 39

4.2 Analytical Techniques 42

4.2.1 Conventional Silicate Line 42

4.2.2 Laser Fluorination 42

4.2.3 Hydrogen – Isotopes 44

4.2.4 Stable Isotope Mass Spectrometry 45

4.2.5 Rb – Sr Isotopes 45

4.2.6 Sm – Nd Isotopes 46

4.2.7 Trace Element Concentrations 46

4.3 Quartz Zonation 47

5 RESULTS 48

5.1 Oxygen - Isotopes 48

5.1.1 Quartz 48

5.1.2 Quartz zoning 52

5.1.3 Zircon 52

5.1.4 Biotite 52

5.1.5 Amphibole 53

5.1.6 Feldspar 53

5.1.7 δ – δ Plots 54

5.2 Hydrogen Isotopes 56

5.2.1 Wt% Water 58

5.3 Radiogenic Isotopes 59

5.3.1 Sr – Isotopes 59

5.3.2 Nd – Isotopes 62

6 DISCUSSION 66

6.1 Affects of Alteration 66

6.2 Isotope Composition of Fluid Involved in Alteration 69

6.3 Original Magma $\delta^{18}O$ 72

6.4 Comparison with Related Regions and Units 74

6.4.1 Comparison with the RLS 78

6.5 Comparison with Felsic Rocks in other LIPs 80

6.5.1 Karoo, Parana/Etendeka and Chon Aike LIPs 80

6.6 Comparison with A-Type Granites 83

6.6.1 A-Type Granites from Brazil, Namibia, Turkey and Eastern China 83

6.7 Are the Bushveld Felsic Rocks Formed from Low $\delta^{18}O$ Magmas? 87

6.8 Comparison with Low $\delta^{18}O$ Felsic Magmas 89

6.8.1 Seychelles, Iceland, Yellowstone and Snake River Plain Low ^{18}O Magmas 91

6.9 Origin of the Bushveld Felsic Magmas 94

7 CONCLUSIONS 97

1 INTRODUCTION

Large Igneous Provinces (hereafter referred to as LIPs) are a record of past magma production of vast size, that have the potential to cover areas the size of many countries kilometers deep and are some of the most studied geological features on Earth. LIPs can contain evidence of many different processes and may provide glimpses into the workings of some less well understood phenomena, such as possible upper mantle chemical and isotopic heterogeneity/homogeneity, mantle plumes and mantle/crust interactions. The importance of LIPs is not merely geological as their formation or emplacement is a phenomenon that may be witnessed by most species only once and are now thought to have been the driving forces behind at least some of the major extinctions since life began (Rampino & Stothers, 1988; Courtillot, 1990 & 1994; Wignall, 2001). LIPs are the remnants of such occurrences, found across the globe, ranging from the ancient (> 2500 Ma Onverwacht and Ventersdorp), to fairly recent (< 300 Ma Bryan & Ernst, 2008, Fig. 1 eg. Siberian and Deccan Traps). Any one of these LIPs had the potential to affect every aspect of the Earth's climate system within a geological moment and thus provided the conditions for our own evolution as a species. The large amount of information that can be gathered from LIPs about the Earth's history and internal processes make LIPs one of the few geological features that have significance across many fields of study, including physics, chemistry, zoology and botany. It is therefore essential that these markers of significant change (Fig. 2) and their global significance are better understood.

The majority of preserved LIPs are composed mainly of mafic/ultramafic rock units with any associated felsic rock units generally in the minority or totally absent (Bryan *et al*., 2002) thus the felsic units of most LIPs if preserved are not as well studied as their mafic/ultramafic counterparts. The Palaeoproterozoic Bushveld Large Igneous Province has been studied by many workers (e.g. Kleemann & Twist, 1989; Schweitzer, 1995; Schweitzer *et al*., 1995; Barnes *et al*., 2004; Kinnaird, 2005; Clarke *et al*., 2009) due to the geological significance and economic importance of the Rustenburg Layered Suite (SACS, 1980) (hereafter referred to as the RLS), which accounts for the majority of the worlds platinum, chrome and vanadium resources. The Bushveld LIP is anomalous in that most of the preserved magmatism is felsic as is the case for the Chon Aike LIP (Fig. 1), with approximately 1/3 being ultramafic/mafic cumulates of the RLS.

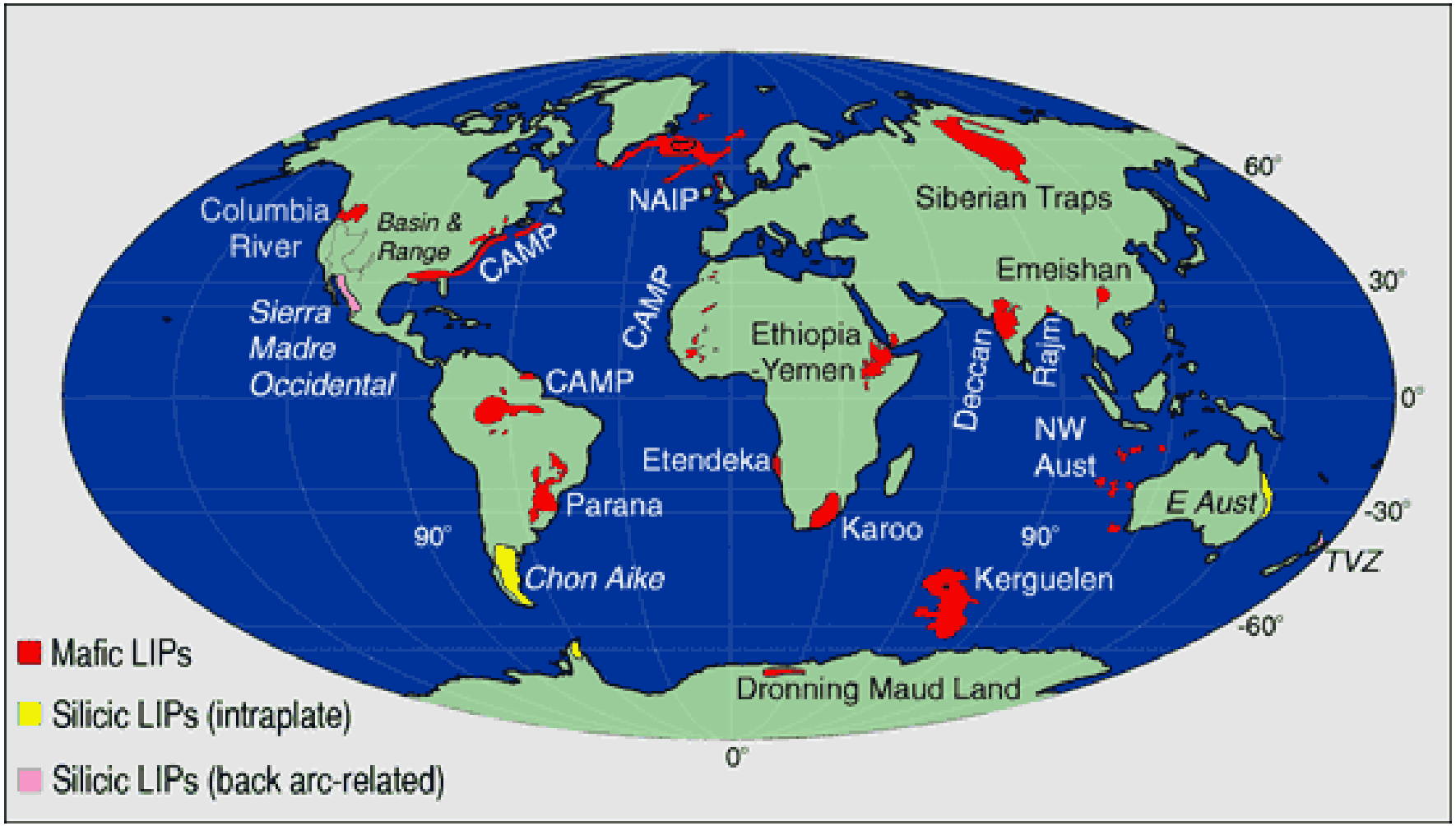

Fig. 1: Location of LIPs around the world during the last 300 Ma.

Source: www.mantleplumes.org/SLIPs.html

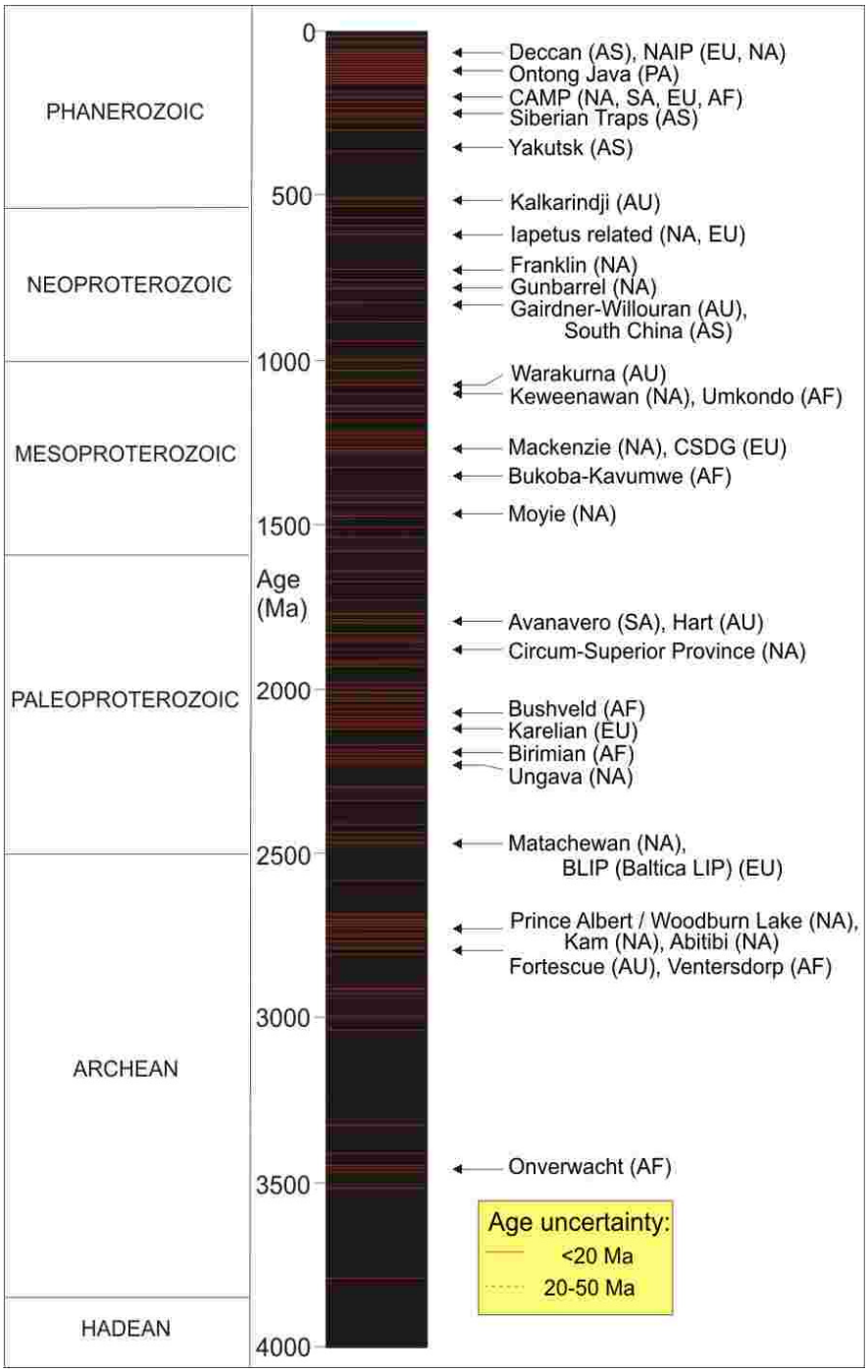

Fig 2: LIPs through time.

Source: Ernst and Buchan, 2004. 'Age spectrum ('bar code') of LIP events through time. LIP abbreviations are: BLIP, Baltic Large Igneous Province; CAMP, Central Atlantic Magmatic Province; CSDG, Central Scandinavian Dolerite Group; HALIP, High Arctic Large Igneous Province; NAIP, North Atlantic Igneous Province; OJHMP, Ontong Java–Hikurangi–Manihiki Plateau. Locations for LIP events are: NA, North America; SA, South America; EU, Europe; AF, Africa; AS, Asia; AU, Australia; AN, Antarctica; and PA, Pacific Ocean.'

The Bushveld Complex has been studied for almost 100 years (Hall, 1932; Buchanan, 1975; Kleemann & Twist, 1989; Hatton, 1995; Hatton & Schweitzer, 1995; Cawthorn *et al*., 1998; Harris *et al*., 2005; Clarke *et al*., 2009) but the petrogenesis of the felsic units is, as yet, not well understood. Similar geochemical characteristics (similar bulk rock composition, similar REE patterns and emplacement dynamics) are interpreted to infer a common source for the Rashoop Granophyre, Nebo Granite and to a lesser extent the Rooiberg Felsite (Schweitzer *et al*., 1997) but the exact relationship between the felsic units remains debateable (Twist & Harmer, 1987; Kleemann & Twist, 1989; Cawthorn *et al*., 2006). The petrogenesis of the magma that formed the Bushveld felsic units, their emplacement and their relationship to the RLS provides an opportunity to investigate a LIP that is both very old and (the remaining extent which can be studied) is well preserved. The Bushveld LIP formation and emplacement has remained difficult to interpret due to a number of factors that range from extensive late stage alteration of the initial Rooiberg volcanic units to the lack of a comprehensive data set for the Bushveld Complex Felsic units as a whole.

The geographical arrangement of the Bushveld Complex lobes, as well as the uniformity of lithological units across the complex, suggest connection of the complex at depth, (Cawthorn *et al.,* 1998) with the general shape of the complex reflecting that of a saucer (Kruger, 2005). Gravity modelling (Cawthorn *et al.,* 1998) shows that dip decreases with depth and towards the centre of the complex to form the wide shallow 'saucer' shape, indicating that crustal loading may be responsible for the shape and not as a result of emplacement from below. The method of emplacement is important to consider, as it may affect the source and degree of post emplacement hydrothermal alteration and thus the isotopic signature of the complex. The general theory is that the production of a large magma chamber below the LIP is connected by a set of feeder pipes that allow the transportation of melt from depth to emplacement level. Alternative theories include; emplacement of a LIP from a source not directly below the LIP or that the magma path to emplacement level does not follow the shortest path i.e. straight upwards, rather a path of least resistance.

The central position of the Bushveld Complex within the Kaapvaal Craton suggests that if emplacement was from a large magma chamber produced by a mantle plume below the complex, then the root or keel of the craton would need to be the path of least resistance for magma transport, resulting in hydrothermal alteration or even thermal erosion of the cratonic root. The great age (> 2.7 Ga. de Wit *et al*., 1992), thickness and relatively cool temperatures of the Kaapvaal root zone do not seem ideally suited to the formation of a large magma chamber.

The Bushveld Complex must have been emplaced from a source via a magma chamber that did not affect the cratonic root zone significantly enough to prevent diamond formation, from a source not directly connected to emplacement level, below the complex or a source not below the Bushveld Complex's current position, with the bulk of the magma flowing/injected into their current location laterally or sub-laterally via feeder dykes or sills (Clarke *et al*., 2009). The effect of magmatic and metamorphic waters relating to emplacement could be reduced if this was the case, with meteoric waters forming the bulk of any post emplacement hydrothermal circulation.

Minerals, especially feldspar and to a lesser extent biotite and amphibole within most of the felsic units record alteration processes, (seen in thin section as the speckled brown alkali feldspar grains) indicative of the beginnings of alkali feldspar break down, resorption and recrystallisation. Recrystallisation of alkali feldspar grains is observed by the embayments and irregular grain boundaries, while varying degrees of chloritisation can be seen affecting the biotite and amphibole grains. Within the Rooiberg Felsite very few unaltered minerals can be observed; the implication of this is that hydrothermal alteration has affected the felsic volcanic units and possibly the other felsic units as well. The resistance of the minerals analysed in this study, quartz and zircon, to alteration and their high closure temperatures for oxygen diffusion are ideally suited to provide original magmatic oxygen isotope values and can be compared to other units such as the RLS. Alkali feldspar, biotite and amphibole are more easily affected by post emplacement alteration and are used to determine the degree of alteration and source of any hydrothermal fluids identified.

The intrusive felsic units of the Rashoop and Lebowa suites and are by contrast some of the least well studied units despite economic significance for fluorite and tin. The extrusive Rooiberg Group has been studied to a greater degree than some of the intrusive felsic units but a modern isotope data set is lacking. Placing constraints on the nature of the Bushveld LIP source is important in understanding the possible processes occurring during emplacement of the world's largest, relatively well preserved, igneous complex.

The great age and subsequent phases of metamorphism assumed to have affected the Bushveld felsic units makes the use of isotopes of particular importance as the isotopic ratios of resistant minerals such as quartz and zircon are not easily altered. Comparisons of the felsic rocks with the mafic RLS is important and as the RLS consists of cumulates, conventional trace element ratio comparisons would not be useful, making isotope data for comparison essential. The findings of previous studies have alternatively suggested a strong relationship between the three distinct felsic units (Maier *et al*., 2000; Buchanan *et al.,* 2004) while others indicate separate source regions for each of the three felsic rock types found in the Bushveld LIP (Twist, 1985; Twist & Harmer, 1987). All the units of the Bushveld Complex have been emplaced within a geologically short period of time. Recent dating by Harmer, (2000, Granite ~ 2055 Ma) and Buick et al., (2001, RLS ~ 2059 Ma) constrain the Bushveld magmatic episode, adding the range in age errors, to < 10 Ma which is comparable to many other LIPs such as the Deccan ~1 Ma (Ernst & Buchan, 2001; Ernst & Buchan, 2004; Ernst *et al*., 2005; Chenet *et al*., 2007).

The Bushveld Complex samples display typical anorogenic (A-type, Kleemann & Twist, 1989) granite characteristics such as hypersolvus alkali feldspar, high silica content, presence of interstitial hornblende and absence of muscovite (low Mg and high Fe) (Loiselle & Wones, 1979; Collins *et al*., 1982). S-Type granites generally contain abundant muscovite and biotite with hornblende being absent, crystallisation of two feldspars (subsolvus feldspar more hydrous) with high silica and variable calcium content (Chappell & White, 1974). I-Type granites are generally characterised by the presence of two crystallising feldspars (subsolvus feldspars), contain hornblende and usually abundant primary biotite with no primary muscovite (Chappell & White, 1974).

The term ‘A-type granite’ is ambiguous in the literature with numerous definitions suggested for this group of granites. Most researchers agree that A-Type granites are distinct but constitute a fairly large range in chemical properties, source materials and formation environments (Bonin, 2006 and references therein). Loiselle & Wones, (1979) first described A-Type granites as ‘anorogenic’ that occur in rift zones and stable continental blocks, are usually mildly alkaline and crystallised under low H_2O and oxygen fugacities and relatively high HF/H_2O ratios in the magma. A-Type granites are enriched in incompatible trace elements, including LILE and HFSE, but low in trace elements compatible in mafic silicates (Co, Sc, Cr, & Ni) and feldspars (Ba, Sr, Eu). The meaning of the A in A-Type Granite was not definitive enough to encompass the entire ‘A-Type field’ for many researchers with A taking to alternately mean (mildly) alkaline, anhydrous and aluminous (Bonin, 2006). The problem with the A-Type nomenclature is in large part due to the assumptions on the origin and formation of granite types in general and classified using the I, S and M system which is still debated by granite researchers. In this study the term A-Type will refer to granites not associated with orogenic processes (anorogenic granites) (Kleemann & Twist, 1989).

1.1 Previous Work

Theories on the emplacement of the Bushveld Complex abound, but definitive evidence for a particular geological setting is lacking at present. Presently a mantle plume source (Walraven, 1987; Hatton, 1995; Schweitzer *et al*., 1997; Gibson & Stevens, 1998; Buchanan *et al*., 2004), providing the heat nessecary to cause melting on such a large scale within a stable cratonic block is favoured. Other theories include a back-arc (Willmore *et al*., 2002) setting, that was responsible for the melting and emplacement by decompression due to crustal thinning and or fracturing along a suture zone with no additional heat input and bolide impact induced melting (Elston, 1992) similar to that observed for the Vredefort Complex south west of Johannesburg.

1.1.1 Review of Major and Trace Element Data for the Bushveld Complex

Geochemical analysis of the Bushveld Complex felsic rocks has been undertaken by a number of workers (Kleemann, 1987; Kleemann & Twist, 1989; Schweitzer, 1995; Schweitzer *et al*., 1995; Hatton & Schweitzer, 1995; Buchanan *et al*., 1999, 2002, & 2004) to characterize the Bushveld Complex felsic rocks. The following paragraphs are a review of the geochemical analyses (major and trace element data) by previous workers and are important to better understand and constrain possible formation and emplacement processes.

1.1.2 Rooiberg Felsite

The Rooiberg Felsite units have been studied in detail by Buchanan *et al*., (1999, 2002 & 2004) and Hatton & Schweitzer, (1995). The four discernable formations are thought to represent different lava flows of slightly different composition with the basal Dullstroom Fm. being the likely parental magma of the overlying formations. The lower Dullstroom Formation can be further divided on the basis of Ti percentage with a low Ti (< 1 wt %) and a high Ti (> 1 wt %) described by Hatton & Schweitzer, (1995) and Buchanan *et al*., (1999, 2002).

The Rooiberg Felsite consists of interbedded sedimentary and volcanic units ranging from basaltic basal units to rhyolites in the upper units. A general trend of increasing SiO_2 upwards with a corresponding decrease in MgO upward is reported by Schweitzer *et al*., 1995; Buchanan *et al*., 1999. The trends seen for major element proportions from the basal section upward are reflected in the trace element data, with increasing abundances of REEs as SiO_2 increases (Cawthorn *et al*., 2006) with a more pronounce Eu anomaly also prominent towards the uppermost Kwaggasnek Formation. The lower mafic Rooiberg units have on average ~ 5 wt.% MgO, ~ 53 wt.% SiO_2, 16 ppm to 158 ppm Ni and ~ 367 ppm Cr. The upper felsic units have < 1 wt.% MgO, ~ 35 ppm Ni, and ~ 10 ppm Cr (Hatton & Schweitzer, 1995). Zr, Nb and Y generally increase upwards, whereas the reverse is observed for P_2O_5, TiO_2 and Sc (Hatton & Schweitzer, 1995). ε_{Nd} and ε_{Sr} values (Fig. 31) average –8.4 ± 1.05 (n = 29) ranging from –10 to –7 and –9.4 ± 241.43 (n = 34) ranging from –859 to 157 respectively. The relatively neagative ε_{Nd} isotope values for the Rooiberg Felsite is interpreted to represent crustal contamination and the large range in ε_{Sr} values representing hydrothermal alteration in the upper more felsic units probably from the emplacement of the Nebo Granite (Buchanan *et al*., 2004).

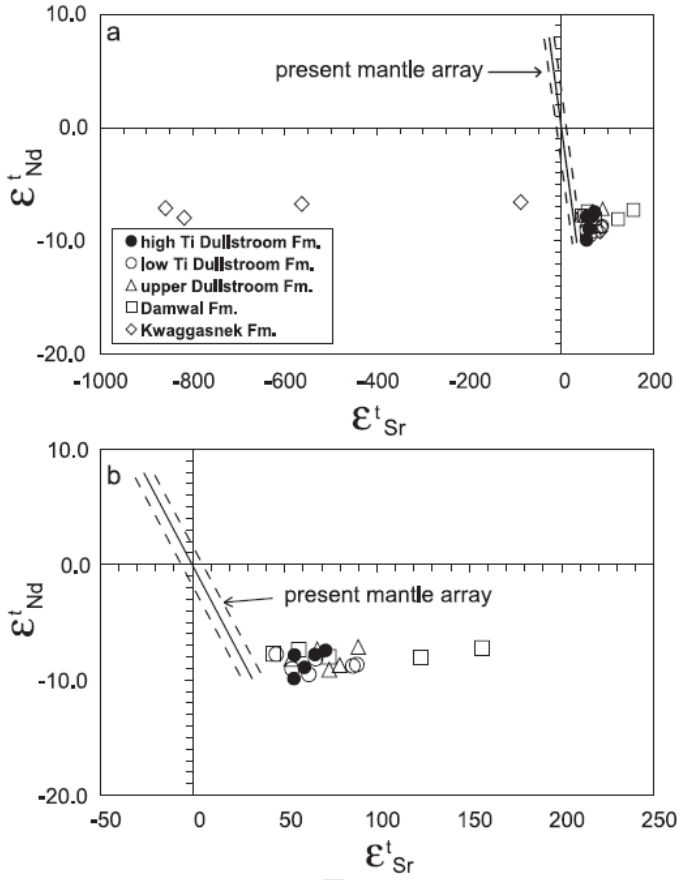

Fig. 3: (a) Plot of Sr vs. Nd for Rooiberg Felsite units. after Buchanan *et al*., 2004; Calculations made for t = 2057.3 Ma (Harmer & Armstrong, pers. comm., 2000 in Buchanan *et al*., 2004). (b) Expanded plot of the right-hand portion of (a).

1.1.3 Rashoop Granophyre

The main component of the Rashoop Granophyre in the Bushveld Complex is the Stavoren Granophyre with smaller volumes of different composition granophyre scattered throughout the complex. The Stavoren Granophyre displays a decrease in grain size toward the upper sections of the sheet (Kleemann, 1987) with the uppermost units classified as micro-granophyres. Accessory hornblende, biotite and clinopyroxene (hedenbergite) have been observed in thin section as well as trace amounts of sphene, apatite, calcite, magnetite, allanite and ilmenite (Kleemann, 1987). The granophyres plot in the hypersolvus field of Luth *et al*., (1964) on the Q-Ab-Or diagram and plot around 90 % to 93 % region on the differentiation index (Kleemann, 1987). Major and trace element characteristics are very similar to those of the Nebo Granite (Walraven, 1987). The Rashoop Granophyre has not been studied in detail since Walraven, (1987) who interpreted the granophyre to be closely related to the main Nebo Granite intrusion.

1.1.4 Nebo Granite

The youngest units of the Bushveld Complex have been studied by Kleemann & Twist, (1989), Walraven & Hattingh, (1993) and Hatton & Schweitzer, (1995) among others. The largely tabular granitic sheet is composed predominantly of quartz, perthite and minor plagioclase (Kleemann & Twist, 1989) and shows more evolved compositions roofward with the basal sections of the sheet containing 10 % to 20 % mafic minerals (mostly hornblende with minor biotite) that decrease to less than 1% in the more evolved upper portions of the sheet (Kleemann & Twist, 1989). Other compositional trends observed by Kleemann & Twist (1989) are; the increase in albite content in the more evolved Klipkloof Granite roof facies, increasing perthite and quartz content (69 % to 76 %) with decreasing plagioclase (~ 8 % at base of the sheet to < 1 % in the upper sections) content upward, increasing K & Rb concentrations and corresponding decreases in Fe, Ti, Ca, P, Ba, Sr and Zr (Fig. 32).

Aluminium concentration shows a similar trend and decreases with increased SiO_2 content in all but the most evolved Klipkloof Granite while Na concentrations do not vary through the sheet and K_2O content increases from 4.6 % near the base of the sheet to 5.7 % at the top (Kleemann & Twist, 1989). The hypersolvus nature observed in the Nebo Granite and generally low proportions of hydrous phases suggest low initial water contents (e.g. Martin & Bonin. 1976; Kleemann & Twist, 1989) and abundances of Ce, Y, Zr & Nb suggesting that the Bushveld Complex granites form the largest exposed example of 'A-Type granite' (Fig. 33) (Kleemann & Twist, 1989). Radiogenic isotope data (mainly Rb/Sr) for the Nebo Granite have been discussed by workers such as Kleemann and Twist, (1989) but a multi-isotope (stable & radiogenic) dataset is not currently available for the Bushveld Complex felsic units making petrogenetic studies on the Bushveld Complex incomplete at best.

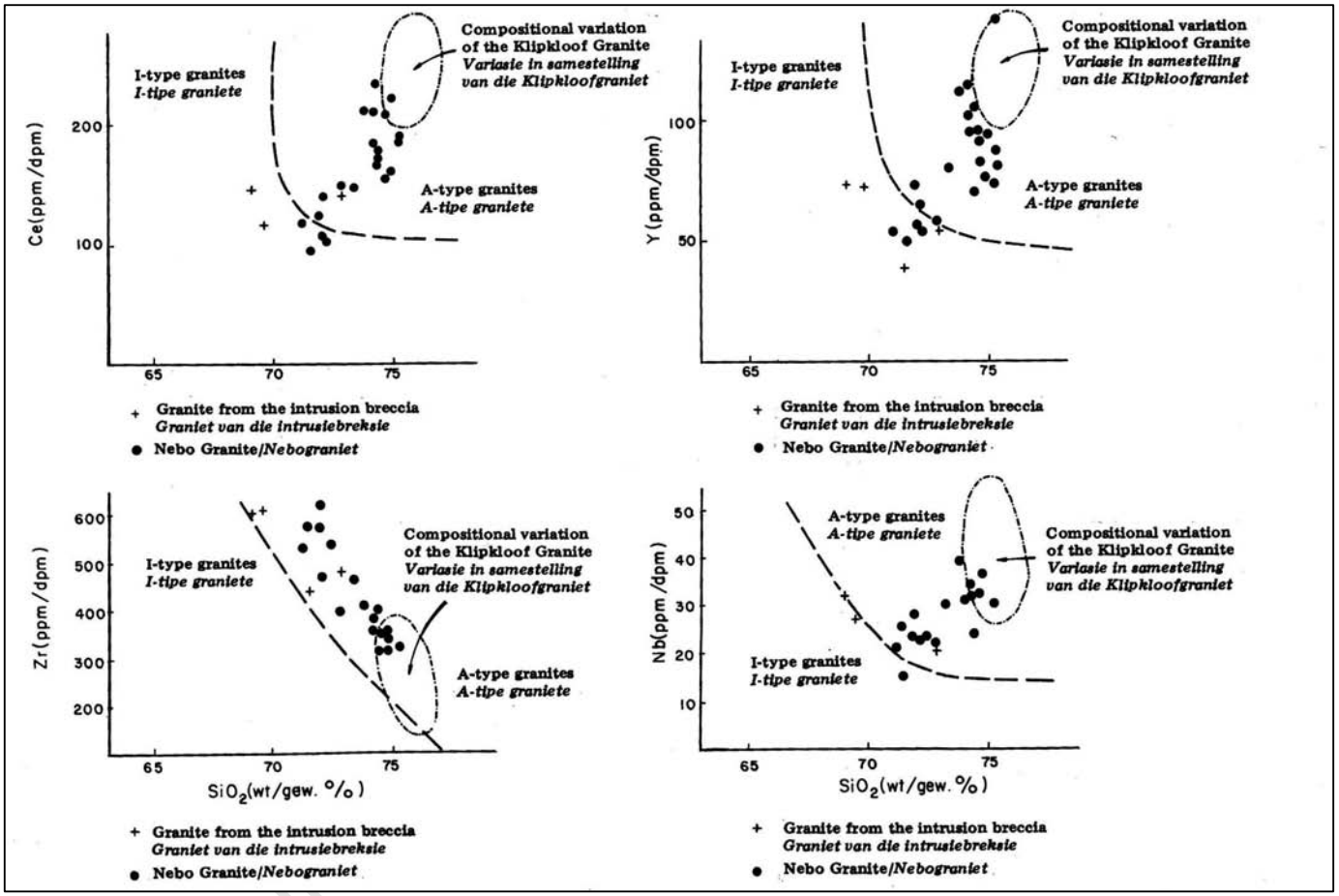

Fig. 4: Graphs showing the A-Type character of the Bushveld granites using Harker diagrams for Ce, Y, Zr and Nb.
Source: Kleemann, (1987).

Oxygen and hydrogen isotopes can often provide robust information regarding the source region of a magma and its subsequent interaction with fluids. The isotope composition of a particular rock or magma is extremely helpful in determining contamination effects and post emplacement alteration as these processes produce distinctive isotope ranges that differ greatly from typical isotope values for rocks that have not been affected by contamination and alteration.

The use of stable isotopes as a petrogenetic indicator has previously been used on the RLS by Schiffries & Rye (1989), Reid *et al*., (1993), Maier *et al*., (2000) and Harris *et al.*, (2005), and will be extended to include the felsic units of the Bushveld LIP in this study. The resistance of quartz and zircon to alteration and high closure temperatures for oxygen diffusion will provide stable isotope data, which in conjunction with previous radiogenic isotope analyses, will more accurately constrain the nature of the source region.

1.2 The aims of this study are:

1. To determine the variation of $\delta^{18}O$ values within the felsic units across the complex.
2. To determine the petrogenesis of the felsic units.
3. To explain any $\delta^{18}O$ variation within and between the different felsic units within each lobe.
4. To investigate the relationship if any, of the felsic units, to the mafic RLS.
5. To determine which mineral/s provide the best estimate for magma $\delta^{18}O$.
6. To understand better the origin of so called A-Type granites.
7. To compare the $\delta^{18}O$ values of the Bushveld Complex Felsic units with other anorogenic granites and explain any differences or similarities.

2 GEOLOGICAL SETTING

The Bushveld Complex has been dated by various workers, with the most recent age data for the Granites of ~ 2055 Ma ± 3.6 produced by Harmer & Armstrong (2000). A calc-silicate xenolith in the RLS gave a single titanite evaporation age of 2058.9 ± 0.8 Ma (Buick *et al*., 2001), and a single zircon from the volcanic Rooiberg Group has been dated by Walraven, (1997) giving an age of 2061 ± 2 Ma). This age data constrains the emplacement of the Bushveld Complex to < 10Ma. The ~ 2.06 Ga Bushveld Complex is classified as a layered igneous complex, and is situated on the Kaapvaal Craton, South Africa, north of Pretoria. The 65000 km^2 complex consists of the layered ultramafic/mafic RLS, preceded by the volcanic Rooiberg Felsite and intruded by the Rashoop Granophyre and Lebowa Granite suites (Fig. 5). The Bushveld Complex units generally overlie the Magaliesberg Fm. quartzites, of the Pretoria Group within the Transvaal Supergroup sedimentary sequence, with the Rooiberg Felsite classified as the last unit of the Transvaal Supergroup (SACS, 1980). The intercratonic Transvaal Basin has preserved the Witwatersrand, Ventersdorp and Transvaal Supergroups representing fluvial clastic to shallow marine platform deposits punctuated by volcanic horizons, with the most famous units being the gold bearing Witwatersrand conglomerates (SACS, 1980; Cawthorn *et al*., 2006).

Suite/Group	Rock Units/Zones		Total Volume Estimate
Lebowa Granite Suite	Nebo, Makhutso, Klipkloof, Bobbejaankop and Verena Granites		~ 180 000 km^3
Rashoop Granophyre Suite	Stavoren and Diepkloof Granophyres, Rooikop Porphyritic Granite, Zwartbank Pseudogranophyre		
Rustenburg Layered Suite	Upper Zone	Subzone C (Ol - Ap diorite) Subzone B (Ol - Mt gabbronorite) Subzone A (Mt gabbronorite)	~ (150 000 km^3 - 400 000 km^3)
	Main Zone	Upper Subzone (gabbronorite) Lower Subzone (gabbronorite, norite)	
	Critical Zone	Upper Subzone (norite, anorthosite, pyroxenite) Lower Subzone (pyroxenite)	
	Lower Zone	Upper Pyroxenite Subzone Harzburgite Subzone Lower Pyroxenite Subzone	
	Marginal Zone (norite)		
Rooiberg Group	Schrikkloof Formation (flow - banded rhyolite) KwaggasnekFormation (massive rhyolite) Damwal Formation (dacite, rhyolite) Dullstroom Formation (basaltic andesite)		~ 300 000 km^3

Fig. 5: Generalised stratigraphy of the Bushveld Complex, including the volcanoclastics of the Rooiberg Group as the initial stage of the Bushveld magmatic event (after Cawthorn *et al*., 2006) Including volume estimates for Rooiberg Group (Twist & French, 1983), RLS; without and with mafics below centre of the complex (Harmer, 2000) and an estimate for the combined Lebowa and Rashoop Suites (Kleemann & Twist, 1989).

The Bushveld Complex can be divided into five lobes (Fig. 6); the far western, western, northern and eastern lobes with the Bethal Lobe not visible but determined from geophysical surveying. The different lobes appear to be separate intrusions, but could possibly be linked at depth. The lobes of the Bushveld Complex are arcuate and suggest an initial more rounded geometry. The eroded far western lobe consists exclusively of the lower units of the RLS (Eales & Cawthorn, 1996) namely the ultramafic/mafic norite, pyroxenite and harzburgite in contact with rocks of the Transvaal Supergroup.

The western lobe of the complex stretches over 100 km N-S from just south of Thabazimbi in the north to Brits in the south. The full RLS sequence is not exposed in the west but has been identified using drill core and geophysical methods (e.g. Eales & Cawthorn, 1996). The observed outcrop in the western lobe reveals a section from the RLS in contact with the Pretoria Group sediments at the base. In the west, the Lebowa Granite suite generally lies conformably above the RLS where the lower and critical zones truncate towards the west, followed by the Rashoop Granophyre and Rooiberg Felsite 'roof' (Cawthorn *et al.,* 2006).

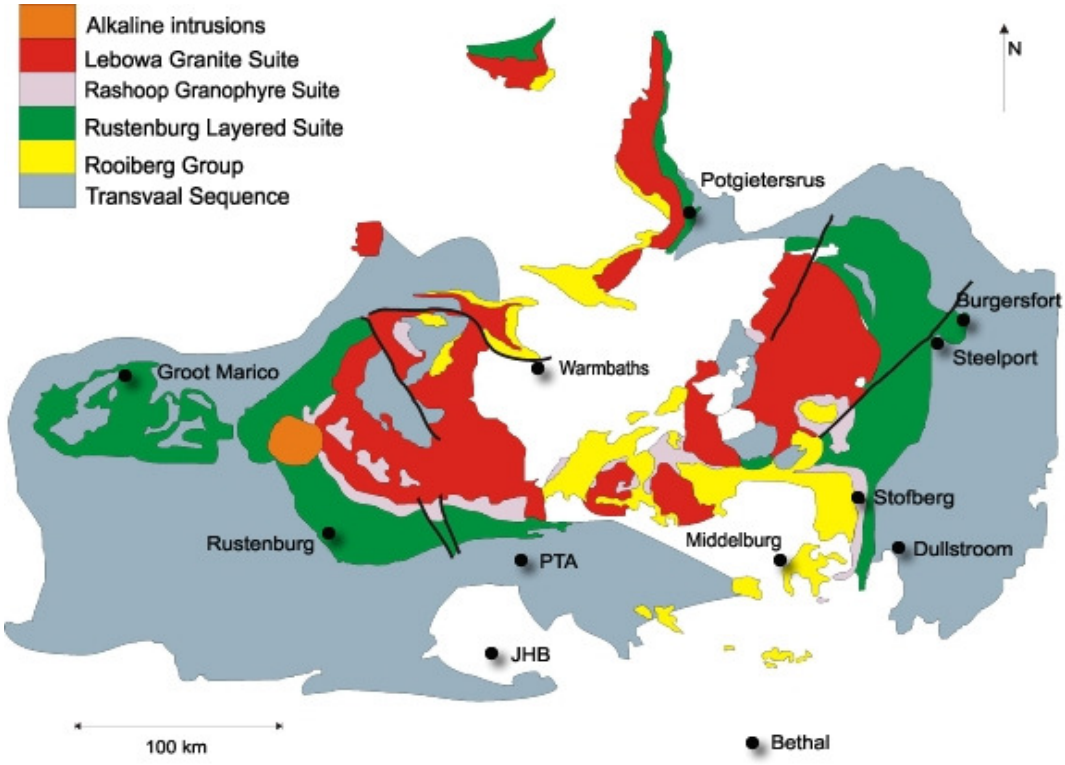

Fig. 6: General geology of the Bushveld LIP, showing the different lobes and geometry of the complex. Source: http://web.wits.ac.za/Academic/Science/Geosciences/Research/bushveld/bushvfthome.htm

Fragments of Rashoop Granophyre occur directly above the RLS, and Pretoria Group sediments are found above the RLS, between the Rashoop Granophyres and Rooiberg Felsites in the Rustenburg and Rooiberg regions respectively (Cawthorn *et al.,* 2006). The Crocodile River fragment (or block) is an inlier of Pretoria Group sedimentary rocks that is situated within the western lobe of the Bushveld Complex and has been deformed and metamorphosed, being forced to 'dome' upwards as the Bushveld was emplaced around and over it and has subsequently re - appeared through erosion of the overlying material (Cawthorn *et al.*, 1998).

The 100 km long Northern Lobe of the complex forms a thin (~ 25 km) north/south trending outcrop from Limburg in the north to in just northeast of Modimolle in the south and includes the Villa Nora fragment ~ 75 km to the northwest of Mokopane. The RLS is not fully developed in the northern limb with the upper units well preserved but the main, critical and lower zones being truncated (Coertze *et al.,* 1978). The RLS is in contact with the Transvaal Supergroup in the east and is conformably overlain by the Lebowa Granite, Rashoop Granophyre and Rooiberg Felsite to the west, where the felsite is in contact with rocks of the Pretoria Group. The stratigraphy of the Villa Nora 'fragment' is characterised by the RLS units cropping out in the north, overlain by the Lebowa Granite and Rooiberg Felsite in the south of the 'fragment'.

The Eastern Lobe is ~ 120 km from north to south and divided by the Steelpoort Fault into northwest and southeast sections, with the southeast section consisting predominantly of RLS with the of Lower, Main and Critical Zones truncating towards the south (Cawthorn, 1998). Northwest the Steelpoort Fault the full RLS sequence is developed (Cawthorn *et al*., 2006) and is in contact with the Lebowa Granite and Rashoop Granophyres in the west with a small occurrence of Rooiberg Felsite in the southern region of the north-western section. Inliers of Transvaal and pre-Transvaal rocks are found to the north of Loskop, near the central region of the complex, almost dividing the Eastern Lobe from the central Bushveld region. The central region consists of Lebowa Granite, Rashoop Granophyre, Rooiberg Felsite and inliers of Transvaal Supergroup rocks (Cawthorn, 1998).

2.1 Rock Types

2.1.1 Rooiberg Felsite

The 4-6 km thick interbedded volcanic and sedimentary package known as the Rooiberg Suite (SACS, 1980) (Figs. 7 & 8) has been divided into 4 distinct geochemical units by Schweitzer *et al.,* (1995) with the Basal Dullstroom Fm. overlain by the younger Damwal, Kwaggasnek and Schrikkloof Fms. respectively. The basal Dullstroom Fm. has been subdivided into four geochemically distinct units or flows (Buchanan *et al.,* 1999) with the volcanic sequence becoming more felsic upwards to the most felsic Schrikkloof Fm. of dacites interbedded with occasional rhyolites and sedimentary units.

Figs. 7 &8: Rooiberg Felsite (BC 32 & BC 33) outcrops NE of Warmbaths in the northern lobe of the Bushveld complex (all photographs, including thin section photos, were taken by Duane Fourie unless otherwise stated).

Dating of zircon from the Rooiberg Felsite (Kwaggasnek Fm.) gives an age of 2057.3 ± 2.8 Ma (Harmer & Armstrong, 2000) which is the same age within error as the RLS emplacement indicating that the RLS was emplaced very soon after the initial Rooiberg Volcanic. The synchronous eruption of the Rooiberg lavas with the RLS and similarity with the Rashoop Granophyre and Nebo Granite units suggest that the current classification of the Rooiberg Suite, as part of the Pretoria Group, may need to be revised (Schweitzer *et al.,* 1995) (Buchanan *et al.,* 1999, 2002 & 2004).

The Rooiberg Felsite is confined to the central regions of the complex and is in contact with the Lebowa Granite Suite in the northern and eastern parts, the Rashoop Granophyre Suite in the southern central part and the mafic RLS in the south-western part of the complex (Schweitzer *et al.,* 1995) (Cawthorn *et al.,* 2006). The Rooiberg Felsite is thought to represent the initial stages of the Bushveld magmatic event (Buchanan *et al*, 2002) that caused large scale melting of predominantly crustal material, by mantle plume upwelling (Hatton & Schweitzer, 1995), subduction zone melting (Hatton, 1988) or even bolide impact (Elston, 1992), which extruded into the proto-Witwatersrand Basin to form the 'roof' and in some places the floor of the subsequent Bushveld Complex units (Cawthorn *et al*., 2006).

2.1.2 Rustenburg Layered Suite (RLS)

The layered ultramafic/mafic units of the RLS generally form the basal section of the Bushveld LIP. The ~ 9 km thick RLS (Fig. 9) contains the bulk of the world's platinum, chrome and vanadium deposits and is the largest layered igneous body in the world. Despite the economic importance and large amount of research being conducted on the RLS, much about the actual emplacement and source region of the parental magmas remains unclear. The RLS as defined by SACS (1980) includes a range of compositions, ranging from diorite to harzburgite with each unit in each limb having a different name. The RLS has generally been divided into five zones (Hall, 1932; Wager & Brown, 1967); Marginal Zone, Lower Zone, Critical Zone, Main Zone and Upper Zone based on lithological similarities and these terms are used by most researchers when speaking about the RLS as a whole. The Marginal Zone underlies most of the RLS in the complex with the exceptions being in the north of the northern limb and in the Burgersfort region of the eastern limb (Eales & Cawthorn, 1996). The Marginal Zone is classified as an 800 m thick norite unit according to SACS (1980). The harzburgite/pyroxenite Lower Zone (SACS, 1980) lies above the Marginal Zone and below the economically important Critical Zone. The Critical Zone of the RLS is divided into a lower zone of pyroxenite and an upper zone of cyclic layered anorthosite, norite and pyroxenite (SACS, 1980) and contains the famous Merensky Reef. Above the Critical Zone lies the Main Zone which can be divided into a lower region of norite, an intermediate zone of anorthosite and an upper zone of anorthosite separated from the intermediate zone by a pyroxenite unit (SACS, 1980). The uppermost unit of the RLS is the Upper Zone which is further divided into three zones with the magnetite gabbronorite zone overlain by the olivine-magnetite gabbronorite zone and olivine-apatite diorite zone respectively (SACS, 1980).

The Sr-isotope variation between the RLS zones has been attributed to the influx and mixing of different magma pulses (Wager & Brown, 1968; Cawthorn *et al*., 1981; Kruger & Marsh, 1982; Harmer & Sharpe, 1985) during the emplacement of the Bushveld LIP. Variations in magnesium number and plagioclase compositions as well as trace element variations in the RLS give evidence of a complex emplacement history. The use of strontium isotopes in plagioclase (Sharpe, 1985; Kruger, 2005) has led to the hypotheses that many injections or pulses of isotopically distinct magma were emplaced to form the RLS.

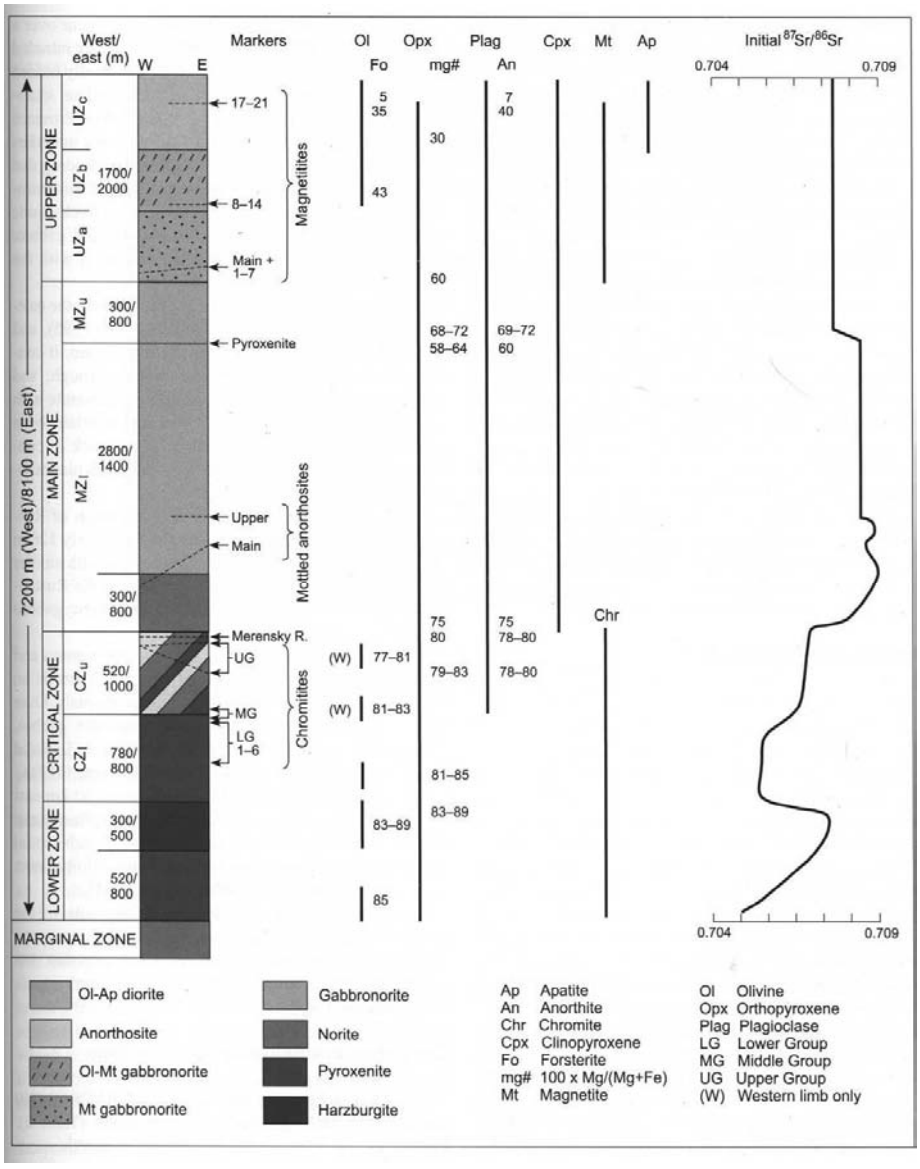

Fig. 9: Stratigraphic sections through the RLS in the eastern and western lobes of the Bushveld complex indicating rock type, major divisions, maximum thickness, magnetite layers, Mg# and $^{87}Sr/^{86}Sr$ variation with stratigraphic height are also shown.
Source: Cawthorn *et al*., 2006.

The layering of the RLS is mimicked on a much larger scale in the overlying felsic units, with the granites, granophyres and felsites seeming to have been emplaced in a generally tabular geometry (Cawthorn *et al*., 2006). The very shallow (~ 10º) centripetal dip (Cawthorn *et al*., 1998) of the Nebo Granite sheet is considered a late stage development due to crustal loading and downwarping, meaning that when emplaced the original felsic units were nearly horizontal. The emplacement geometry seems to indicate that the RLS and felsic units flowed into their current position and were not injected from below (Clarke *et al*., 2009). Stable isotope studies on the mafic/ultramafic units have been carried out by Schiffries & Rye, (1989); Reid *et al*., (1993); Maier *et al*., (2000) and Harris *et al*., (2005) to acertain the petrogenesis of the RLS cumulates. The large amount of research performed on the RLS suggests that the RLS parental magma was of mantle origin but was contaminated at depth by crustal material and possibly other magmas to yield the characteristic isotope composition of the RLS (Maier *et al*., 2000; Harris *et al*., 2005). The RLS magma travelled upward, due to a negative pressure gradient, to lower crustal depths and was emplaced in the proto-Witwatersrand Basin above and below the Rooiberg Felsite (Cawthorn *et al*., 2006). Magmatic differentiation, settling and possible magma mixing within the basin is thought to be responsible for the RLS layering (Cawthorn *et al*., 2006) but consensus on the formation of the RLS layering has not yet been reached.

2.1.3 Rashoop Granophyre

The 2061.8 ± 5.5 Ma age for the Rooikoppies Porphyry, obtained by Harmer & Armstrong, (2000) indicates that the Rashoop Granophyre Suite, (Figs. 10 & 11) was emplaced (within error) at the same time. Evidence of this from the field is seen most clearly north of Grobelaarsdal, within the Stavoren Granophyre in the eastern Bushveld and the Rooiberg fragment where granophyric dykes intrude into the Rooiberg Felsite units above and Nebo Granite intrudes into the Stavoren Granophyre (Crocker *et al*., 2001). The Rashoop Granophyre Suite is thought to represent shallow intrusions of magma and small volumes of partially re-melted Rooiberg volcanics (Walraven, 1987; Hatton & Schweitzer, 1995) and two types of granophyre have been identified. Walraven (1987) identified the distinct characteristics of magmatic and metamorphic granophyre units.

The ‘magmatic granophyres’ show well developed micrographic texture of quartz and alkali feldspar (Walraven, 1985), while the ‘metamorphic granophyres’ show irregular micrographic intergrowth between quartz and alkali feldspar, thought to be formed by replacement of minerals in ‘magmatic granophyres’ during metamorphism of granophyres and felsites when the Bushveld Granites were emplaced (Walraven, 1985). The magmatic granophyres have been named the Stavoren Granophyre and the metamorphic granophyre the Diepkloof Granophyre and Zwartbank Pseudogranophyre. Studies on the granophyres (Walraven, 1985 & 1987b; Hatton & Schweitzer, 1995) have indicated a similarity in chemical composition with lavas of the Rooiberg Group. Geochemical variation between units and suites may reflect a slightly different emplacement or formation history.

Figs. 10 & 11: Rashoop Granophyre (BC 5 & BC 25) outcrop situated in the western and northern lobe respectively.

Dating and field observations of the Rashoop Granophyre Suite suggest that it was emplaced before the Nebo Granite but not before the RLS. A study by Von Gruenewaldt, (1971) led to the hypothesis that the granophyres formed by melting of the Rooiberg Felsite during the emplacement of the RLS while Walraven, (1982) suggested that the granophyres represent the intrusive equivalent of the Rooiberg Felsite lavas. Some workers (Schweitzer *et al.*, 1997) believe a petrogenetic link exists between the Rashoop Granophyres, Nebo Granite and the Rooiberg Felsite, so a widely accepted petrogenetic model of the granophyres is still lacking.

2.1.4 Lebowa Granite Suite

The majority of the granitic units encompassed within the Lebowa Suite are relatively minor compared to the Nebo Granite (Figs. 12 & 13) (Kleemann, 1987) which is the most voluminous and widespread of the granitic units, and is estimated to be ~ 30000 km^2 (Kleemann & Twist, 1989) in aerial extent and possibly up to ~ 100000 km^3 in volume. The 2-3 km thick Nebo Granite sheet will be the focus of this study as the other granitic units are often localised and thought to be evolved from the main Nebo Granite sheet. The main minerals associated with the Nebo Granite are quartz, K-feldspar (perthite), plagioclase and in some cases hornblende and biotite, with accessory zircon, apatite and sphene. The coarse-grained, mostly pink granite has been dated at 2054.2 ± 2.8 Ma (Harmer & Armstrong, 2000). The Granitic sheet becomes progressively more albitized, with biotite and hornblende depleted roofward (Kleemann, 1987) with the topmost section severely stained and altered by fluids.

Figs. 12 & 13: Nebo Granite Samples (BC 3 & BC 39) taken in the western and eastern lobes.

Granitic bodies within the main Nebo Granite sheet have been divided into three main groups (Cawthorn *et al.,* 2006). The medium-grained red Bobbenjaankop Granite is found in the upper part of the Nebo Granite sheet and has been heavily altered by fluid interaction and is mineralised in places like the Zaaiplats cassiterite mine (Kleemann, 1987; Crocker *et al*., 2001). The medium to fine-grained Klipkloof Granite forms dykes and sills within the Nebo Granite sheet near the roof of the sheet.

The least abundant and youngest of the three units is the medium-grained Makhutso Granite which has a relatively high mafic mineral content compared to the other evolved granites and does not seem to be a differentiated Nebo Granite melt (Walraven, 1988). Workers (Kleemann & Twist, 1989; Schweitzer et al., 1997; Cawthorn et al., 2006) agree that the Nebo Granite represents the terminal phase of Bushveld Complex magmatism and its intrusion and emplacement into the proto–Witwatersrand Basin was probably responsible for the hydrothermal alteration seen in the felsic units, particularly the Rooiberg Felsite. The Nebo Granite and all its different facies are thought to have formed by the fractionation of a large magma body formed in or intruded into the mid to upper crust (Kleemann & Twist, 1989). The reason for the large magma body formation is not well understood but the anhydrous nature of the granites suggests a magma with high liquidus temperatures, thus melting of source material due to mantle plume upwelling is most likely (Twist & Harmer, 1987), but the exact petrogenesis remains unclear.

3 PETROGRAPHY AND SAMPLE DESCRIPTION

The great size of the Bushveld Complex and the geometry of the 3 largest exposed lobes necessitated good spatial sampling and preferably numerous samples of each felsic unit within each lobe to more accurately characterise the Bushveld Complex's isotope composition and make comparison between and within lobes possible. Sixty samples of the felsic units from the Bushveld Complex were collected in March/April 2008 by Duane Fourie, Jarryd Finkelstein and Andre Fourie from outcrop in the western, northern and eastern lobes of the Bushveld Complex (Table 1 & Fig. 14) and 36 samples were studied with a petrographic microscope in thin section (Fig. 15 & Table 2). The Nebo Granite samples generally contained coarse-grained quartz and feldspar grains, accounting for ~ 90 % of the sample, with the feldspar predominantly perthitic with few distinguishable plagioclase or K-feldspar grains. Some samples of Nebo Granite also exhibited granophyric intergrowth but of limited extent (~ 10 % to 15 %) compared to the granophyre samples. The Rashoop Granophyres samples showed extensive (40 % to 80 %) granophyric intergrowth across the thin sections, with very few discrete quartz or feldspar grains visible.

The Rooiberg Felsites are generally very fine-grained and individual minerals extremely difficult to identify. Spherulitic texture within the groundmass and occasional phenocrysts of quartz and or feldspar could be distinguished. The granite and granophyre samples contained varying amounts of accessory and alteration minerals such as mica (biotite/chlorite) and amphiboles, with sample BC 11 having up to 20 % amphibole. Zircon, sphene and apatite were also observed in many thin sections in trace amounts. Most of the Rooiberg Felsite samples showed signs of alteration in the form of iron oxide staining, leaving the thin section almost opaque and minerals not easy to identify.

Table 1: Location and lithology of the Bushveld Complex Felsic unit samples analysed in this study.

Sample	Rock Type	Latitude	Longitude	Location
BC1	Rashoop Granophyre	25°34′47.8"	27°46′13.7"	Western Lobe
BC2	Nebo Granite	25°28′03.0"	27°39′44.0"	Western Lobe
BC3	Nebo Granite	25°27′04.7"	27°38′04.5"	Western Lobe
BC4	Rashoop Granophyre	25°32′55.5"	27°42′50.7"	Western Lobe
BC5	Rashoop Granophyre	25°23′43.7"	27°33′57.9"	Western Lobe
BC6	Nebo Granite	25°24′03.6"	27°32′25.0"	Western Lobe
BC7	Nebo Granite	25°26′29.4"	27°25′10.5"	Western Lobe
BC8	Nebo Granite	25°25′46.6"	27°22′30.8"	Western Lobe
BC9	Nebo Granite	25°19′27.9"	27°23′43.3"	Western Lobe
BC10	Nebo Granite	25°19′32.0"	27°23′36.0"	Western Lobe
BC11	Rashoop Granophyre	25°19′15.1"	27°22′38.6"	Western Lobe
BC12	Nebo Granite	25°08′40.7"	27°24′32.6"	Western Lobe
BC13	Nebo Granite	25°07′45.1"	27°23′08.1"	Western Lobe
BC14	Nebo Granite	25°08′42.8"	27°15′35.9"	Western Lobe
BC15	Nebo Granite	25°10′58.5"	27°48′45.3"	Western Lobe
BC16	Rooiberg Felsites	25°05′10.9"	27°38′42.0"	Western Lobe
BC17	Nebo Granite	25°04′37.5"	27°38′54.4"	Western Lobe
BC18	Rashoop Granophyre	25°03′28.2"	27°39′08.0"	Western Lobe
BC19	Nebo Granite	25°02′28.4"	27°39′31.1"	Western Lobe
BC20	Rooiberg Felsites	24°55′23.9"	27°45′23.9"	Western Lobe
BC21	Rashoop Granophyre	24°56′07.7"	27°46′25.7"	Western Lobe
BC22	Nebo Granite	24°58′31.1"	27°48′36.7"	Western Lobe
BC23	Rashoop Granophyre	24°41′07.9"	27°39′10.4"	Northern Lobe
BC24	Nebo Granite	24°03′00.9"	28°46′23.1"	Northern Lobe
BC25	Rashoop Granophyre	24°05′14.0"	28°44′34.2"	Northern Lobe
BC26	Rooiberg Felsites	24°06′25.8"	28°43′59.2"	Northern Lobe
BC27	Rooiberg Felsites	24°06′03.2"	28°44′03.0"	Northern Lobe
BC28	Nebo Granite	24°26′31.9"	28°40′00.4"	Northern Lobe
BC29	Rooiberg Felsites	24°28′05.7"	28°36′02.7"	Northern Lobe
BC30	Nebo Granite	24°31′24.6"	28°33′11.5"	Northern Lobe
BC31	Rooiberg Felsites	24°33′30.4"	28°31′37.2"	Northern Lobe
BC32	Rooiberg Felsites	24°34′42.4"	28°30′41.5"	Northern Lobe
BC33	Rooiberg Felsites	24°37′50.6"	28°30′23.9"	Northern Lobe
BC34	Rooiberg Felsites	24°38′51.1"	28°10′36.9"	Northern Lobe
BC35	Nebo Granite	24°39′28.3"	28°06′42.3"	Northern Lobe
BC36	Rooiberg Felsites	24°43′03.5"	28°07′40.6"	Northern Lobe
BC37	Rooiberg Felsites	24°49′58.7"	27°50′52.9"	Northern Lobe
BC38	Nebo Granite	24°50′11.5"	27°51′05.7"	Western Lobe
BC39	Nebo Granite	25°05′30.6"	29°28′23.9"	Eastern Lobe
BC40	Nebo Granite	25°01′10.1"	29°32′45.7"	Eastern Lobe
BC41	Nebo Granite	25°00′29.2"	29°40′40.4"	Eastern Lobe
BC42	Rashoop Granophyre	25°04′31.4"	29°42′00.6"	Eastern Lobe
BC43	Rooiberg Felsites	25°05′10.8"	29°43′14.0"	Eastern Lobe
BC44	Rashoop Granophyre	25°25′35.0"	29°48′14.1"	Eastern Lobe
BC45	Rooiberg Felsites	25°26′44.2"	29°46′04.2"	Eastern Lobe
BC46	Rooiberg Felsites	25°27′34.6"	29°45′58.7"	Eastern Lobe
BC47	Rooiberg Felsites	25°30′06.0"	29°45′16.9"	Eastern Lobe
BC48	Rashoop Granophyre	25°31′18.6"	29°43′14.1"	Eastern Lobe
BC49	Rooiberg Felsites	25°34′38.3"	29°39′28.3"	Eastern Lobe
BC50	Rooiberg Felsites	25°25′57.5"	29°31′36.0"	Eastern Lobe
BC51	Rooiberg Felsites	25°25′19.6"	29°31′39.6"	Eastern Lobe
BC52	Rashoop Granophyre	25°25′07.6"	29°31′31.8"	Eastern Lobe
BC53	Rashoop Granophyre	25°24′14.2"	29°30′07.2"	Eastern Lobe
BC54	Nebo Granite	25°15′02.7"	29°01′22.5"	Eastern Lobe
BC55	Nebo Granite	25°15′58.1"	29°00′00.5"	Eastern Lobe
BC56	Rashoop Granophyre	25°16′25.5"	28°59′25.3"	Eastern Lobe
BC57	Nebo Granite	25°18′05.1"	28°57′24.0"	Eastern Lobe
BC58	Rooiberg Felsites	25°20′18.8"	28°53′47.2"	Eastern Lobe
BC59	Rashoop Granophyre	25°27′48.2"	28°42′38.0"	Eastern Lobe
BC60	Nebo Granite	25°29′31.9"	28°40′52.8"	Eastern Lobe

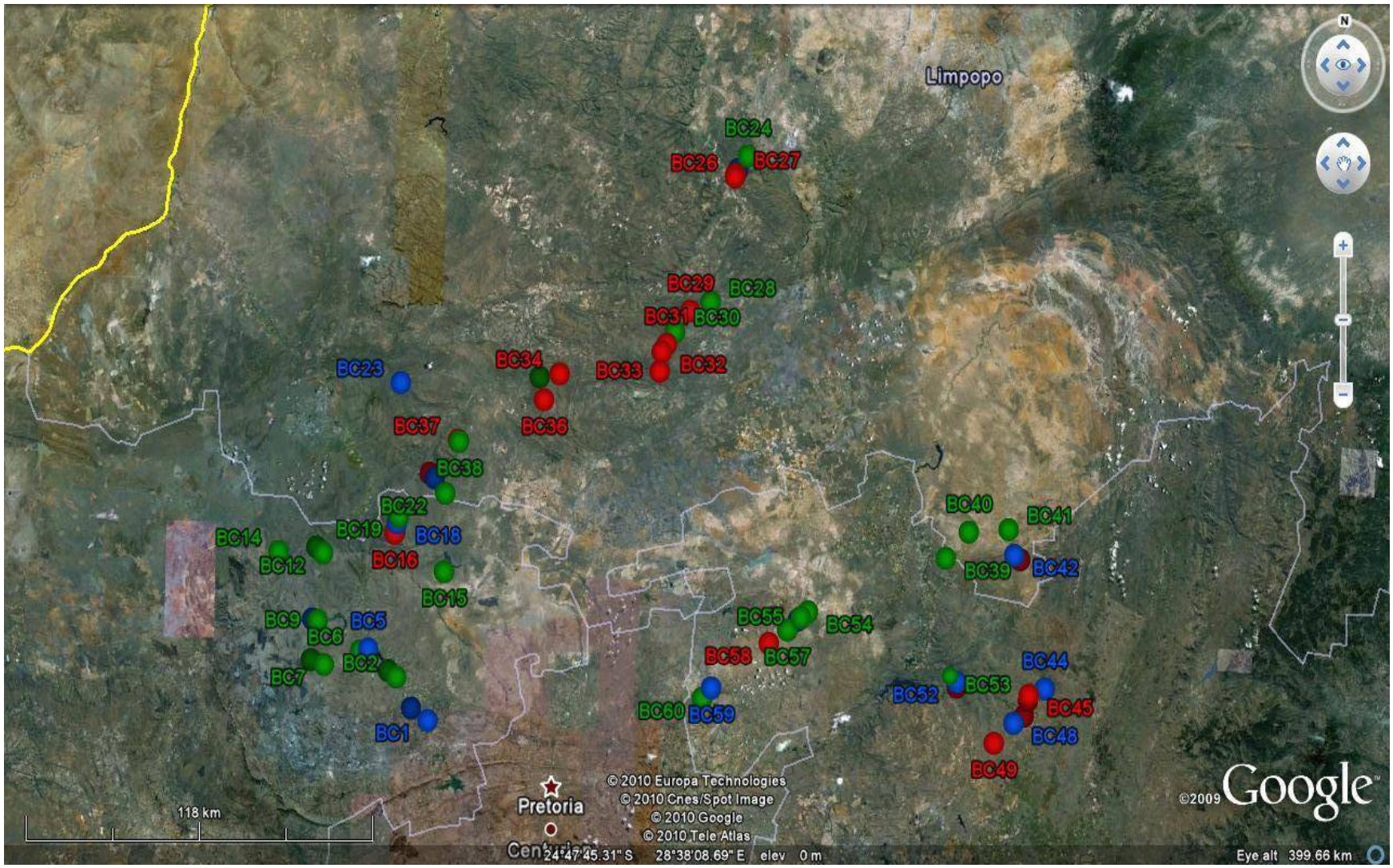

Fig. 14: Google Earth image of the Bushveld Complex sampling points for this study. Red, Blue and Green points represent Rooiberg Felsite, Rashoop Granophyre and Nebo Granite samples respectively.

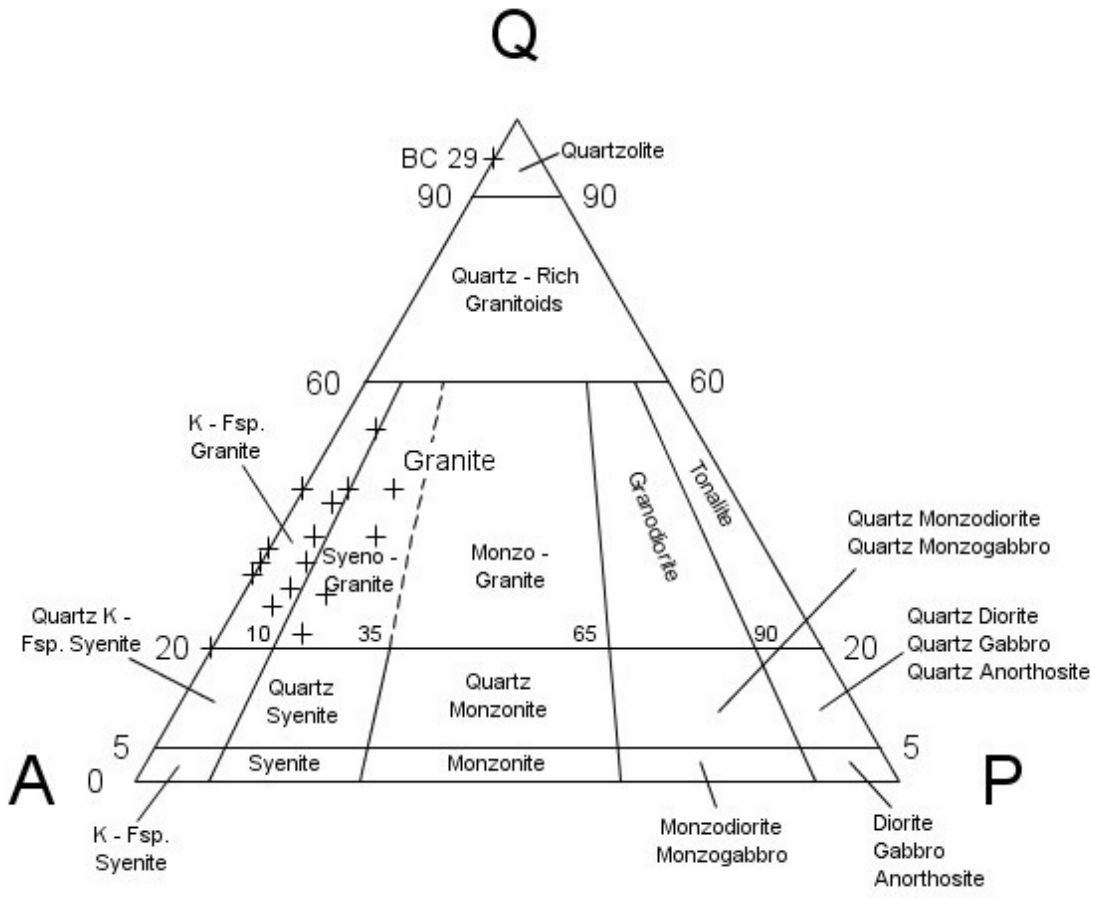

Fig. 15: Modal composition of Bushveld Complex Felsite, Granophyre and Granite samples from visual inspection of thin sections. Q = Quartz, A = Alkali Feldspar, P = Plagioclase. Perthite all plotted as A. Sample BC 29 is a sedimentary horizon within the Rooiberg Felsite. Fields after le Maitre *et al*., (1989)

Table 2. Petrography and Sample Description

Sample #	Type	Mineralogy	Description
BC1	Rashoop Granophyre	Quartz ~ 25 % Feldspar ~ 60 - 65 % Micas ~ 10 % (Biotite/chlorite) Rutile ~ 1 % Zircon ~ 1 %	Bimodal grain size of ~ 1 mm quartz intergrown with larger 4 – 6 mm K-fsp. Grains to form characteristic granophyric texture. Quartz grains irregular and yellow-slightly orange coloured. Plag. occurs as subhedral lathes 6 – 8 mm long and 1 mm wide. Zonation of plag. evident with alteration of rim and or core visible. Chlorite after feldspars and scattered biotite. Medium-large grain size (ave. ~ 1 – 2 mm), showing granophyric intergrowth.
BC4	Rashoop Granophyre	Quartz ~ 50 – 55 % Feldspar ~ 40 – 45 % Micas ~ 5 % (Biotite/white micas) Rutile < 1 % Zircon < 1 %	Fairly equigranular (Ave.~ 0.5 mm – 1 mm) medium-grained texture with distinctive Granophyric intergrowth between quartz and K-fsp.
BC5	Rashoop Granophyre	Quartz ~ 40 % Feldspar ~ 40 – 50 % Biotite ~ 5 % Opaque minerals (oxides) ~ 1 %	Quartz grain size ~ 0.5 – 1 mm and intergrown with 1 – 2 mm K-fsp grains to show granophyric texture. Biotite replacing feldspar in places. Granophyric texture dominant over ~ 80 – 90 % of thin section.
BC9	Nebo Granite	Quartz ~ 30 – 35 % Feldspar ~ 50 – 55 % Micas < 5 % Pyroxene < 5 % Amphibole < 5 % (Hornblende) Sphene < 5 %	Overall texture of medium to large grain size with a few places showing granophyric texture. Scattered fragments of pyroxene and amphibole throughout along with some biotite replacement. Sphene is observed scattered within the thin section as well.
BC11	Rashoop Granophyre	Quartz ~ 30 % Feldspar ~ 40 – 50 % Biotite ~ 5 % Amphibole ~ 15 – 20 % (Hornblende) Zircon < 1 %	Quartz grains (Ave. ~ 1 – 2 mm) irregular and show evidence of deformation: Sutured grain boundaries with pressure solution, sub-grain boundary formation within larger grains and fracturing of grains. No Granophyric texture visible. Feldspar larger grains (Ave. 2 – 3 mm) altered so crystal shape and some original mineral is visible but otherwise totally altered. Amphibole (Ave. ~ 1 – 2 mm) alteration with subhedral-anhedral grains after feldspar as well as some scattered biotite in the thin section.
BC16	Rooiberg Felsite	Quartz ~ 5 % Opaque minerals (Iron Oxides) ~ 5 % Groundmass ~ 80 % (Feldspar, micas, quartz, oxides)	Porphyritic quartz (Ave. ~ 0.25 - 0.5 mm) within very fine-grained groundmass. Sub-grain boundary formation in quartz grains suggests deformation. Groundmass has spherulitic texture (difficult to identify laths but looks like feldspar)

BC18	Rashoop Granophyre	Quartz ~ 30 % Feldspar ~ 55 – 60 % Biotite ~ 5 %	Bimodal irregular quartz grains (~ 0.5 mm), (2 – 4 mm) show sub-grain boundaries and pressure solution. Feldspar grains show bimodal grain size, with the smaller size averaging 1 mm and the larger grains averaging 3 – 4 mm. Feldspar grains are altered with no clear granophyric intergrowth visible.
BC21	Rashoop Granophyre	Quartz ~ 40 % Feldspar ~ 40 – 50 % Micas ~ 5 – 10 % (Biotite, chlorite)	Bimodal grain size for quartz with smaller grain size averaging 0.5 mm and larger grains averaging 2 mm in size. Quartz grains show pressure solution at grain boundaries and 120º grain intersections. Feldspar grains show bimodality between plag. (1 mm prisms) and K-fsp (2 – 3 mm perthitic grains intergrown with quartz). Granophyric texture throughout the thin section with intergrowths on the scale of 0.5 – 1 mm. Biotite scattered within the thin section with some chlorite replacing feldspars.
BC23	Rashoop Granophyre	Quartz ~ 30 – 40 % Feldspar ~ 50 – 60 % Opaque minerals (iron oxides) ~ 5 %	Quartz grains intergrown with K-fsp on a small scale (< 0.5 mm) with the largest 'free' quartz grain < 1 mm. Feldspar grains mostly intergrown with quartz but no grains larger than 2 mm. Spherulitic texture visible with granophyric quartz/K-fsp grains radiating outwards from a 'nucleus', average spherulite size is 2 mm.
BC25	Rashoop Granophyre	Quartz ~ 40 – 45 % Feldspar ~ 45 – 50 % Micas ~ 5 % (Biotite, chlorite, muscovite)	Irregular quartz grains with some grains showing resorption textures. Feldspar shows granophyric intergrowth with quarts with the K-fsp grains being perthitic and averaging 1 – 2 mm in size. Scattered mica throughout thin section with chlorite replacing feldspar in places.
BC26	Rooiberg Felsite	Quartz ~ 60 – 65 % Micas ~ 25 – 30 % (Biotite, white micas) Opaque minerals (iron oxides) ~ 5 – 10 %	Fairly equigranular sub-rounded grains (~ 1 mm) showing sub-grain boundaries, suturing and granulation of larger grains. Some large grains appear totally undeformed. No feldspar visible at all and most quartz grains look to be relict; thin section looks pelitic and is probably a sedimentary unit within the felsite.
BC27	Rooiberg Felsite	Quartz ~ 1 – 3 % Opaque minerals (iron oxides) ~ 1 – 3 % Groundmass ~ 90 – 95 % (Quartz, micas, epidote)	Very small (< 0.5 mm) quartz grains within groundmass which is extremely altered and stained by iron oxides, looks sedimentary.
BC29	Rooiberg Felsite	Quartz ~ 85 – 90 % Feldspar ~ 5 % Opaque Minerals (Iron Oxides) ~ 5 % Zircon ~ 1 %	Larger (~ 2 mm) grains within quartz 'groundmass' that seem to be an alteration/replacement of euhedral crystals by micas. Grains are cemented by iron oxides. The sample looks sedimentary.

BC31	Rooiberg Felsite	Quartz ~ 65 – 70 % Micas ~ 20 – 25 % (Biotite, chlorite) Opaque minerals (iron oxides) ~ 10 %	Grains coated by iron oxides and are irregular in shape. Micas replacing original mineralogy which is not discernable or sample is not igneous, looks like a sedimentary unit.
BC32	Rooiberg Felsite	Quartz ~ 5 % Groundmass ~ 90 – 95 % (Quartz ~ 50 – 60 %, micas ~ 35 – 40 % opaques ~ 5 – 10 %)	Small (~ 0.5 mm) quartz grains within the finer quartz/mica 'groundmass'. Not an igneous rock.
BC33	Rooiberg Felsite	Quartz ~ 5 % Groundmass ~ 95 % (Quartz ~ 50 % Micas ~ 35 – 40 %, opaques ~ 10 – 15 %)	Large (1 – 2 mm) quartz phenocrysts within fine (< 0.5 mm) groundmass. Grains are fairly equigranular and covered by oxides that obscure grain boundaries. The oxide coating is pervasive and in one corner an 'oxide front' can be seen that separates a coated section from a predominantly (75 – 80 %) oxide section.
BC34	Rooiberg Felsite	Quartz ~ 10 – 15 % Feldspar ~ 10 – 15 % Micas ~ 5 % (Biotite, chlorite) Groundmass ~ 70 – 75 % (Quartz, feldspar, micas, opaques)	Sample is coated by iron oxides, obscuring minerals and features, quartz grains are small (< 1 mm) and irregular in shape. Spherulitic feldspar lathes within the groundmass (< 1 mm) in length) and alteration of feldspar by chlorite and biotite. Fractures in the sample are infilled with quartz grains that are totally unstained by iron oxide.
BC35	Nebo Granite	Quartz ~ 30 – 35 % Feldspar ~ 55 – 60 % Opaque minerals (iron oxides) ~ 5 – 10 % Micas ~ 1 %	~ 1 mm, fairly equigranular, quartz grains intergrown with feldspar on a large (1 – 2 mm) scale. Feldspar grains (2 – 3 mm) appear predominantly perthitic and are intergrown with quartz. Mica is scattered sparsely within the sample.
BC36	Rooiberg Felsite	Quartz < 5 % Feldspar < 5 % Mica ~ 5 – 10 % Groundmass ~ 90 – 95 % (Quartz, feldspar, mica, Opaques)	Small (< 1 mm) quartz phenocrysts, with larger, fairly euhedral (~ 1 mm), feldspar crystals also present within the groundmass. Biotite and chlorite after feldspars and scattered throughout the sample. Granophyric texture on a small (< 0.5 mm) scale with groundmass altered and stained by iron oxides.
BC37	Rooiberg Felsite	Quartz ~ 15 – 20 % Feldspar ~ 60 – 65 % Mica ~ 10 – 15 % (Biotite, chlorite) Opaque minerals (iron oxides) ~ 5 %	Granophyric intergrowth between quartz and feldspar where the grains are large enough. Spherulitic feldspar also common with the sample stained by iron oxides.
BC42	Rashoop Granophyre	Quartz ~ 15 – 20 % Feldspar ~ 60 – 65 % Mica ~ 5 – 10 % Opaque minerals (iron oxides) ~ 5 %	Quartz grain size of ~ 1 mm with large (2 – 3 mm) feldspar crystals forming a granophyric texture with spherulitic feldspar lathes also visible. Mica present as alteration/replacement of grains with some feldspar grains already totally replaced.

BC43	Rooiberg Felsite	Feldspar ~ 5 % Mica ~ 5 % Amphibole ~ 1 % (Hornblende) Groundmass ~ 90 – 95 % (Quartz, feldspar, mica)	Large (1 – 2 mm) feldspar and amphibole (1 mm) phenocrysts within the finer (< 0.5 mm) groundmass.
BC44	Rashoop Granophyre	Quartz ~ 20 – 25 % Feldspar ~ 50 – 60 % Amphibole ~ 5 – 10 % (Hornblende) Pyroxene ~ 5 % Mica ~ 5 % Opaque minerals (iron oxides) ~ 5 %	Fairly equigranular quartz (1 mm) and larger (2 mm) perthitic feldspar grains with scattered mica, amphibole and pyroxene in the sample.
BC45	Rooiberg Felsite	Quartz ~ 5 – 10 % Mica ~ 5 % Groundmass ~ 90 – 95 % (Quartz, mica)	Small (< 0.5 mm) phenocrysts of quartz and mica within very fine-grained groundmass. A few large (2 – 3 mm) phenocrysts of an unknown mineral.
BC46	Rooiberg Felsite	Quartz ~ 20 – 25 % Feldspar ~ 55 – 60 % Mica ~ 5 % Opaque minerals (iron oxides) ~ 5 – 10 %	Quartz grains are small (< 0.5 mm) and forms granophyric intergrowth with K-fsp. Spherulitic feldspar and feldspar phenocrysts of plagioclase (1 mm) with scattered mica and opaque minerals.
BC47	Rooiberg Felsite	Quartz ~ 35 – 40 % Feldspar ~ 40 – 45 % Mica ~ 10 – 20 % (Biotite)	Large phenocrysts of perthitic K-fsp and plagioclase grains (1 – 2 mm) are situated in a finer-grained (< 0.5 mm) groundmass of quartz, micas and feldspar. Smaller plagioclase grains (~ 1 mm) are euhedral and the overall texture resembles an altered cumulate.
BC48	Rashoop Granophyre	Quartz ~ 20 – 25 % Feldspar ~ 65 – 70 % Mica ~ 5 % (Biotite)	Large (3 – 6 mm) quartz and perthitic K-fsp phenocrysts in a quartz/feldspar/mica groundmass (0.5 – 1 mm). Granophyric texture visible in smaller (< 2 mm) grains in places with scattered biotite. Overall texture is of a quartz/feldspar porphyry with the groundmass having a cumulate texture.
BC49	Rooiberg Felsite	Quartz < 2 % Feldspar ~ 5 % Opaque Minerals (Iron Oxides) ~ 5 – 10 % Groundmass ~ 80 – 90 % (Quartz, feldspar, opaques)	Phenocrysts of quartz and feldspar (some euhedral plag grains.) within a fine (< 0.5 mm) groundmass of quartz, feldspar and opaque minerals. Groundmass shows devitrification texture.
BC50	Rooiberg Felsite	Quartz ~ 30 % Feldspar ~ 55 – 60 % Mica < 5 % (Biotite) Amphibole ~ trace (Hornblende) Opaque minerals (iron oxides) < 5 %	Overall texture of small to medium (0.5 mm – 1 mm) grains of quartz, feldspar with scattered biotite and fragments of amphibole. Thin section is stained by iron oxide with some discreet opaque minerals also visible.

BC51	Rooiberg Felsite	Quartz ~ 5 – 10 % Feldspar ~ 5 % Opaque minerals (iron oxides) ~ 5 – 10 % Groundmass ~ 80 – 85 % (not discernable)	Phenocrysts of quartz and feldspar (~ 1 mm) within finer (< 0.5 mm) groundmass showing devitrification textures. Quartz phenocrysts are granulated and the feldspar grains altered and stained by iron oxides.
BC52	Rashoop Granophyre	Quartz ~ 20 – 25 % Feldspar ~ 65 – 70 % Mica ~ 5 % (Biotite) Opaque minerals (iron oxides) < 5 %	Large (3 – 5 mm) quartz, K-fsp. (4 – 5 mm) and plagioclase (1 – 2 mm) phenocrysts within the groundmass of smaller (1 – 2 mm) K-fsp, quartz and plagioclase grains. Larger quartz grains show resorption texture. Granophyric texture visible in the smaller grains but not in the large phenocrysts with scattered biotite throughout the thin section. Texture resembles cumulate in places.
BC56	Rashoop Granophyre	Quartz ~ 40 – 45 % Feldspar ~ 45 – 50 % Mica ~ 5 % (Biotite) Opaque minerals (iron oxides) ~ 5 %	Large (4 – 5 mm) phenocrysts of quartz and perthitic K-fsp with smaller (1 – 3 mm) altered plagioclase grains within groundmass of medium sized (~ 1 mm) grains of quartz and feldspar. Large quartz grains show suturing and pressure solution textures with the thin section stained by iron oxides. No granophyric texture visible.
BC57	Nebo Granite	Quartz ~ 40 – 45 % Feldspar ~ 50 – 55 % Mica ~ 5 % Opaque minerals (iron oxides) ~ 5 %	Phenocrysts of quartz (~ 1 mm) situated within granophyric 'groundmass'. Opaque minerals and biotite/chlorite scattered throughout thin section. Granophyric texture visible over 80 – 85 % of the thin section with 2 – 3 mm K-fsp grains intergrown with quartz.
BC58	Rooiberg Felsite	Quartz ~ 40 – 45 % Feldspar ~ 50 – 55 % Mica ~ trace Opaque minerals (iron oxides) ~ 5 %	Phenocrysts of quartz (~ 1 mm) situated within granophyric 'groundmass'. Opaque minerals and biotite/chlorite scattered throughout thin section. Granophyric texture visible over 80 – 85 % of the thin section with 2 – 3 mm K-fsp grains intergrown with quartz.
BC59	Rashoop Granophyre	Quartz ~ 40 – 45 % Feldspar ~ 45 – 50 % Mica ~ 5 % (Biotite) Opaque minerals (iron oxides) ~ 5 %	Discreet quartz grains (~ 1 mm) situated within 'groundmass' of granophyric quartz and K-fsp. Granophyric textured intergrowth of quartz and K-fsp cover 80 % of the thin section with the remainder of the slide covered by quartz grains and scattered mica.
BC60	Nebo Granite	Quartz ~ 35 – 40 % Feldspar ~ 35 – 40 % Amphibole ~ 5 – 10 % (Hornblende) Mica ~ 5 % (Biotite) Opaque minerals (iron oxides) ~ 5 %	60 – 70 % of the thin section occupied by granophyric intergrowth of quartz and k-fsp (1 – 2 mm). Fragments of hornblende scattered throughout the thin section along with mica and opaque minerals. A few quartz grains (1 – 2 mm) scattered in the thin section that are not intergrown with K-fsp..

Petrography of the 36 thin sections from the Bushveld Complex Felsic units. The mica observed in most thin sections, with the exception of a few Rooiberg Felsite samples, are biotite and chlorite, not muscovite.

3.1 Rooiberg Felsite

The general appearance of Rooiberg Felsite samples in thin section is of a very fine-grained groundmass of feldspars, micas and quartz, often showing devitrification textures. Distinguishable features within the groundmass are spherules of feldspar laths (Figs. 16 & 17) which may or may not surround a grain of quartz or feldspar, often displaying chloritisation (Fig. 19) and or oxide infiltration. Alteration and magmatic disequilibrium textures of feldspar and quartz grains are seen in some samples with the majority of the feldspar being perthitic and some quartz grains showing evidence of deformation in the form of sutured and sub-grain boundaries (Figs. 20 & 21) and 120º grain intersections. The deformation features are not usually observed in the other minerals and may be inherited from a sedimentary or metamorphic precursor.

Primary hydrous phases are very difficult to discern and most biotite and amphibole seen in thin section looked to be formed by alteration of feldspars or other primary minerals. The presence of oxides (Fig. 18) in the Rooiberg Felsite samples varies dramatically from sample to sample, with most samples showing ~ 10 % oxide staining but a few samples have up to 70 % of their total areas covered by oxide staining. The Rooiberg Felsite samples are not easily separated into igneous and sedimentary units in the field but in thin section 4 samples were not of igneous origin consisting of > 80 % quartz and showing inherited sedimentary textures such as bedding and sorting of grains.

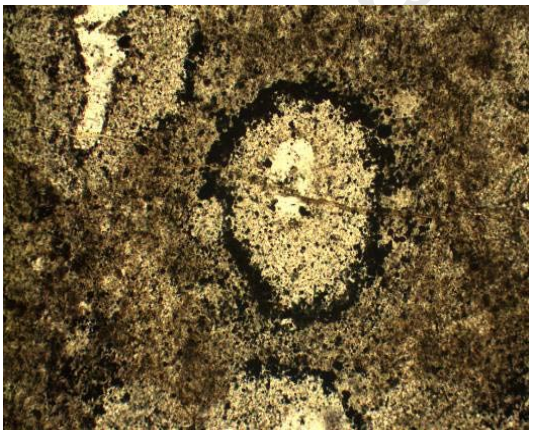

Fig. 16: BC 51 Quartz grains forming nuclei in the matrix surrounded by an alteration halo. Field of view (FOV) is 2 mm wide.

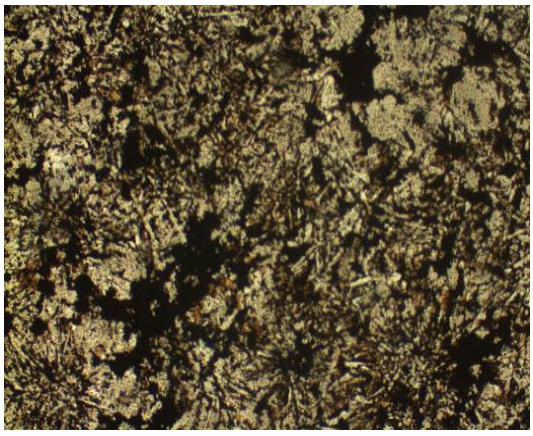

Fig. 17: BC 29 Spherulitic texture and oxide staining. FOV is 2 mm wide.

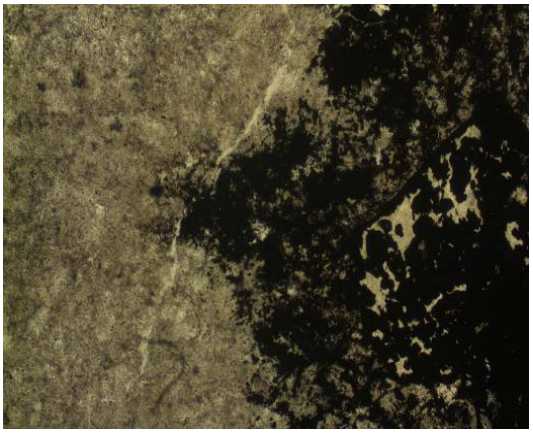

Fig. 18: BC 33 Oxide front meeting fine grained felsite matrix. FOV is 4 mm wide.

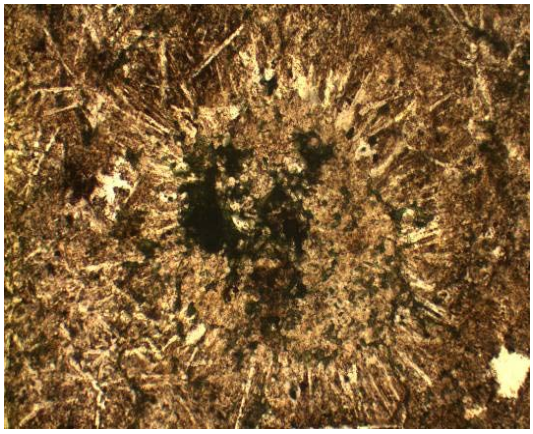

Fig. 19: BC 37 Spherulites of feldspar and micas with chloritisation beginning. FOV is 2 mm wide.

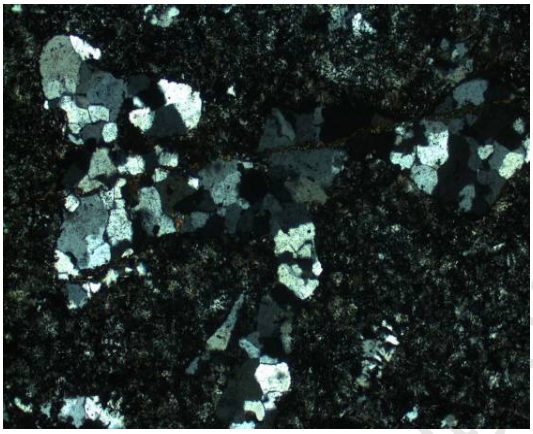

Figs. 20 & 21: BC 51 Granulated quartz 'grain', in fine altered matrix under XPL and PPL. FOV is 4 mm wide.

3.2 Rashoop Granophyre

The Bushveld Complex Granophyre samples are medium to coarse-grained (0.5 mm to 2 mm) in thin section, displaying the characteristic granophyric intergrowth of alkali feldspar and quartz (Fig. 22) in the majority of samples. Alkali feldspar is perthitic generally accounting for 50 % to 70 % of the sample with small amounts (< 5 %) of free plagioclase observed in the Rashoop granophyre samples. Quartz crystals appear subhedral to anhedral, surrounded by larger grained perthitic and granophyric alkali feldspar with free quartz forming ~ 10 % to 15 % of most samples. Accessory minerals include zircon (Fig. 23), iron oxides, biotite and amphibole (hornblende) with the hydrous phases forming 10 % to 15 % of the sample in some cases. Features typical of deformation are observed in thin section as suturing of grain boundaries and resorption textures in quartz and alkali feldspar crystals (Figs. 24, 25 & 26) with infiltration of iron oxides and chloritisation also visible in some samples (Figs. 26 & 27). A number of amphibole grains also show suturing (Fig. 25) and may represent a primary hydrous phase.

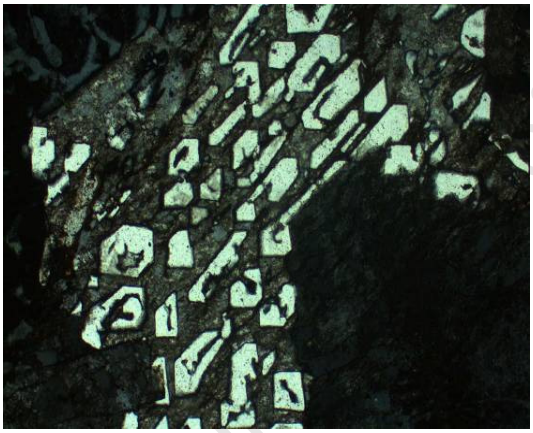

Fig. 22: BC 59 Granophyric texture in XPL. FOV is 4 mm wide.

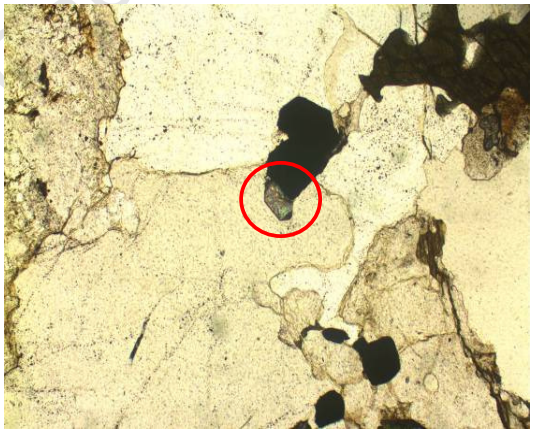

Fig. 23: BC 11 Zircon in quartz viewed in PPL. Suturing and resorption of quartz is also visible. FOV is 4 mm wide.

Fig. 24: BC 21 Embayed quartz grain in finer matrix of quartz, feldspar and micas. FOV is 4 mm wide.

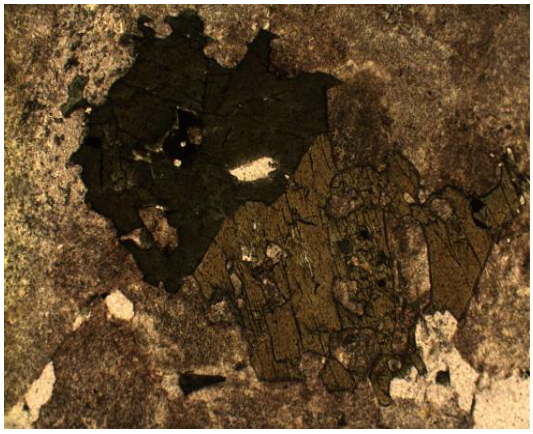

Fig. 25: BC 44 Amphibole grains showing break down of surrounding feldspars and suturing. FOV is 2 mm wide.

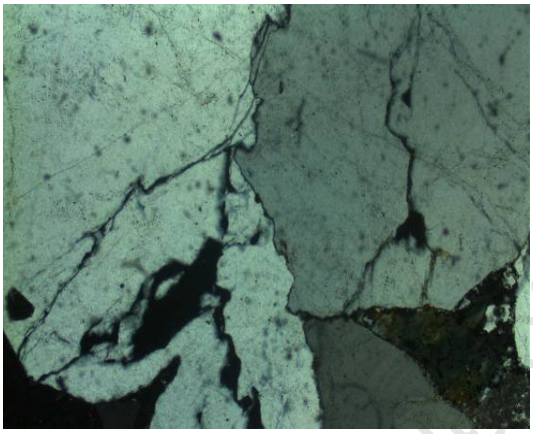

Fig. 26: BC 56 Sutured grain boundaries and fluid inclusion trails in quartz and chloritisation of biotite or feldspars also visible. FOV is 4 mm wide.

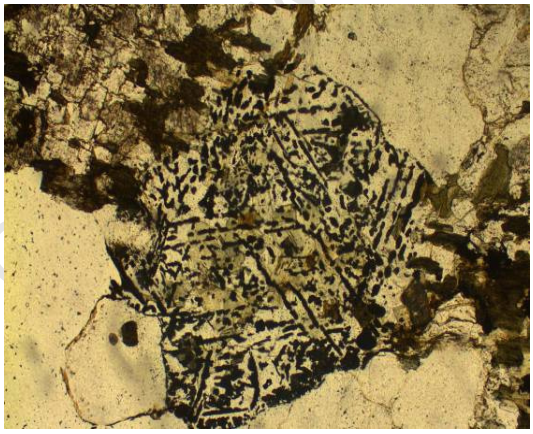

Fig. 27: BC 56 Infiltration of oxides, staining fractures in quartz. FOV is 2 mm wide.

3.3 Nebo Granite

The mineralogy of the coarse-grained (1 mm to 3 mm) Nebo Granite is essentially the same as the Rashoop Granophyre with less granophyric intergrowth (Figs. 28 & 29) between alkali feldspar and quartz. Quartz and alkali feldspar in the Nebo Granite exhibit disequilibrium features such as resorption embayments (Figs. 31, 32 & 33) with fluid alteration indicated by chloritisation and the presence of iron oxide staining in selected samples (Figs. 30, 32 & 33). While such features conclusively indicate the effects of alteration and disequilibrium, they are not pervasive within the Nebo Granite and are generally not observed in more than 20 % to 30 % of samples. Annealing of quartz grains and fluid inclusion trails accompanied by grain boundary suturing (Figs. 30 & 32) and sub-grain boundary formation are more prevalent than fluid alteration features. Biotite and hornblende form up to 30 % of some samples with a corresponding drop in visible free quartz but the majority of samples contain < 5 % hydrous minerals with biotite seen mostly as either an interstitial or alteration mineral.

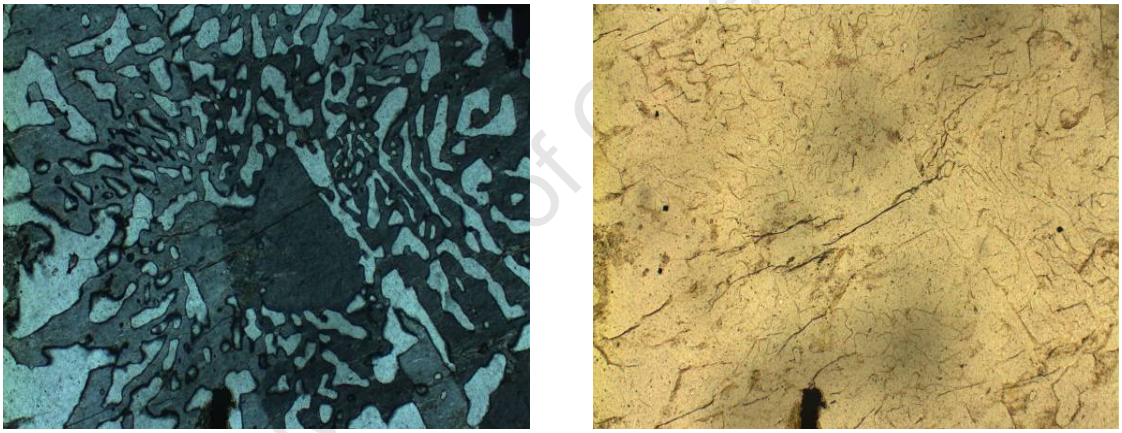

Figs. 28 & 29: BC 60 (Nebo Granite) showing Granophyric texture, visible in XPL and PPL. FOV is 4 mm wide.

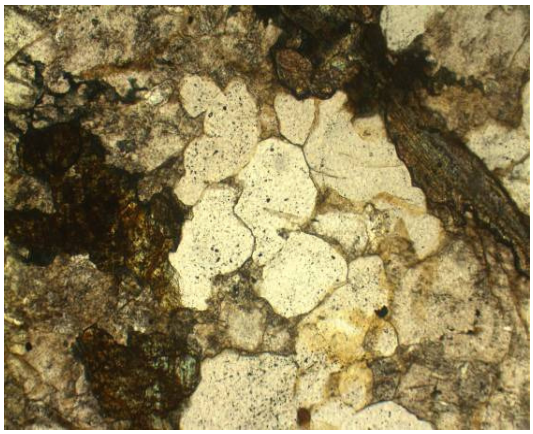

Fig. 30: BC 9 Sutured quartz grain boundaries and chloritisation after feldspar and biotite in Nebo Granite. FOV is 4 mm wide.

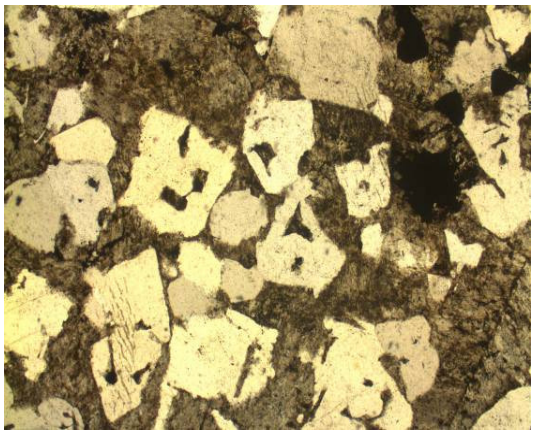

Fig. 31: BC 35 Embayed Nebo Granite quartz grains and oxide staining of perthite visible. FOV is 4 mm wide.

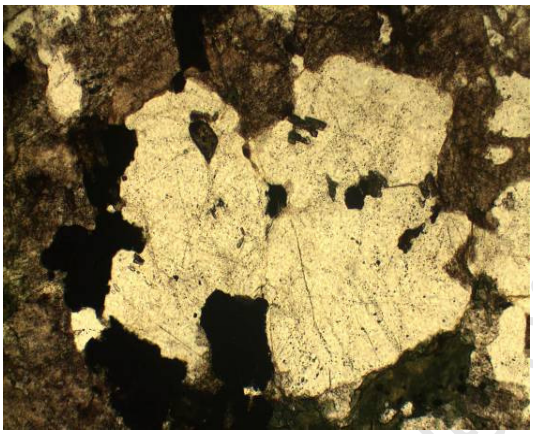

Figs. 32 & 33: BC 57 Quartz grains (centre) showing irregular grain boundaries and fluid inclusion trails surrounded by perthitic feldspar, chlorite and iron oxides (black minerals). FOV is 4 mm wide.

Petrographic study of Nebo Granite thin sections reveals a predominance of perthitic alkali feldspar and lesser quantities of free quartz with minor hydrous phases forming the bulk of the analysed samples; accessory minerals such as zircon, sphene, some calcite and iron oxide are also observed. Deformation and alteration features are observed in most samples but less so in the coarser - grained Rashoop Granophyre and Nebo Granite. No metamorphic minerals and lack of metamorphic textures indicate that metamorphism, if any, was confined to lower grades without significant amounts of fluid to form metamorphic minerals.

4 METHODOLOGY

The samples collected for this study encompass the Western, Northern and Eastern Lobes of the Bushveld Complex. Samples were collected from as many of the felsic units that outcrop within each lobe as possible. Samples were collected by Duane Fourie, Jarryd Finkelstein and Andre Fourie from areas identified by using the Council for Geoscience (1978) and Geological Survey of South Africa (1981) Geological maps of the region, and collected by driving and walking the area over a period of 10 days in March/April 2008. As many as 80 sample sites were initially identified but due to access constraints and lack of outcrop 60 samples were collected, of which 26 were from the Lebowa Granite Suite (Nebo Granite), 15 were from the Rashoop Granophyre Suite and 19 from the Rooiberg Felsite Group. Samples were taken using a 5 kg sledge hammer, with between 3-5 kg of sample collected from each site. Each site was marked using an E-trex GPS for accurate location. The samples were transported to UCT to be prepared for analysis with the aim of separating quartz, amphibole, biotite and zircon from the different felsic units to analyse for oxygen and hydrogen isotopes. Zircon separation, radiogenic isotope data extraction and trace element analyses were carried out by the scientists responsible at the Council for Geosciences in Pretoria, the radiogenic isotope laboratory at UCT and ICPMS laboratory at UCT respectively due to time constraints.

4.1 Mineral Separation

All Bushveld Complex felsic rock samples were crushed and sieved to < 600 µm at UCT in preparation for mineral separation. The samples were crushed using a 25 ton hydraulic crusher followed by a jaw crusher and then sieved to collect the relevant (< 600 µm) size fraction. Separation/picking of ~ 30 grains (depending on the analytical procedure and grain size) of quartz, amphibole, biotite and alkali feldspar from selected granite and granophyre samples proceeded. Mineral grains (except alkali feldspar) were not picked if they appeared altered or weathered. The felsite is too fine-grained to separate any minerals visually. Quartz, amphibole, biotite and alkali feldspar grains were washed in distilled water and then ethanol to remove any dust particles and dried overnight in an oven at 50°C. The clean grains from each sample that were being analysed using the conventional silicate and hydrogen lines (quartz, alkali feldspar, amphibole & biotite), were then ground to a powder in an agate pestle and mortar in preparation for analysis.

Zircon separation from the Nebo Granite, Rashoop Granophyre and Rooiberg Felsite samples was first attempted in geological sciences at UCT using sieved size fraction between 425 µm and 63 µm. The size fraction was washed in distilled water and placed in an ultrasonic bath for 15 min. to remove dust from the sample and dried in an oven at 60ºC overnight. The dry sample was put through a magnetic separator at 0.2 A to separate any highly magnetic minerals from the fraction. The sample was then poured into a separating funnel containing a heavy liquid (Fig. 34) (lithium heteropolytungstate) with a density of 2.85 g/cm^3 at 25ºC to separate the lighter minerals of quartz and feldspar from the heavy fraction. The heavy minerals were caught in filter paper below the separating funnel and washed with distilled water to wash off the heavy liquid and dried overnight in an oven at 60ºC. The heavy minerals were then put through the magnetic separator at 0.2 A, 0.4 A, 0.8 A, 1.2 A and 1.4 A respectively to separate zircon from the heavy mineral fractions.

Fig. 34: Separating funnel containing heavy liquid (lithium heteropolytungstate) used to separate the heavy mineral fraction which was then magnetically separated to extract zircon.

The zircons (Figs. 35 & 36) were studied using a reflected light microscope and any non-zircon mineral was removed with a steel tweezer. The average quantity of zirconium in the Bushveld rocks is ~ 400 ppm and many zircon grains were visible in thin section but all were less than 50 µm in diameter. The very small grain size makes working with the zircon samples a challenge and results in the necessity of analysing pooled samples of hundreds of grains by laser fluorination compared to the single grain analysis of the larger quartz grains. The small size and small quantity of zircon obtained from the samples from geological sciences at UCT prompted the sample fractions being sent to the Council for Geoscience laboratories in Pretoria for zircon extraction.

A representative subset of 12 samples (7 Nebo Granite, 3 Rashoop Granophyre & 2 Rooiberg Felsite) was selected for determining radiogenic Sr and Nd values. The selected samples were crushed and milled to a powder at UCT using a sieb mill. The whole rock powder was then sent for analysis at the AEON EarthLAB, Department of Geological Sciences, UCT.

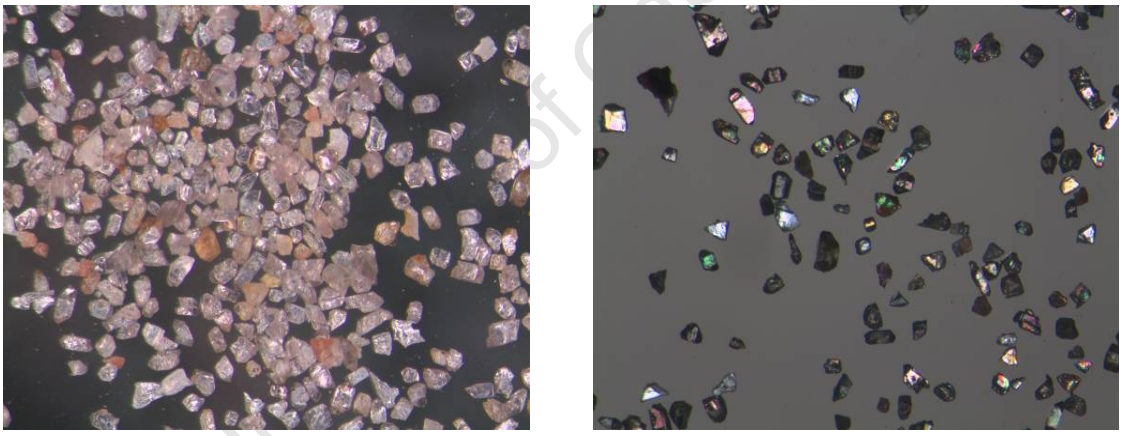

Figs. 35 & 36: Zircon fraction after magnetic separation of sample BC 6 (Nebo Granite), viewed under PPL and XPL. All zircon grains smaller than 50 µm in size.

4.2 Analytical Techniques

4.2.1 Conventional Silicate Line

Eighteen samples (8 quartz & 10 alkali feldspar samples) were analysed using the conventional silicate line analytical technique (Harris & Ashwal, 2002). Ten milligrams of quartz or alkali feldspar sample, dried overnight in an oven at 60ºC, were loaded into the nickel sample chambers on the conventional silicate line under the pressure of dry N_2 and degassed under vacuum at 200ºC for 2 h before the introduction of the ClF_3 reagent. The samples were then reacted at 550ºC for 4 hours with the liberated O_2 converted to CO_2 using a hot platinized carbon rod. At UCT, duplicate splits of the quartz standard (NBS28) are used to calibrate $\delta^{18}O$ values with each run of eight samples and used to convert the raw data to the SMOW scale using the $\delta^{18}O$ value of 9.6 % for NBS28 recommended by Coplen *et al*., (1983). The average difference between analyses of the NBS28 standard for this study was 0.16 ‰ (n = 61).

4.2.2 Laser Fluorination

A total of 39 quartz samples, 9 biotite samples, 19 amphibole samples and 8 zircon samples were analysed at UCT using the laser fluorination analytical process, described in Munteanu *et al*., (2010, Fig. 37). Ten additional quartz samples were selected from those already analysed to be used as duplicates, to ascertain any inherent heterogeneity of the quartz and any analytical error within the laser fluorination procedure. Greater variation in laser line $\delta^{18}O$ values is expected due to the nature of the analysis, with the laser line technique analysing 1 to 3 grains at a time compared to the fairly homogenised (typically ~ 10 crushed quartz grains) sample required for conventional silicate line analysis. Any impurities (inclusions or fragments) or $\delta^{18}O$ heterogeneity within quartz grains would therefore be greatly exaggerated and more easily alter the 'average' $\delta^{18}O$ value of the quartz grain using the laser line technique, reducing the precision of the technique.

The washed grains were weighed on a digital balance to ensure 2 to 3 mg (1 to 10 grains depending on the size) of each mineral was transferred into each highly polished chamber on the pure nickel sample holder in preparation for laser fluorination. Normally 10 samples and 2 standards were loaded onto a sample holder at any one time. The sample holder was loaded into the reaction chamber directly from an 110^{o}C oven to prevent absorption of any moisture. After the reaction chamber was evacuated, about 10 kPa of BrF_5 was expanded into the reaction chamber, left for about 30 seconds, and then removed cryogenically. A second batch of BrF_5 (~ 10 kPa) was then left in the reaction chamber overnight before extraction of oxygen from the samples was attempted. Each day, before extraction of any samples was attempted, a blank was run and the amount of gas measured using a pirani gauge. The blank pressure was typically < 1/200 of the sample volume.

Each sample was reacted in the presence of approximately 10 kPa BrF_5 and on completion of the reaction, the excess BrF_5 and the free Br formed by dissociation were frozen out into a cold finger and the remaining gases were allowed to pass through a KCl trap maintained at about 200^{o}C. The gasses were then expanded into the stainless steel double-U trap immersed in liquid nitrogen and the purified O_2 was collected onto a 5 Å molecular sieve contained in a glass storage bottle

In-house laser silicate standard (Monastery garnet hereafter referred to as MON. GT.) is derived from a single garnet megacryst from the Monastery Kimberlite pipe (Moore, 1986). Details of the composition of this standard are given by Harris *et al*., (2000). MON. GT. was recalibrated against the UWG-2 garnet standard of Valley *et al.,* (1995) using the current laser system, and has a revised $\delta^{18}O$ value of 5.38 ‰, assuming a $\delta^{18}O$ value of 5.80 ‰ for UWG-2. If this garnet formed in $\delta^{18}O$ equilibrium with mantle olivine of 5.2 ‰ (average value of Mattey *et al*., 1994) at 1150^{o}C, then it would have a $\delta^{18}O$ value of 5.46 ‰ (using the $\Delta_{garnet - olivine}$ equation of Rosenbaum & Mattey, 1995). In all cases, data were normalised so that the average MON. GT. $\delta^{18}O$ value was 5.38 ‰. The very small grain size of the zircons resulted in the loss of grains during laser fluorination as some of the grains 'exploded' out of the nickel sample holder (Fig. 38) to be lost or contaminate the adjacent samples of zircon. The average difference between MON. GT. $\delta^{17}O$ and $\delta^{18}O$ values of duplicates standards analysed for the period of this study was 0.19 ‰ ± 0.20 (n = 10).

Fig. 37: Laser Fluorination line at UCT that was used to collect the oxygen isotopes from the bulk of the Bushveld samples.

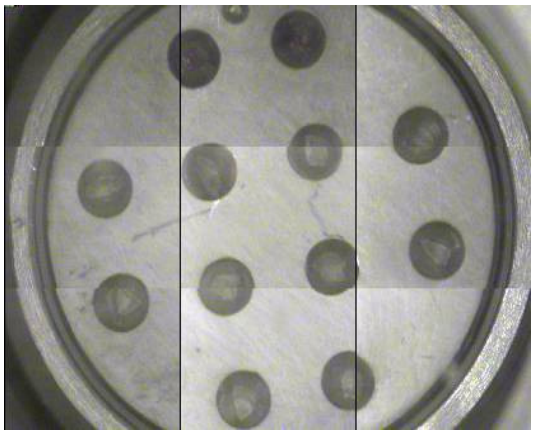

Fig. 38: The nickel sample holder containing 2-3 mg of sample in each hole ready for laser fluorination.

4.2.3 Hydrogen – Isotopes

The analyses of hydrogen isotopes was carried out only on the most abundant hydrous mineral phases, namely biotite and amphibole with whole rock δD values deemed not to be as useful as mineral data. Approximately100 mg of amphibole and 50 mg of biotite (due to the greater proportion of water within mica) was required for hydrogen isotope analyses; the powdered samples were weighed to the correct amounts on a digital balance and added to quartz tubes, followed by quartz grains and quartz wool to prevent loss of sample under vacuum. The tubes containing samples were left in an oven at ~ 110ºC overnight to remove any absorbed H_2O. Each tube was attached individually to the hydrogen line and the sample degassed under vacuum at 200ºC.

Hydrogen was extracted from the samples using the method of Venneman and O'Neil, (1993) with the sample being heated with an oxypropane torch until molten to liberate the hydrogen as water vapour. The water vapour was continuously frozen into liquid nitrogen during heating and then transferred into evacuated break seal tubes containing100 mg of 'Low–blank Indiana Zinc'. This reduced the hydrogen in the H_2O to elemental H_2 that could be isotopically analysed. Two internal water standards; CTMP3 ($\delta D = -7$ ‰ & $\delta^{18}O = -1.95$ ‰) and Evian ($\delta D = -70$ ‰ & $\delta^{18}O = -10.2$ ‰) were used to calibrate the data to the SMOW scale and for the period of this study (n = 2). The std. deviations of voltage measurements on the mass 2 collector for CTMP3 (n = 2) and Evian (n = 2) in this study were 0.04 V and 0.05 V (from an actual voltage measurement of 6 V) equivalent to 0.01 mg water.

4.2.4 Stable Isotope Mass Spectrometry

All samples were analysed off–line in dual–inlet mode, using a Finnigan Delta XP mass spectrometer at UCT, to measure the oxygen and hydrogen isotope ratios (all data reported in the familiar δ notation where $\delta^{18}O$ = (Rsample/Rstandard –1)*1000 and R = measured ratio i.e. $^{18}O/^{16}O$ or D/H). All samples analysed using laser fluorination O-isotope ratios were measured on O_2 gas. The isotope composition of the O_2 reference gas was determined by converting an aliquot of O_2 to CO_2 using the carbon convertor on the conventional extraction line. This value was assumed to remain constant and was used to calculate a raw δ value of each sample relative to the SMOW scale. Measured values of MON. GT. were used to normalise raw data and correct for drift in the reference gas, the average difference of MON. GT. standards during the period of this study was 0.24 ‰ for ^{17}O and 0.21 ‰ for ^{18}O. The inlet pressure of gas from each sample was measured at a constant volume. Samples where the measure and expected pressure did not correspond were discarded.

Samples analysed using the conventional silicate and hydrogen lines were measured on CO_2 and H_2 gas, respectively. For hydrogen, water contents were determined from the voltage measured on the mass 2 collector of the mass spectrometer using an identical sample inlet volume (Venneman and O'Neil, 1993) using a Finnigan Delta XP dual inlet gas–source mass spectrometer.

4.2.5 Rb – Sr Isotopes

Radiogenic Sr-isotope analysis (whole rock) was performed on twelve samples, including three Rooiberg Felsite samples and three Rashoop Granophyre samples. The Sr–isotope data was obtained using a Nu instruments NuPlasma HR mass spectrometer in the AEON EarthLAB, Department of Geological Sciences, at UCT, following the chemical separation procedure described by Miková & Denková, (2007). The Sr was analysed as 200 ppb 0.2% HNO_3 solutions using NIST SRM987 as a reference standard. The average value obtained for the NIST SRM987 standard was 0.710302 ± 0.000021 (2σ, n = 5) A value of 0.710225 was used to normalize the $^{87}Sr/^{86}Sr$ data. All Sr isotope data were corrected for Rb interference and instrumental mass fractionation using the exponential law and a $^{86}Sr/^{88}Sr$ value of 0.1194.

4.2.6 Sm – Nd Isotopes

Radiogenic Nd-isotope analysis (whole rock) was performed on twelve samples, including three Rooiberg Felsite samples and three Rashoop Granophyre samples. The Nd-isotope data was obtained using a Nu instruments NuPlasma HR mass spectrometer in the AEON EarthLAB, Department of Geological Sciences at UCT, following the chemical separation procedures described by Miková & Denková, (2007). Nd isotopes were analysed as 50 ppb 2 % HNO_3 solutions using the Nu Instruments DSN-100 desolvating nebuliser. The La Jolla Nd-isotope standard gave an average value of 0.512078 ± 0.000018 (2σ, n = 5) during the Nd-isotope runs. The Nd-isotope values were normalized to a value of 0.512115 (JNdi-1) after Tanaka *et al.*, (2000). All Nd-isotope data corrected for Sm and Ce interference as well as instrumental mass fractionation using the exponential law and a $^{146}Nd/^{144}Nd$ value of 0.7219.

4.2.7 Trace Element Concentrations

The concentrations of the radiogenic Rb/Sr and Sm/Nd element pairs was carried out using solution inductively coupled plasma mass spectrometry (ICP-MS) at UCT (updated from the procedure used by le Roex *et al.*, 2003). ICP-MS analyses were determined on a ThermoFisher Xseries2 ICP-MS using the following analytical procedure: 50 mg of 300 # sample powder were dissolved in a 4:1 HF/HNO_3 acid mixture in sealed Savilex1 beakers on a hotplate for 48 h, followed by evaporation to incipient dryness and two treatments of 2 ml concentrated HNO_3. The final dried product was then taken up in 5 % HNO_3 solution containing 10 ppb Re, Rh, In and Bi as internal standards. Standardization was against artificial multi-element standards. The average measurement errors for ^{85}Rb and ^{88}Sr were 0.26 % ± 0.16 (n = 12) and 1.96 % ± 2.40 (n = 12). The average measurement errors for ^{152}Sm and ^{144}Nd were 21.11 % ± 43.36 (n = 12) and 4.79 % ± 13.35 (n = 12). Two samples (BC 15 & BC 29) had very small amounts of ^{152}Sm (1.32 ppm & 2.05 ppm) resulting in two very large measurement errors; the average measurement error for ^{152}Sm drops to 3.70 % ± 2.73 (n = 10) with these values removed. Three samples (BC 7, BC 15 & BC 29) had large measurement error associated with small amounts of ^{144}Nd (35.6 ppm, 4.18 ppm & 11.79 ppm) with the average value becoming 0.42 ‰ ± 0.23 (n = 9) when they are removed.

4.3 Quartz Zonation

Significant variation in $\delta^{18}O$ values for some of the quartz samples from the Bushveld Complex felsic units (1 ‰ to 2 ‰) was observed after analysis prompting the investigation into the possibility of $\delta^{18}O$ heterogeneity within quartz grains. Samples from the Bushveld LIP felsic untis were visually inspected for the presence of large (≥ 3 mm diameter) quartz crystals to be broken up and rim and core fragments visually selected. Four samples were chosen and ~ 10 quartz crystals were picked from each sample. Four Nebo Granite samples were selected with quartz grains being too small in the Rashoop Granophyre and Rooiberg Felsite samples. The quartz grains/fragments were picked from the > 600 μm size fraction and stuck to transparent tape (Fig. 39) to keep the spatial position of the crystals. The relatively large quartz crystals were broken using a hammer and the resulting fragments (Fig. 40) inspected to identify core and rim fragments. The 'core' fragments were washed in distilled water and dried in an oven at 60°C. The rim fragments were cleaned using ethanol and ultrasonic vibration after selection as they still had vestiges of glue and other minerals on the outer edge of the fragments and dried overnight at 60ºC. The clean core and rim fragments were then sent to be analysed using laser fluorination.

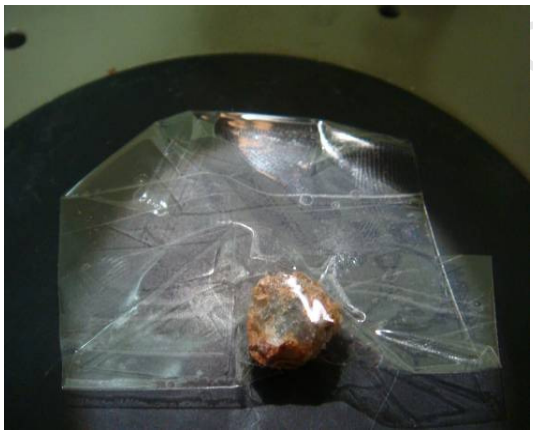

Fig. 39: Quartz grain covered in tape in preparation hammering. Quartz grain ~ 4 mm^2.

Fig. 40: Broken quartz grain from which rim for and core fragments were picked for oxygen isotope analysis.

5 RESULTS

Isotope data from the various analytical techniques used in this study are reported in tables 3 to 6 and supported by figs. 41 to 49 in the following chapter. Interpretation of this data is presented in the discussion chapter to follow.

5.1 Oxygen - Isotopes

5.1.1 Quartz

The $\delta^{18}O$ values for quartz (Table 3) analysed using the laser line averaged 7.95 ‰ ± 1.03 (1σ, n = 39) ranging from 4.8 ‰ to 10.8 ‰ (Fig. 41). The average $\delta^{18}O$ value for quartz analysed on the conventional silicate line was 8.49 ‰ ± 0.59 (1σ, n = 8). Quartz $\delta^{18}O$ values (laser line) of Nebo Granite from the northern and eastern lobes of the complex are compared to those of the Rashoop Granophyre from the same lobes, all falling within the same range, (Figs. 41 & 42) as well as the $\delta^{18}O$ values of each unit within each lobe. Ten duplicate samples were analysed using laser fluorination, producing an average value of 6.86 ‰ ± 1.23 (1σ, n = 10). Omitting the anomalously high value of 10.75 ‰ (one BC 12 sample value), the average $\delta^{18}O$ quartz value from all Bushveld Complex granophyre and granite analyses is 7.78 ‰ ± 1.05 (1σ, n = 56).

Table 3. $\delta^{18}O$ and δD Data for the Bushveld Complex Felsic Units

Sample	Oxygen $\delta^{18}O$								Hydrogen δD	
	Qtz. C/L	Qtz. L/L	Qtz. Duplicates L/L	K - Fsp.	Biotite	Amph.	Zircon A	Zircon B	Biotite	Amph.
BC1		6.9	5.5	9.1		4.5				-82
BC2		8.3			2.4	6.0				-99
BC3	8.4	8.5	7.9	7.4		3.9				-94
BC4		6.1								
BC5		6.5								
BC6		8.1				2.2	5.4	5.6		-83
BC7		8.2	8.2		3.6	4.4				-105
BC8		8.2			2.9	4.9				-103
BC9		8.2								
BC10	7.4	8.2	6.8	7.6						
BC11		7.7				3.9				
BC12	8.6	10.8	8.4			4.0				-121
BC13		8.4				4.4				-114
BC14		8.2				3.7				-94
BC15	8.4	7.9								
BC17		8.1								
BC18		8.7	6.7							
BC19		7.7								
BC21		9.3								
BC22	8.6	8.0			1.6	4.2				-82
BC24		7.8			1.9	3.5				
BC25		7.1	6.4	9.1			5.5	5.5		
BC28		8.4		9.7	2.1				-66	
BC30		8.3		7.7						
BC35		9.3					5.3	5.3		
BC36							5.3			
BC38		9.2	7.8	8.4		3.5				-77
BC39	8.8	7.8			1.2	2.7			-95	-133
BC40	8.4	7.7		10.2	9.1				-90	
BC41		8.0			1.7	4.9				-104
BC42		6.9						5.4		
BC44		6.8	6.2							
BC48		7.9				2.1				
BC52		8.1				2.8				
BC53						5.3				
BC54		8.6								
BC55	9.5	8.7		9.8						
BC56		9.1					2.5	4.0		
BC57		6.5		9.9		3.5				
BC58								7.3		
BC59		7.2	4.6							
BC60		4.8								

Qtz. – Quartz; Amph. – Amphibole (Hornblende); C/L – Conventional Silicate Line; L/L – Laser Fluorination Line; Zircon A – initial batch of zircon analyses; Zircon B – A second run of zircon separates; Quartz duplicates are re – analyses quartz by laser fluorination to check for any $\delta^{18}O$ heterogeneity within samples.

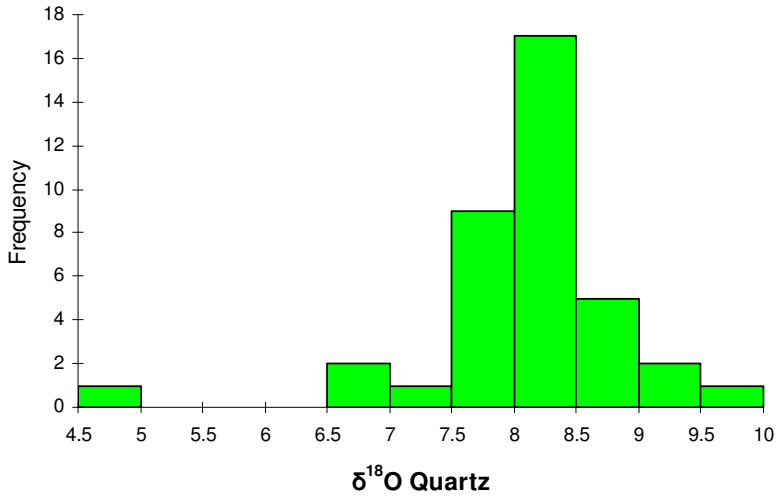

Fig. 41: Histogram showing the range in quartz $\delta^{18}O$ values for the Nebo Granite samples.

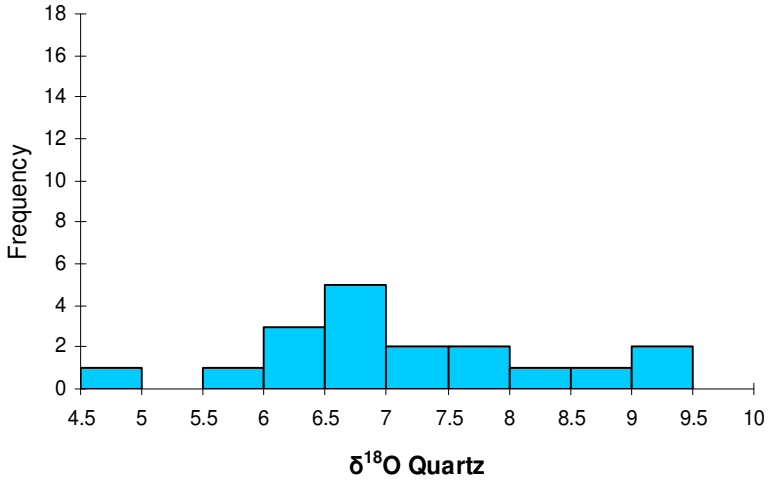

Fig. 42: Histogram showing the range in quartz $\delta^{18}O$ values for the Rashoop Granophyre samples.

The western lobe average $\delta^{18}O$ value is 7.91 ‰ ± 0.85 (1σ, n = 32) ranging from 6.1 ‰ to 9.3 ‰, the northern lobe $\delta^{18}O$ average is 7.87 ‰ ± 1.02 (1σ, n = 6) ranging from 6.4 ‰ to 9.3 ‰ and the eastern lobe average is 7.53 ‰ ± 1.37 (1σ, n = 18) with a range between 4.6 ‰ and 9.5 ‰ (Fig. 43). $\delta^{18}O$ values of the Nebo Granite from the western lobe averaged 8.15 ‰ ± 0.45 (1σ, n = 24) and the Rashoop Granophyre $\delta^{18}O$ values from the western lobe averaged 7.17 ‰ ± 1.29 (1σ, n = 8). The northern lobe Nebo Granite produced a $\delta^{18}O$ average value of 8.44 ‰ ± 0.62 (1σ, n = 4) while the Rashoop Granophyre samples from the northern lobe have an average value of 6.73 ‰ ± 0.46 (1σ, n = 2). The eastern lobe Nebo Granite and Rashoop Granophyres show $\delta^{18}O$ values averaging 7.86 ‰ ± 1.35 (1σ, n = 10) and 7.11 ‰ ± 1.36 (1σ, n = 8) respectively.

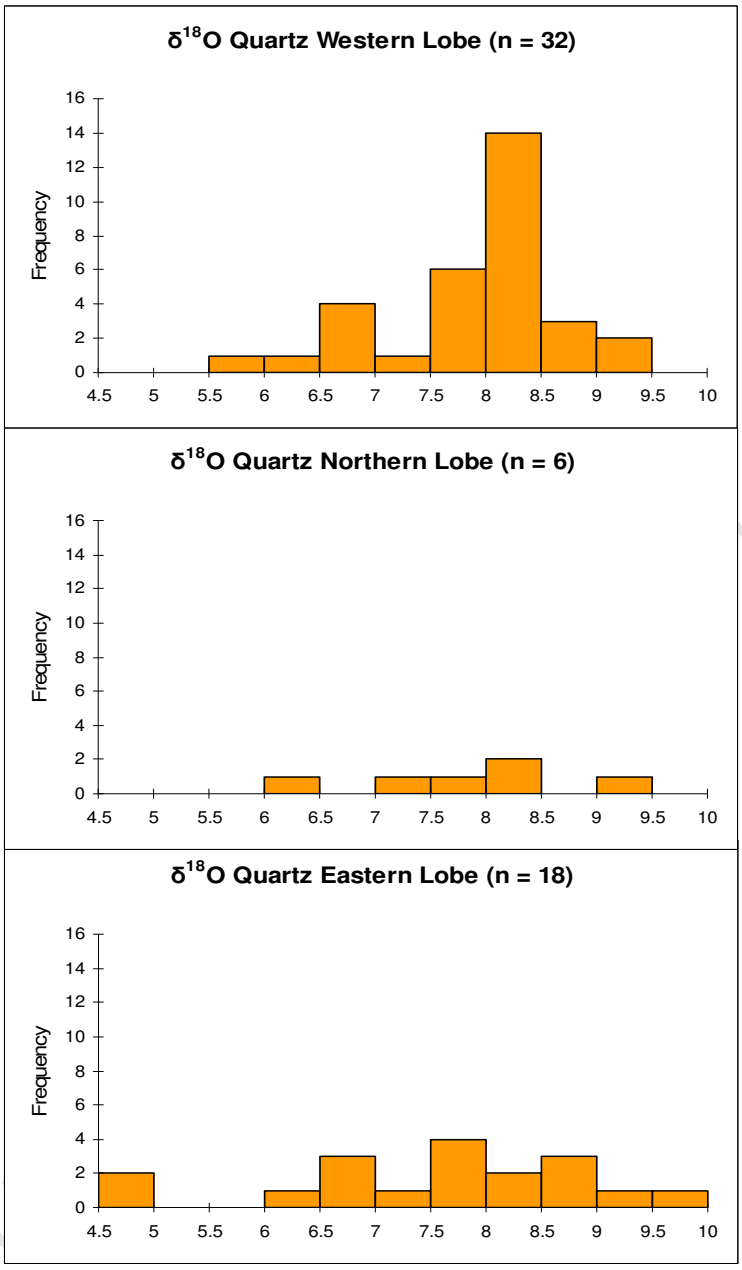

Fig. 43: Rashoop Granophyre and Nebo Granite $\delta^{18}O$ quartz values, comparing the western, northern and eastern lobes of the Bushveld Complex.

5.1.2 Quartz zoning

The $\delta^{18}O$ values for quartz rim and core (Table 4) from the 4 samples selected was 8.11 ‰ ± 0.33 (1σ, n = 10) of which a set of rim and core values were another quartz crystal sample BC15 Nebo Granite. The average value of the 'rim' fragments from the complex are 8.20 ‰ ± 0.33 (1σ, n = 5) and the average $\delta^{18}O$ values for the 'core' fragments are 8.02 ‰ ± 0.33 (1σ, n = 5). The $\delta^{18}O$ values for the quartz rim and core are very similar, with an average difference of 0.28 ‰, almost within error (± 0.1 ‰) for $\delta^{18}O$ measurement.

Table 4: $\delta^{18}O$ values for Bushveld quartz 'rim' and 'core' analyses.

Sample #	Rock Type	Rim	Core
BC15	Nebo Granite	7.8	8.0
		8.0	7.5
BC28	Nebo Granite	8.3	8.0
BC39	Nebo Granite	8.2	8.1
BC55	Nebo Granite	8.7	8.4

5.1.3 Zircon

Zircon separates were obtained from 11 samples, of which 6 had sufficient amounts of zircon to be analysed. Zircon separates were obtained from the Rooiberg Felsite sample BC 58, 3 Rashoop Granophyre samples and 2 Nebo Granite samples (Table 3). The average $\delta^{18}O$ value for zircon was 5.19 ‰ ± 1.17 (1σ, n = 11) ranging from 2.5 ‰ to 7.3 ‰. The average value rises to 5.41 ‰ ± 0.12 (1σ, n = 8) with the standard deviation falling dramatically due to the removal of the much lower sample values of 2.5 ‰ & 4.0 ‰ (BC 56 Rashoop Granophyre) and the highest zircon $\delta^{18}O$ value of 7.3 ‰ (BC 58 Rooiberg Felsite).

5.1.4 Biotite

The average $\delta^{18}O$ value of biotite for the entire complex (Table 3) being 2.94 ‰ ± 2.42 (1σ, n = 9) ranging from 1.2 ‰ to 9.1 ‰. The average western lobe biotite $\delta^{18}O$ value is 2.62 ‰ ± 0.83 (1σ, n = 4) ranging between 1.6 ‰ and 3.6 ‰, the average northern lobe value is 1.99 ‰ ± 0.10 (1σ, n = 2) ranging between 1.9 ‰ and 2.1 ‰ and the average eastern lobe value of 3.99 ‰ ± 4.43 (1σ, n = 3) ranging between 1.2 ‰ and 9.1 ‰.

5.1.5 Amphibole

The $\delta^{18}O$ values for amphibole (Table 3) in all samples ranges from 2.1 ‰ to 6.0 ‰ with an average value of 3.91 ‰ ± 1.01 (1σ, n = 19). An average $\delta^{18}O$ value, for the western lobe, of 4.12 ‰ ± 0.89 (1σ, n = 12) ranging from 2.2 ‰ to 6.0 ‰ was recorded. A $\delta^{18}O$ value of, 3.5 ‰ (n = 1) was determined for the northern lobe and an average $\delta^{18}O$ value of 3.56 ‰ ± 1.29 (1σ, n = 6) ranging from 2.1 ‰ to 5.3 ‰ was observed for the eastern lobe. The $\delta^{18}O$ values of amphiboles from the Nebo Granite and Rashoop Granophyre were also compared for each lobe where possible. The average amphibole $\delta^{18}O$ values for the western lobe Nebo Granites and Rashoop Granophyres were found to be 4.11 ‰ ± 0.97 (1σ, n = 10) ranging from 2.2 ‰ to 6.0 ‰ and 4.18 ‰ ± 0.43 (1σ, n = 2) ranging from 3.9 ‰ to 4.5 ‰. The northern lobe did not have a sufficient number of amphibole $\delta^{18}O$ analyses to compare to other lobes. The average eastern lobe Nebo Granite $\delta^{18}O$ value is 3.72 ‰ ± 1.12 (1σ, n = 3) ranging from 2.7 ‰ to 4.9 ‰, with the Rashoop Granophyre average value being 3.40 ‰ ± 1.68 (1σ, n = 3) ranging between 2.1 ‰ and 5.3 ‰.

5.1.6 Feldspar

The average $\delta^{18}O$ value of the feldspar was 8.64 ‰ ± 1.03 (1σ, n = 10) ranging from 7.4 ‰ to 10.2 ‰ (Table. 3). The average $\delta^{18}O$ value for the western lobe was 8.10 ‰ ± 0.76 (1σ, n = 4), the average northern lobe $\delta^{18}O$ value was 8.85 ‰ ± 1.01 (1σ, n = 3) and the eastern lobe $\delta^{18}O$ value averaged 9.92‰ ± 0.2 (1σ, n = 3). The $\delta^{18}O$ values of all alkali feldspar and quartz samples (Fig. 44) show a Δqtz-fsp of 0.90 ‰ which is consistent with equilibrium at magmatic temperatures but a Δqtz-fsp of 2.02 ‰ between 6 samples is not consistent with equilibrium at magmatic temperatures. The 6 sample values that do not show $\delta^{18}O$ equilibrium at magmatic temperatures are labelled, representing an increase in alkali feldspar $\delta^{18}O$ values relative to the $\delta^{18}O$ values of quartz.

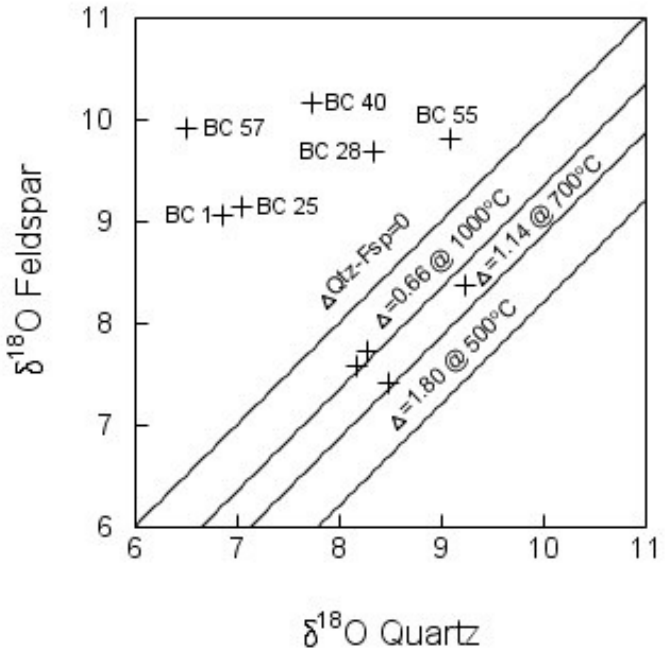

Fig. 44: Plot of $\delta^{18}O$ of Feldspar vs. $\delta^{18}O$ of quartz. The fractionation factor between qtz–fsp used in this graph from Clayton *et al*., (1989) assuming an average composition of An_{13} (Δquartz–albite & Δquartz–orthoclase is the same.) for the Bushveld feldspar (Marlow, 1976).

5.1.7 δ – δ Plots

The $\delta^{18}O$ values of amphibole (hornblende), zircon and biotite from the Bushveld Complex felsic units were plotted against the $\delta^{18}O$ values of quartz (Fig. 45) from the same sample to determine the degree of internal oxygen isotope equilibrium. The diagonal isotherm lines drawn on the graph array represent the typical per mille differences in $\delta^{18}O$ values between the specific mineral pairs at specific temperatures and are generally determined by laboratory experiments and known $\delta^{18}O$ ranges. $\delta^{18}O$ values falling outside these boundaries generally represent $\delta^{18}O$ disequilibrium between minerals, produced by a number of processes, including alteration and metamorphism.

All three graphs exhibit greater $\delta^{18}O$ variation in one mineral compared to the other, suggesting that the $\delta^{18}O$ values for some minerals preserve magmatic $\delta^{18}O$ values better than others. Looking at the graph array this trend would be (in order of descending robustness) zircon $\delta^{18}O$ > quartz $\delta^{18}O$ > amphibole $\delta^{18}O$ > biotite $\delta^{18}O$. The majority of the $\delta^{18}O$ values for zircon vs. quartz (Fig. 45) show isotopic equilibrium for magmatic temperatures to a temperature of 500ºC. Due to the higher closure temperature for oxygen diffusion in zircon, quartz continues to exchange $\delta^{18}O$ after $\delta^{18}O$ exchange has ceased in zircon while in equilibrium, but two samples are in disequilibrium (BC 56 Rashoop Granophyre, the solid black circle is the duplicate split) with variable zircon $\delta^{18}O$ values while quartz $\delta^{18}O$ values remain constant. The $\delta^{18}O$ biotite vs. $\delta^{18}O$ quartz plot shows $\delta^{18}O$ values ranging between 1.2 ‰ and 9.1 ‰ with Δqtz-bt > 4.56 ‰ in all but one sample (BC 40 with Δqtz-bt < 0) at all temperatures down to 550º C (Fig. 45) falling outside of typical equilibrium $\delta^{18}O$ values at magmatic temperatures. The $\delta^{18}O$ values of biotite are more variable than the $\delta^{18}O$ quartz values which remain relatively constant. The amphibole vs. quartz graph indicates that approximately 50 % of the samples have Δamph-qtz consistant with equilibrium at magmatic temperatures, while the remaining half of the samples are not in $\delta^{18}O$ equilibrium with quartz at magmatic temperatures.

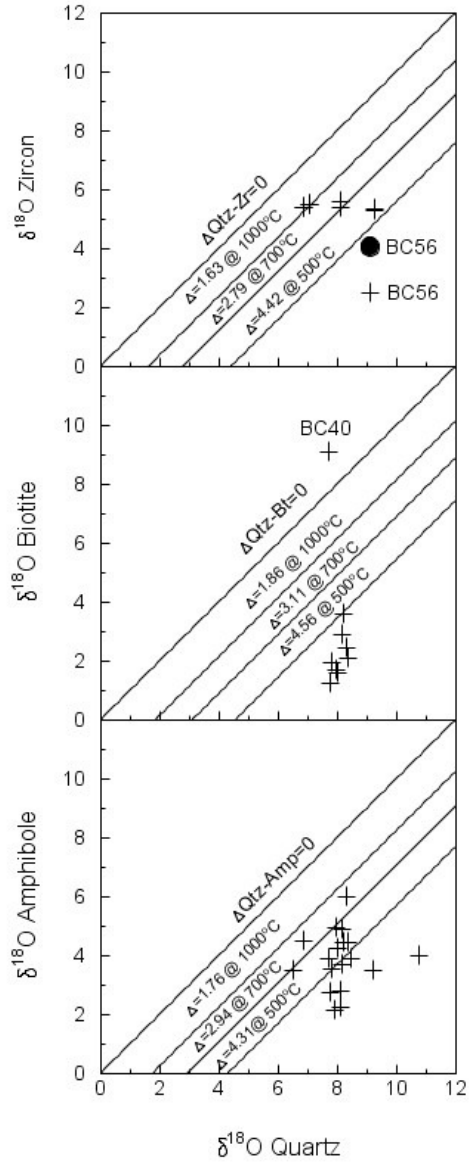

Fig. 45: δ – δ plot showing the $\delta^{18}O$ quartz vs. $\delta^{18}O$ zircon (including a duplicate of sample BC56, filled circle.), biotite & amphibole. Δqtz-zr used in this study from Valley *et al*., (2003). Δqtz-bt. & Δqtz-hbl used in this study from Zheng, (1993b).

5.2 Hydrogen Isotopes

The large range in δD values and their high degree of overlap within rocks of different origin make the definitive identification of source waters difficult. The large standard deviation (~ 15 ‰) for δD in samples is observed for the Bushveld Complex felsic units but is within typical standard deviation values for δD (~ 20 ‰) (Hoefs, 1987; Sharp, 2007).The hydrogen isotope data from the Bushveld Complex felsic units is important as it provides a good indication of fluid interaction within the complex and assists in defining the fluid source.

The average δD value for the Bushveld Complex Felsic units is –96 ‰ ± 17 (1σ, n = 16) ranging from –133 ‰ to –66 ‰ (Table 3). Removing outlying sample values for BC 28 (Nebo Granite biotite) and BC 39 (Nebo Granite amphibole) the average value becomes –96 ‰ ± 13 (1σ, n = 14).

The change in δD with wt% water (Fig. 46) is important as water contents > 2 wt% for amphibole and > 3.5 wt% for biotite indicates that alteration has occurred. On the other hand, low wt% water and δD values may provide evidence for possible magma degassing (Taylor, 1986). Constraining the type/s and amount of fluids using isotopic hydrogen values provides a way of assessing post crystallisation alteration.

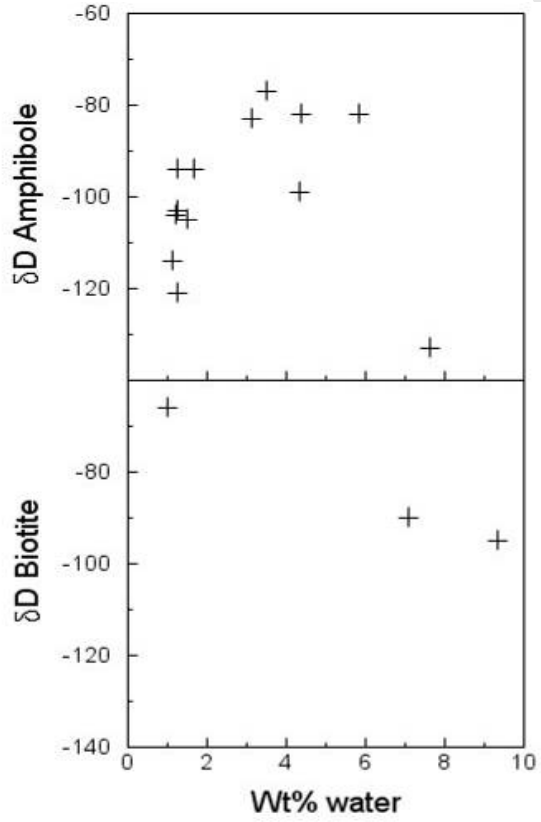

Fig. 46: Plot of δD vs. wt% water for amphibole and biotite.

The average δD value for the amphibole samples from the Bushveld felsic units is –99 ‰ ± 17 (1σ, n = 13) and ranges between –133 ‰ and –77 ‰ (Table 3). Amphibole grains could not be picked in sufficient quantity from the northern lobe samples so no comparison to this lobe can be made. The western lobe has an average δD value for amphibole of –96 ‰ ± 14 (1σ, n = 11) ranging from –121 ‰ to –77 ‰ while the eastern lobe has an average δD value of –119 ‰ ± 21 (1σ, n = 2) ranging from –133 ‰ to –104. The average biotite δD value for the Bushveld Complex felsic units is –84 ‰ ± 16 (1σ, n = 3) ranging between –95 ‰ and –66 ‰ (Table. 3). The western lobe has a δD value of –66 ‰ (n = 1) and the average δD value for the eastern lobe is –93 ‰ ± 4 (1σ, n = 2).

5.2.1 Wt% Water

The amphibole samples have average wt% water values of 2.94 % ± 2.11 (1σ, n = 13) with a range of 1.1 % to 7.6 % (Table. 3). Alteration (chloritisation) of the amphibole grains has occurred as indicated by the > 2 wt% water values measured for some amphiboles. The average value for wt% water from the western lobe is 2.59 % ± 1.72 (1σ, n = 10) and the eastern lobe average wt% water is 4.13 % ± 3.24 (1σ, n = 3). The average wt% water for the biotite samples is 5.83 % ± 4.32 % (1σ, n = 3) ranging from 1.0 in the northern lobe to 9.4 % in the eastern lobe (Table. 3). The high wt% water values (> 3.5) for 2 of the 3 biotite samples reveals post crystallisation alteration to chlorite. Ignoring the lowest value, the average becomes 8.23 % ± 1.61 % (1σ, n = 2) for the eastern lobe.

5.3 Radiogenic Isotopes

5.3.1 Sr – Isotopes

Strontium data is reported in table 5, including initial $^{87}Sr/^{86}Sr$ values and ε_{Sr} values calculated for an age of 2058.9 Ma. The extremely negative and positive ε_{Sr} values measured for the Bushveld Complex felsic units are not useful in determining magmatic values as they indicate open source processes. The average initial $^{87}Sr/^{86}Sr$ value for the Bushveld Complex felsic units is 0.26 ± 0.88 (n = 12) ranging from –2.0 to 0.08. The western, northern and eastern lobes have average initial $^{87}Sr/^{86}Sr$ values of 0.66 ± 0.06 (n = 4), 0.11 ± 0.84 (n = 4) and 0.02 ± 1.34 (n = 4) respectively. The average initial $^{87}Sr/^{86}Sr$ value for the Nebo Granite samples is 0.12 ± 1.06 (n = 6) with the Rashoop Granophyre and Rooiberg Felsite having average initial $^{87}Sr/^{86}Sr$ values of 0.75 ± 0.10 (n = 3) and 0.06 ± 0.96 (n = 3) respectively. Omitting the two outlying negative initial Sr values (BC 26 Rooiberg Felsite & BC 40 Nebo Granite) the average initial Sr value becomes 0.62 ± 0.21 (n = 10). The average ε_{Sr} value for the Bushveld Complex felsic units is –6272 ± 12503 (n = 12), ranging from –38420 to 2264. Omitting the three lowest values (BC 26, BC 30 & BC 40) and the highest value (BC 25), the average becomes –660 ± 894, still many times less and more than typical unaltered Sr ranges. All the Bushveld Complex felsic units Sr data points, except 3 values (Fig. 47), are reasonably closely grouped but do not form an isochron, with a best fit line corresponding to an age of ~ 1102 Ma (including outliers) and ~ 2365 Ma (excluding 3 outliers), which is removed from the 2059 Ma reference line depicted on the graph.

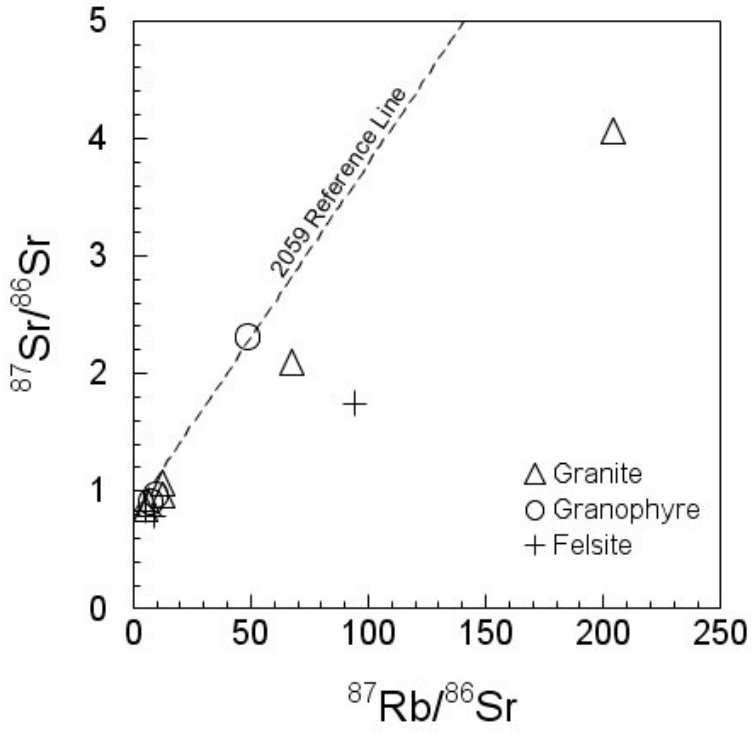

Fig. 47: Isochron diagram for the Rb/Sr system. The best fit isochron calculated for the Bushveld felsic units data, corresponds to an age of ~ 1102 Ma. The dashed line represents a reference line for an age of 2059 Ma with arbitrary initial ratio.

Table 5: Rb/Sr - isotope data for the Bushveld Complex Felsic units including measurement error

Sample	Rock Type	Rb (ppm) ± error	Sr (ppm) ± error	($^{87}Rb/^{86}Sr$) ± error	($^{87}Sr/^{86}Sr)_m$ ± error	Sr_O ± error	ε_{Sr}
BC1 WR	Granophyre	140.00 ± 0.24	43.86 ± 0.67	9.46 ± 0.16	0.965514 ± 0.000028	0.684791 ± 0.004814	-246
BC7 WR	Granite	168.40 ± 0.40	76.71 ± 0.13	6.46 ± 0.03	0.884807 ± 0.000020	0.693263 ± 0.000804	-126
BC15 WR	Granite	79.46 ± 0.52	18.36 ± 0.16	12.81 ± 0.20	0.953746 ± 0.000021	0.573594 ± 0.005903	-1830
BC19 WR	Granite	182.60 ± 0.46	42.85 ± 0.48	12.74 ± 0.17	1.059518 ± 0.000023	0.681454 ± 0.005172	-294
BC25 WR	Granophyre	251.40 ± 0.59	17.28 ± 0.34	48.59 ± 1.07	2.301876 ± 0.000069	0.860406 ± 0.031761	2255
BC26 WR	Felsite	297.30 ± 0.32	10.07 ± 0.54	94.21 ± 5.11	1.743896 ± 0.000061	-1.051057 ± 0.151604	-24970
BC29 WR	Felsite	69.28 ± 0.34	23.44 ± 0.56	8.62 ± 0.25	0.793056 ± 0.000032	0.537251 ± 0.007384	-2348
BC30 WR	Granite	374.40 ± 0.36	18.14 ± 0.13	67.65 ± 0.55	2.085498 ± 0.000033	0.078455 ± 0.016230	-8883
BC40 WR	Granite	333.10 ± 0.56	6.293 ± 0.51	204.13 ± 16.95	4.058230 ± 0.000072	-1.997996 ± 0.502898	-38458
BC48 WR	Granophyre	179.50 ± 0.54	71.3 ± 0.32	7.42 ± 0.06	0.909195 ± 0.000022	0.689016 ± 0.001662	-186
BC50 WR	Felsite	174.20 ± 0.40	104.3 ± 0.55	4.89 ± 0.04	0.835607 ± 0.000015	0.690557 ± 0.001106	-164
BC60 WR	Granite	183.00 ± 0.26	106.9 ± 0.33	5.02 ± 0.02	0.843948 ± 0.000019	0.695163 ± 0.000681	-99

($^{87}Sr/^{86}Sr)_M$ = Measured Sr values for this study; Sr_O = Original Sr values calculated from measured values for an age of 2058.9. $^{87}Rb/^{86}Sr$, Sr_O and ε_{Sr} values were calculated using the equations of Harmer and Eglington, (1990). ^{87}Rb values are calculated. Error reported as the difference between the highest and lowest calculated $^{87}Rb/^{86}Sr$, Sr_O and ε_{Sr} values. Sr Sample BC 24 (Granite) has the only positive ε_{Sr} value compared to the other samples which show moderate to extremely negative ε_{Sr} values.

5.3.2 Nd – Isotopes

The average initial $^{143}Nd/^{144}Nd$ value for the Bushveld Complex felsic units is 0.509490 (n = 12) ranging from to 0.506110 to 0.510498 (Table 6). Average initial values of 0.508826 (n = 4), 0.509915 (n = 4) and 0.509728 (n = 4) were found for the western, northern and eastern lobe respectively. The Nebo Granite whole rock samples have an average initial Nd value of 0.509127 (n = 6) while the average Rashoop Granophyre initial Nd value is 0.509726 (n = 3) and the Rooiberg Felsite units have an average initial Nd value of 0.509979 (n = 3). All the Bushveld Complex felsic units Nd data points, except 2 values (Figs. 48a & 48b), are reasonably closely grouped but do not form an isochron, with a best fit line corresponding to an age of ~ 1569 Ma, which is removed from the 2059 Ma reference line depicted on the graph. The ε_{Nd} data is mostly negative, having an average value of –8.26 ± 21.35 (n = 12), ranging between –74.90 and 11.16 (Table 5), dropping to a value of –3.98 ± 1.30 (n = 10) when the highest (BC 29 Rooiberg Felsite) and lowest (BC 15 Nebo Granite) values omitted. The error calculated for the age uncertainty (Figs. 49a & 49b) is very small compared to the measurement error and does not increase the total error, so is not included in the following tables. The total error associated with the Nd values is on average 67 % ranging from 13 % to 194 %. The very large error associated with three samples (BC 7, BC 15 & BC 29) are due to small amounts of Sm and Nd in the sample and large measurement errors associated with them, propagated through the calculations for Nd_o and ε_{Nd} this causes a very large total error. Omitting these 3 large total error values the average total error becomes 38 %. Taking this value of 38 % average total error into account the average ε_{Nd} value (–2.78 ± 1.64) is less negative but remains negative indicating the negative ε_{Nd} values are not a product of error.

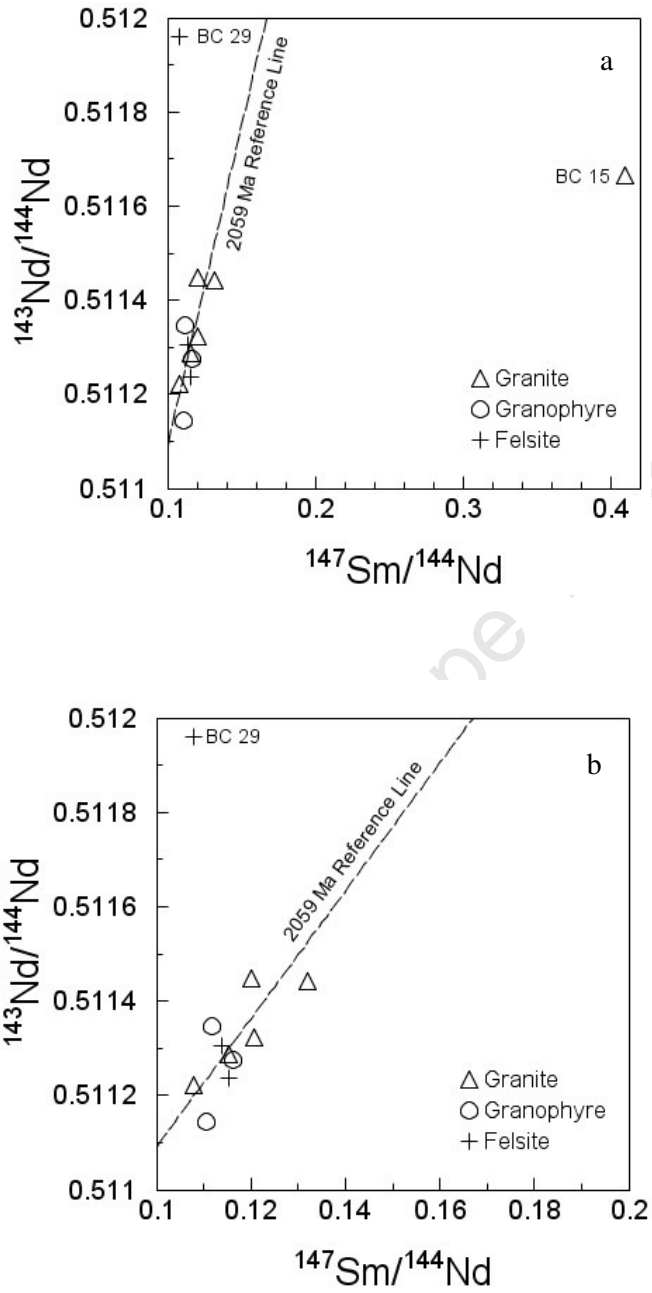

Fig. 48: a) Isochron diagram for the Sm/Nd system including the outlying value of BC 15. b) Isochron diagram for the Sm/Nd system excluding the outlying value of BC 15. The best fit isochron calculated for the Bushveld felsic units data (omitting the 2 outliers), corresponds to an age of ~ 1569 Ma. The dashed line represents a reference line for an age of 2059 Ma with arbitrary initial ratio.

Table 6: Sm/Nd - isotope data for the Bushveld Complex Felsic units showing measurement and age determination error

Sample	Rock Type	Sm (ppm) ± error	Nd (ppm) ± error	$^{147}Sm/^{144}Nd$ ± error	$(^{143}Nd/^{144}Nd)_M$ ± error	Nd_O ± error	ε^t_{Nd} ± measurement error
BC1 WR	Granophyre	13.78 ± 0.51	75.39 ± 0.05	0.1105 ± 0.0042	0.511144 ± 0.000016	0.509647 ± 0.000072	-5.56 ± 1.42
BC7 WR	Granite	6.76 ± 0.61	35.60 ± 1.21	0.1152 ± 0.0143	0.511287 ± 0.000009	0.509725 ± 0.000202	-4.02 ± 3.97
BC15 WR	Granite	1.32 ± 1.89	4.18 ± 1.97	0.4099 ± 0.4658	0.511665 ± 0.000021	0.506110 ± 0.006332	-74.95 ± 124.23
BC19 WR	Granite	15.27 ± 0.39	76.92 ± 0.43	0.1200 ± 0.0037	0.511448 ± 0.000006	0.509822 ± 0.000057	-2.12 ± 1.11
BC25 WR	Granophyre	15.40 ± 0.64	83.28 ± 0.40	0.1118 ± 0.0052	0.511346 ± 0.000007	0.509832 ± 0.000077	-1.93 ± 1.52
BC26 WR	Felsite	23.94 ± 0.25	125.60 ± 0.26	0.1152 ± 0.0014	0.511237 ± 0.000013	0.509676 ± 0.000032	-4.99 ± 0.63
BC29 WR	Felsite	2.06 ± 1.51	11.79 ± 0.38	0.1080 ± 0.0808	0.511961 ± 0.000010	0.510498 ± 0.001105	11.15 ± 21.69
BC30 WR	Granite	16.83 ± 0.19	77.03 ± 0.41	0.1321 ± 0.0022	0.511442 ± 0.000009	0.509652 ± 0.000039	-5.45 ± 0.76
BC40 WR	Granite	10.15 ± 0.12	56.95 ± 0.48	0.1077 ± 0.0022	0.511223 ± 0.000008	0.509763 ± 0.000037	-3.28 ± 0.73
BC48 WR	Granophyre	12.88 ± 0.57	67.02 ± 0.17	0.1162 ± 0.0055	0.511275 ± 0.000010	0.509701 ± 0.000084	-4.50 ± 1.65
BC50 WR	Felsite	14.61 ± 1.09	77.69 ± 0.26	0.1137 ± 0.0089	0.511304 ± 0.000008	0.509763 ± 0.000128	-3.28 ± 2.52
BC60 WR	Granite	13.39 ± 0.30	67.09 ± 0.37	0.1206 ± 0.0034	0.511322 ± 0.000011	0.509687 ± 0.000057	-4.77 ± 1.11

($^{143}Nd/^{144}Nd)_M$ = Measured Nd values for this study; Nd_O = Original Nd values calculated from measured values for an age of 2058.9 Ma. Sample BC 15 (Granite) has a very negative ε^t_{Nd} value due to the very small quantity of Sm and Nd present in the sample, samples BC 7 & BC 29 also show large ε^t_{Nd} error due to a very large measurement uncertainty which is propagated through the calculations. $^{147}Sm/^{144}Nd$, Nd_O and ε^t_{Nd} values were calculated using the equations of Harmer and Eglington, (1990). Error reported as the difference between the highest and lowest calculated $^{147}Sm/^{144}Nd$, Nd_O and ε^t_{Nd} values. The error calculated for the age uncertainty (2058.9 ± 0.8, Buick *et al.* 2001) is small compared to the measurement error so does not affect the total error seen in the last column.

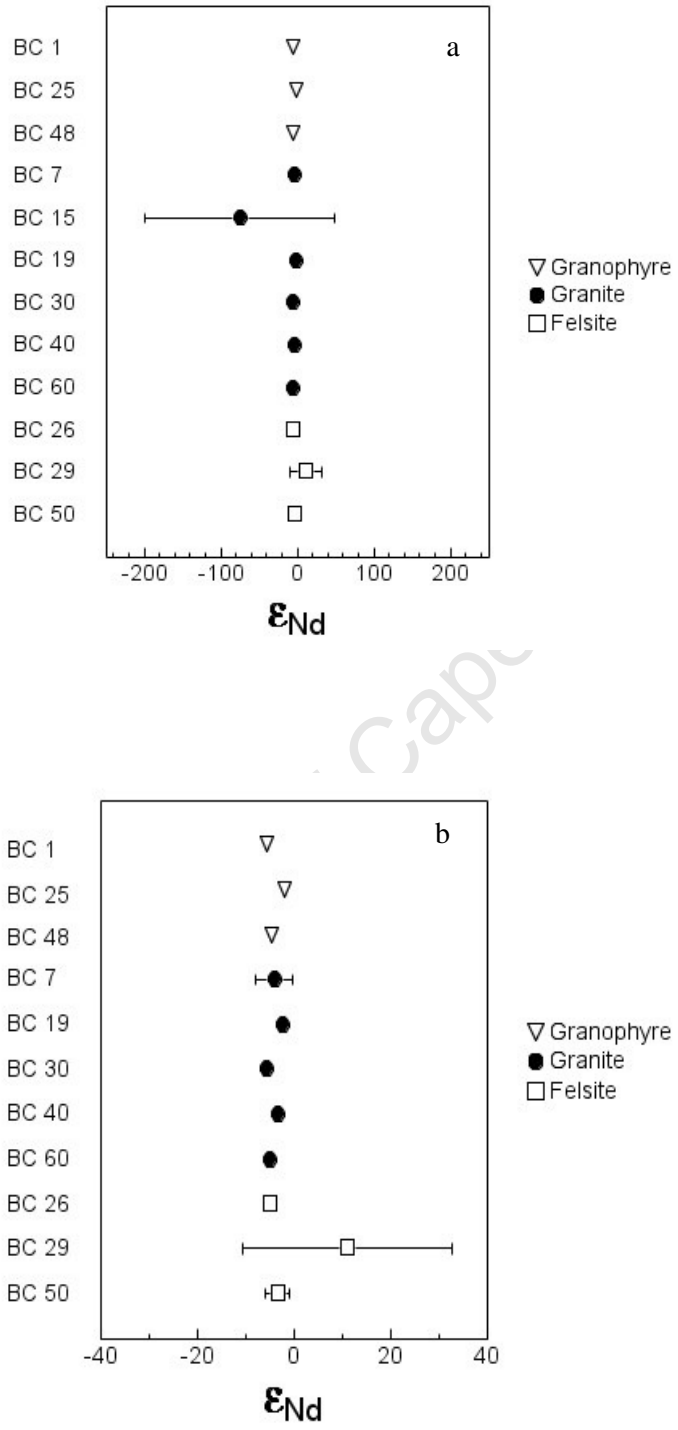

Fig. 49: a) Plot of the ε_{Nd} values and their associated measurement and age error for each sample from those analysed for Nd from the Bushveld Complex, including the large error for BC 15. b) Plot of the ε_{Nd} values and their associated measurement and age error for each sample from those analysed for Nd from the Bushveld Complex, excluding the large error for BC 15. Sample BC 7, BC 15 & BC 29 shows larger error due to the very small amounts of Sm and or Nd in the sample that produce large measurement and re – calculation errors.

6 DISCUSSION

In the following section the data produced from the various analytical methods will be discussed. The focus of this section will be to consider the effects of alteration on the Bushveld Complex felsic units so as to determine the $\delta^{18}O$ values for the original magma and the type of fluid involved during alteration. The data will then be compared to various similar units including the RLS and A-Type granites from around the world before discussing the petrogenesis of the Bushveld Complex felsic units.

6.1 Affects of Alteration

The effect of ~ 2 Ga of geological processes at work on the Bushveld LIP cannot be ignored and the large scale alteration of most of the Rooiberg Felsite is evidence of post emplacement fluid interaction and metamorphism. The interaction of the Bushveld LIP with hydrothermal fluids through time could help explain a small number of anomalous $\delta^{18}O$ values (< 5 ‰ & > 10 ‰) and the resultant large range in $\delta^{18}O$ values (4.6 ‰ to 9.5 ‰) observed for the Bushveld Complex felsic units. The range in Δqtz-fsp, Δqtz-hbl and Δqtz-bt values in the Bushveld Complex felsic units is an argument for hydrothermal alteration during a metamorphic episode during its history.

Change in isotopic $\delta^{18}O$ values in minerals can be achieved by:

1. Alteration due to hydrothermal fluid circulation
2. Overgrowth of magmatic 'core' quartz and zircon with metamorphic rims.
3. Metamorphism, involving fluid interaction in an open system, causing resetting of the isotopic signature at high temperatures, i.e. temperatures above the closure temperature for oxygen diffusion for that mineral.

There does not seem to be any significant quartz $\delta^{18}O$ variation from granite and granophyre samples across the complex with all the lobes sampled having as much variation within the lobe as between the lobes. The lack of significant $\delta^{18}O$ variation between quartz rim and core samples is definitive evidence for the lack of change in $\delta^{18}O$ values in quartz in the Bushveld Complex felsic units as any alteration ought to have altered the $\delta^{18}O$ value of the rim of the quartz grain compared to the $\delta^{18}O$ value of the core. The similarity in $\delta^{18}O$ values for the majority of samples from the complex supports the notion that the Bushveld Complex felsic units were emplaced as part of a single large intrusion and not as five disconnected lobes. The emplacement of smaller discontinous sheets might be expected to show more isotopic heterogeneity than a single larger connected body, as more magma is in contact with the host rocks and assimilation/alteration is more likely.

The similarity in isotopic $\delta^{18}O$ values within the majority of the Rashoop Granophyre and Lebowa Granite Suite samples within the Bushveld Complex and within each lobe suggests a fairly homogenous magma being intruded into upper crustal material with smaller (< 1 ‰) differences occurring as a result of localised post emplacement hydrothermal alteration or assimilation of isotopically dissimilar units. The quartz/zircon $\delta - \delta$ plot (Fig. 45) shows that quartz and zircon were in isotopic equilibrium at magmatic temperatures indicating that the $\delta^{18}O$ values of quartz from the Bushveld Complex felsic units has not been affected by hydrothermal alteration since crystallisation.

The average $\delta^{18}O$ value of amphibole (hornblende) is 3.91 ‰ ± 1.01 (1σ, n = 19). The range in $\delta^{18}O$ values is fairly restricted but some large variations were noted. The average values of the western and eastern lobes are very similar in value and spread, while the northern lobe appears to be slightly raised with respect to $\delta^{18}O$ values. Nebo Granite hornblende $\delta^{18}O$ values were very similar to that of the granophyre within the eastern lobe with both units showing up to a 2 ‰ spread from the mean. The amphibole/quartz $\delta - \delta$ plot (Fig. 45) indicating that roughly half of the 19 amphibole samples are not in isotopic equilibrium with quartz at magmatic temperatures. Post crystallisation interaction of amphibole with a fluid at temperatures which were not sufficiently high enough to affect the quartz $\delta^{18}O$ values (seen as a trend to lower $\delta^{18}O$ values for amphibole while the quartz $\delta^{18}O$ values remain relatively constant on the amphibole/quartz $\delta - \delta$ plot) are thought to be responsible for the sometimes large variation between amphibole samples and the disequilibrium $\delta^{18}O$ values between amphibole and quartz.

Biotite from the Bushveld Complex felsic units was observed in thin section mainly as an accessory mineral, interstitial in most samples is interpreted to indicate late formation/growth after crystallisation. The biotite/quartz δ – δ plot (Fig. 45) reveals that biotite from the Bushveld Complex felsic units is not in isotopic equilibrium with quartz. The large range in biotite $\delta^{18}O$ values, seen on the biotite/quartz δ – δ plot (~ 1 ‰ to ~ 4 ‰ compared to a fairly constant quartz $\delta^{18}O$ value ~ 8 ‰), support a multi-phase formation/growth and/or alteration hypothesis. The large spread in $\delta^{18}O$ values and deviation from the mean value, seen in all lobes, also provides evidence for alteration from the Bushveld Complex felsic units.

The susceptibility of feldspar to alteration is often used to identify post magmatic alteration in rocks as it shows disequilibrium with more resistant minerals such as quartz (e.g. Taylor, 1968; Criss *et al*., 1986). The quartz/feldspar δ – δ plot (Fig. 44) indicates average Δqtz-fsp = 0.90 ‰ with 6 samples having Δqtz-fsp < 0 ‰ with 4 samples showing equilibrium $\delta^{18}O$ values between quartz and alkali feldspar at magmatic temperatures and cooling (~0.60 ‰ < Δqtz-fsp < ~ 1.14 ‰). The average alkali feldspar $\delta^{18}O$ value shows equilibrium with that of quartz for the Bushveld Complex felsic unit samples but six of the ten samples do show higher, disequilibrium alkali feldspar $\delta^{18}O$ values, consistent with oxygen exchange at low temperatures as opposed to the trend of lowering alkali feldspar $\delta^{18}O$ values if high temperature alteration had taken place.

6.2 Isotope Composition of Fluid Involved in Alteration

The average $\delta^{18}O$ ranges for fluids in equilibrium with igneous and metamorphic rocks are 7 ‰ to 10 ‰ and 2 ‰ to 20 ‰ respectively. Typical $\delta^{18}O$ values for meteoric waters range from –20 ‰ to 0 ‰ (Sharp, 2007). δD values for a typical fluid in equilibrium with igneous rocks have a range of values from ~ –50 ‰ to –80 ‰ while those in equilibrium with metamorphic rocks range from –70 ‰ to 0 ‰ (Sharp, 2007). The lowest δD values are associated with organic waters (Sharp, 2007) i.e. waters affected by organic processes and range from –90 ‰ to –160 ‰. The designated fields as presented by Sharp (2007) (Fig. 50) are not absolute and a degree of overlap and uncertainty is inherent in isotopic δD values. Typical Δmineral–water values for $\delta^{18}O$ and δD are shown in tables 7 and 8 with biotite and amphibole having very similar values over the entire temperature range. Minerals from the Bushveld granite and granophyre units have $\delta^{18}O$ and δD values ranging from 1.6 ‰ to 10.8 ‰ and δD values ranging from –66 ‰ to –133 ‰. Water in equilibrium with minerals in the Bushveld granite and granophyre units would have $\delta^{18}O$ values of 0.9 ‰ to 7.1 ‰ (quartz at 450ºC to 850ºC), 5.3 ‰ to 8.4 ‰ (zircon from 450ºC to 850ºC) and 5.8 ‰ to 10.4 ‰ (Alkali feldspar from 450ºC to 850ºC). The hydrous phases have $\delta^{18}O$ values of 3.9 ‰ to 11.4 ‰ (biotite) and 4.0 ‰ to 8.1 ‰ (amphibole) over the temperature range of 450ºC to 850ºC. δD values would range from –22 ‰ to –68 ‰ for biotite and –39 ‰ to –95 ‰ for amphibole over the temperature range of 450ºC to 850ºC. Only three samples would have maximum $\delta^{18}O$ values above 10 ‰ and four samples δD values less negative than –50 ‰ suggesting that the fluid responsible for the alteration was of magmatic origin.

Table 7.

$\delta^{18}O$					
Temperature (K)	**Quartz - H_2O (‰)**	**Zircon - H_2O (‰)**	**Alkali Feldspar - H_2O (‰)**	**Biotite - H_2O (‰)**	**Hornblende - H_2O (‰)**
722	3.70	-2.77	1.60	-2.31	-1.96
822	2.54	-2.90	0.77	-2.51	-2.23
922	1.81	-2.85	0.28	-2.52	-2.28
1022	1.33	-2.72	0.00	-2.43	-2.22
1122	1.02	-2.54	-0.16	-2.30	-2.11

Equations used for calculation of quartz–H_2O factors, Alkali feldspar–H_2O factors and zircon–H_2O factors from Zheng, (1993a). Equations used for calculation of biotite–H_2O factors and horneblende–H_2O factors from Zheng, (1993b). Temperature values in Kelvin (K) representing a Celsius temperature range of 450ºC to 850ºC.

Table 8.

δD		
Temperature (K)	**Biotite – H_2O (‰)**	**Hornblende – H_2O (‰)**
722	-44	-38
822	-34	-28
922	-28	-20
1022	-23	-15
1122	-20	-11

Equations used for calculation of biotite–H_2O factors and horneblende–H_2O factors from Suzuoki & Epstein, (1976). Temperature values in Kelvin (K) representing a Celsius temperature range of 450°C to 850°C.

Some Bushveld Complex felsic unit samples show δD values (Fig. 50) that are slightly more negative than those typically associated with magmatic processes, with δD values less than –120 ‰ (BC 12 & BC 39). Taking the standard deviation and inherent heterogeneity into account, these Bushveld Complex felsic unit sample values still plot outside the typical fields for hydrothermal fluids.

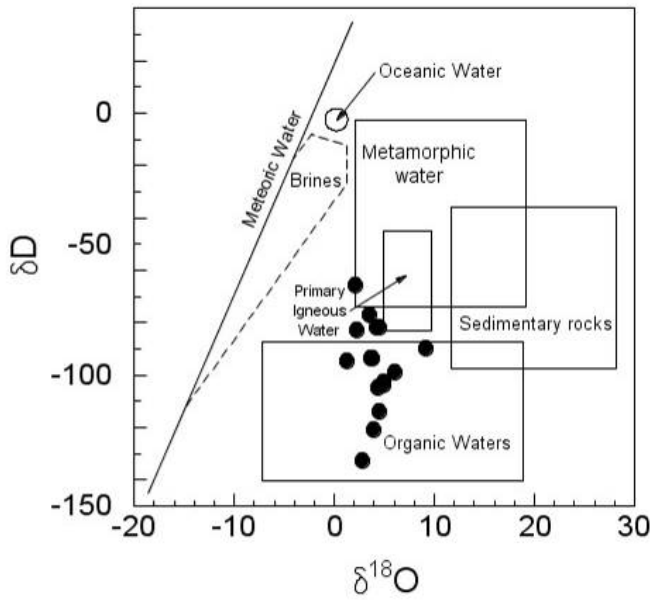

Fig. 50: Graph showing the $\delta^{18}O$ vs. δD values of amphibole and biotite from the Bushveld Complex felsic units, plotting into the more negative δD and slightly lower $\delta^{18}O$ fields for 'organic water. All fields shown representing general trends after Sharp, (2007).

A lowering of δD values, corresponding to a decrease in wt % water is observed (Fig. 51) for the hydrous phases within Bushveld Complex felsic rocks. A trend to more negative δD values with decreasing water content is typically due to loss of ^2H relative to H during magma dagassing before and during emplacement. Loss of water through degassing of the magma during ascent and or during emplacement could account for the more negative δD values seen in some samples that may have been less affected by later fluid alteration.

Further evidence to support the magmatic/igneous nature of the fluid is the $\delta^{18}O$ data for alkali feldspar from the qtz/fsp $\delta - \delta$ plot that indicates continued oxygen isotope exchange at lower temperatures to higher $\delta^{18}O$ values (~ 9 ‰), consistent with post emplacement alteration with magmatic fluids.

Biotite and some amphibole samples also show a post emplacement alteration trend in the lowering of δD values with an increase in water content (Fig. 51). The majority of samples have less than 2 wt% water but some samples show wt% water values of ~ 5 %, 7 % and 9 % (2 biotite & 6 amphibole samples), indicating varying degrees of chloritisation of these phases after the initial magmatic degassing. While it is unlikely that organic water had any significant effect on the Bushveld Complex felsic units δD values, the relatively low percentages of water and relatively impermeable nature of the igneous body may have resulted in localised influx of meteoric waters that lowered some sample δD values.

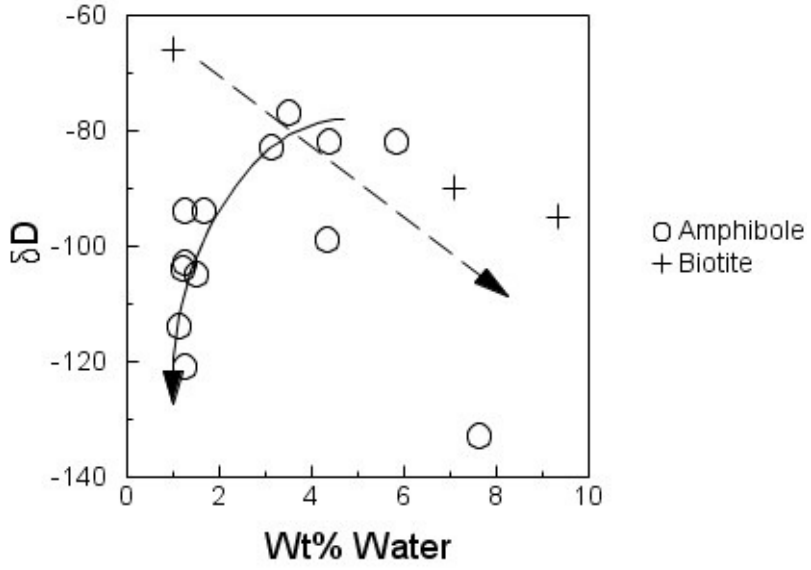

Fig. 51: Plot of δD vs. Wt% water for amphibole and biotite samples from the granites and granophyres of the Bushveld Complex, with half the samples showing an alteration trend (dashed line) and the remaining half showing a degassing trend (curve).

6.3 Original Magma $\delta^{18}O$

The $\delta^{18}O$ values for zircon from the Bushveld Complex granite and granophyre units are consistent with average mantle zircon values of 5.3 ‰ ± 0.3 (Valley *et al.,* 1998). Thin sections of the Bushveld Complex felsic unit samples show no evidence for metamorphism but deformation features in quartz and alteration of amphibole are apparent in the majority of samples. The lack of evidence to support anything but the lowest levels of metamorphism (Fig. 45) eliminates the possibility of the zircon isotope signature being that of a metamorphic episode in the past, reset from near magmatic values. The use of zircon as an indicator for magmatic $\delta^{18}O$ values is due to the relatively recent development of the laser fluorination analytical method (Valley *et al*., 1995; Spicuzza *et al*., 1998) and where applicable, assuming zircon inheritance is not a factor, is preferable to quartz, as zircon is less prone to alteration and isotopic resetting. The disequilibrium between alkali feldspar, amphibole, biotite and quartz $\delta^{18}O$ values at crystallisation temperatures and cooling indicate that the most reliable original $\delta^{18}O$ values are most likely those from zircon and to a lesser degree quartz. The relationship between the $\delta^{18}O$ signatures of quartz and zircon may give further information of $\delta^{18}O$ changes at higher temperatures and potentially resolve smaller scale magmatic processes. Oxygen isotope data from quartz and zircon have been successfully employed in areas such as the Yellowstone Volcanic Province (Bindeman & Valley, 2001) and the A-Type granites of Eastern China (Wei *et al*., 2000, 2008) to determine more accurately the isotope composition of original magmas.

A consistent $\delta^{18}O$ value is found for the Bushveld Complex granite and granophyre zircons from each of the three lobes studied. Samples were situated up to 120 km apart, indicating a homogenous source and the apparent lack of post emplacement hydrothermal alteration. The Bushveld granite and granophyre zircon also indicate crystallisation temperatures of the felsic magmas at ~ 840ºC (using the equation $1000\ln\alpha_{qtz\text{-}zrc} = (2.33\pm0.24)\times10_6/T_2$ .from Bindeman *et al*., 2009) which reflect high temperature melts, in agreement with the anhydrous character of the Bushveld granite and granophyre units. The amount of ^{18}O in quartz is significantly higher than the other minerals with which it is in equilibrium and Δqtz-magma typically ranges between 1 ‰ to 2 ‰ (Zheng. 1993a) suggesting that the $\delta^{18}O$ values of the Bushveld felsic units parental magma $\delta^{18}O$ values ranged between 5.8 ‰ and 6.8 ‰.

When the fractionation factor is taken into account between zircon and magma, 0.6 ‰ to 1.0 ‰ (Chiba *et al*., 1989; King *et al*., 2001; Valley *et al*., 2003), the average $\delta^{18}O$ value, for the parental magma, ranges between 5.8 ‰ and 6.2 ‰. Although a relatively small number of zircon analyses were possible, the consistent equilibrium Δqtz-zr values and large number of quartz $\delta^{18}O$ analysed in this study suggest that these 'low' $\delta^{18}O$ values are characteristic of the Bushveld Complex felsic rocks. The zircon grains observed in this study from Nebo Granite and Rashoop Granophyre samples were all of igneous/magmatic origin using the classifications of Pupin (1980) thus ruling out the possibility of inherited zircons from other sources.

Magmatic differentiation of a portion of the RLS magma to form the more felsic units of the Bushveld Complex could be a possible formation process but poses a number of challenges. The differentiation from a mafic magma to a felsic magma would involve large amounts of fractional crystallisation, producing a $\delta^{18}O$ increase of between 0.6 ‰ to 0.8 ‰ (e.g. Sharp, 2007). This trend would result in an increased ratio of ^{18}O to ^{16}O in the more felsic minerals/melt (~ 0.5 ‰ to 1.0 ‰) compared to that of the mafic/ultramafic RLS which has a $\delta^{18}O$ value of 7.1 ‰ (Harris *et al*. 2005). This trend is not observed in the felsic units with the lower than RLS $\delta^{18}O$ values for quartz and zircon suggesting that fractional crystallisation was not the dominant mechanism affecting the $\delta^{18}O$ values of the felsic units.

The original magma/s $\delta^{18}O$ values (Table 9) would have been in the range of ~ 5.8 ‰ to 6.8 ‰, depending on the fractionation factor used for zircon and quartz $\delta^{18}O$ data. As the $\delta^{18}O$ data for the other minerals analysed in this study (amphibole, biotite and alkali feldspar) show evidence of $\delta^{18}O$ disequilibrium at magmatic temperatures they will not be used to constrain the Bushveld Complex felsic units parental magma $\delta^{18}O$ values. The quartz zircon δ – δ plot (Fig. 45) indicates that quartz and zircon were in isotopic equilibrium during crystallisation, constraining the average quartz $\delta^{18}O$ values for the original magma to values ~ 6 ‰.

Table 9.

Mineral	**$\delta^{18}O$ range and average for minerals (‰)**	**Δmineral – magma (‰)**		**$\delta^{18}O$ Magma (‰)**
Quartz	4.6 – 9.5 **(7.78; n = 56)**	ΔQtz – Magma	(1 – 2)	5.78 – 6.78
Zircon	5.3 – 5.6 **(5.41; n = 8)**	ΔZrc – Magma	(– 0.4 to – 0.8)	5.8 – 6.2

Summary of the $\delta^{18}O$ values for quartz and zircon analysed during this study as well as typical Δmineral–magma values based on Δqtz–magma = 1.5 (Zheng, 1993a). Also shown are the likely $\delta^{18}O$ value ranges for the felsic units parent magma.

6.4 Comparison with Related Regions and Units

The comparison of the Bushveld Complex felsic units isotope characteristics with that of the RLS is useful to establish the relationship between the mafic and felsic units of the Bushveld Complex. Comparison of isotope characteristics with other regions and units, of known petrogenesis, around the world (Figs. 52, 53 & 54) are needed to determine a likely petrogenetic model for the Bushveld Complex as a whole. The Bushveld Complex Felsic units will be compared to the following:

1. RLS
2. Other felsic rocks in LIP's (Parana/Etendeka, Karoo and Chon Aike LIPs).
3. Other A-Type granites (A-Type granites from Brazil, Namibia, Eastern China and Turkey).

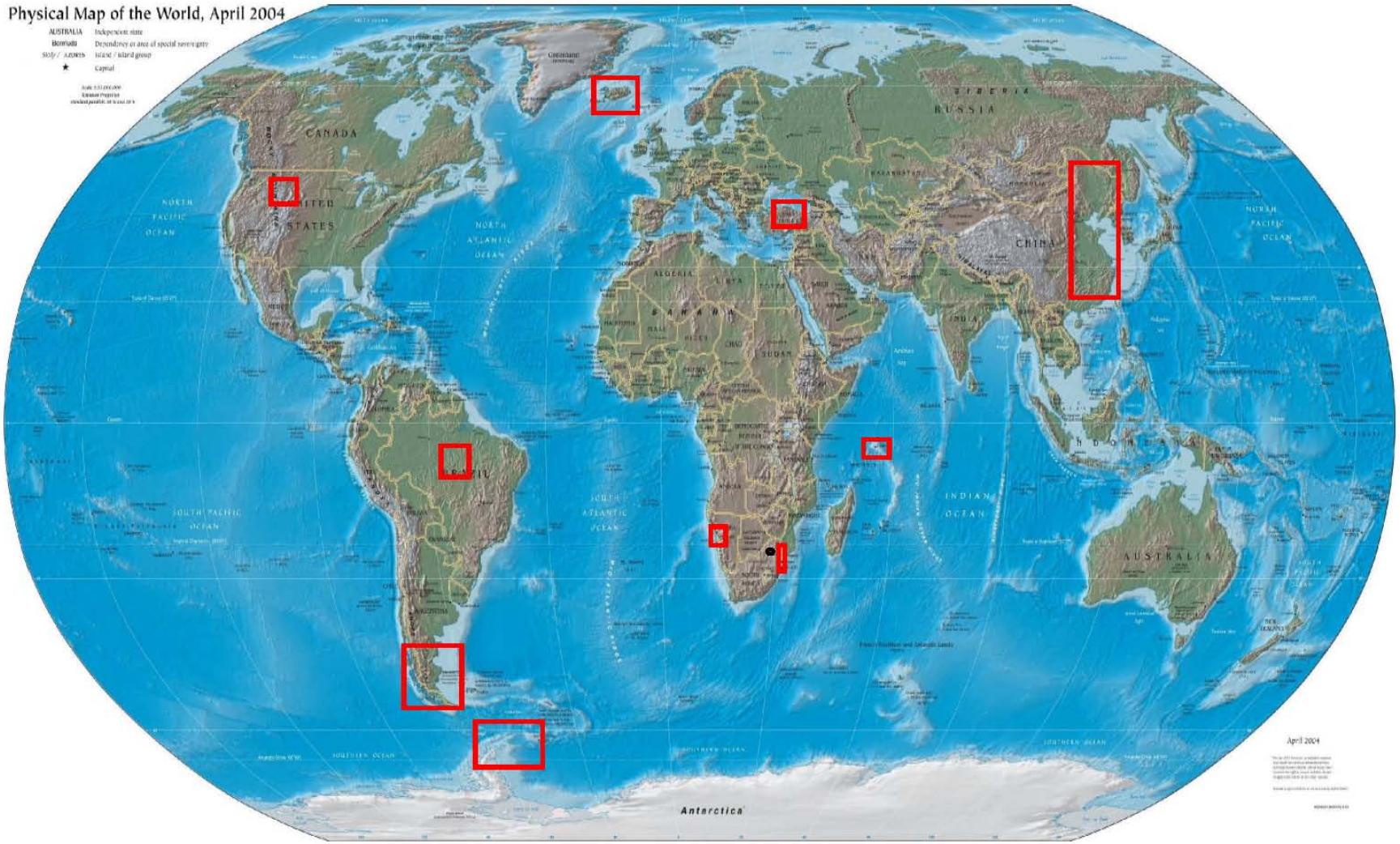

Fig. 52: Map of the Earth showing the Bushveld Complex and all other regions used for comparison in this study.

Source Map: http://www.printableworldmap.org/printable_world_map_wiki1.htm

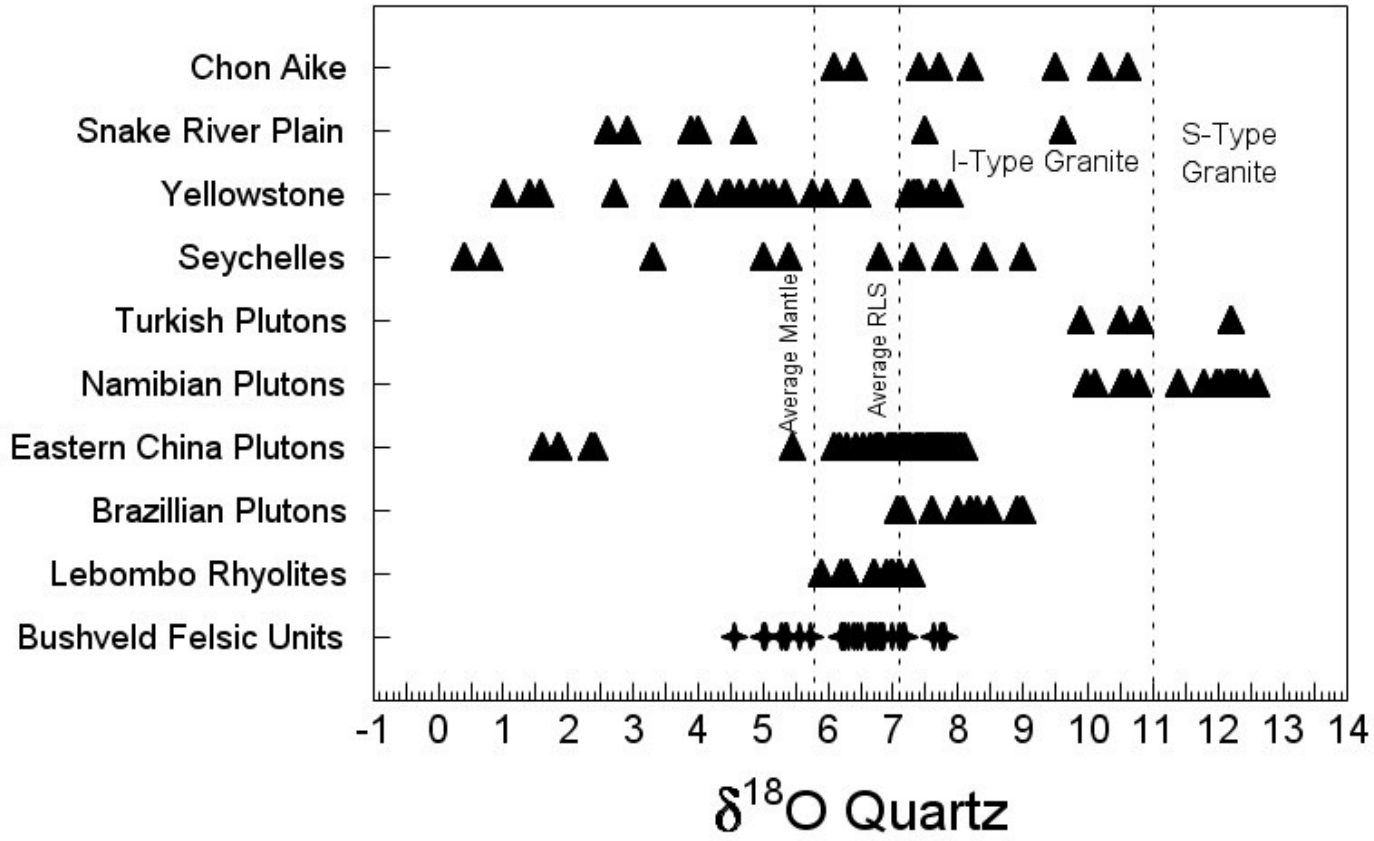

Fig. 53: Plot showing the ranges in $\delta^{18}O$ values for the Bushveld Complex felsic units (referring to the granite and granophyre units only) vs. other LIPs (Lebombo Rhyolites from Karoo LIP), A–Type granites and low $\delta^{18}O$ magmas.

Sources: Brazillian Pluton data from Dall'Agnol *et al*., (2005) and references therein, Lebombo Rhyolites data from Miller & Harris, (2007), Chon Aike Rhyolite data from Riley *et al*., (2001), Namibian A–Type Granite data from Harris, (1995) &Trumbull *et al*., (2004), A–Type Granite data from Turkey from Boztuğ *et al*., (2007), South – Eastern China $\delta^{18}O$ data from Wei *et al*., (2008), Seychelles $\delta^{18}O$ data from Harris & Ashwal, (2002), Yellowstone $\delta^{18}O$ data from Bindeman & Valley, (2001) & Snake River Plain $\delta^{18}O$ data from Boroughs *et al*., (2005).

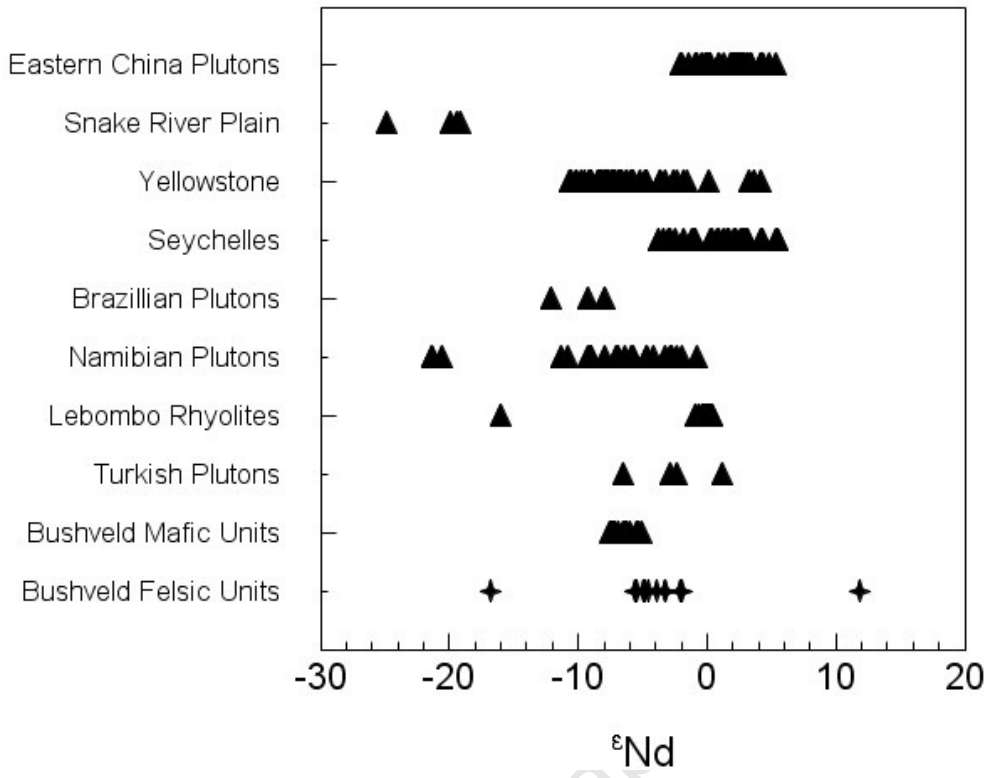

Fig. 54: Plot showing the range in ε_{Nd} values for the Bushveld Complex Felsic units compared to the RLS, A–Type Granites, felsic rocks from other LIPs and low $\delta^{18}O$ provinces.

Sources: Brazillian Pluton data from Dall'Agnol *et al*., (2005) and references therein, Lebombo Rhyolites data from Miller & Harris, (2007), Chon Aike Rhyolite data from Riley *et al*., (2001), Namibian A–Type Granite data from Harris, (1995) &Trumbull *et al*., (2004), A–Type Granite data from Turkey from Boztuğ *et al*., (2007), South – Eastern China ε_{Nd} data from Wei *et al*., (2008), Seychelles ε_{Nd} data from Harris & Ashwal, (2002), Yellowstone ε_{Nd} data from Bindeman & Valley, (2001), Snake River Plain ε_{Nd} data from Kellogg *et al*. (1994) and RLS ε_{Nd} from Maier *et al*. (2000).

6.4.1 Comparison with the RLS

The average δD and $\delta^{18}O$ values of the RLS magmas are –71 ‰ and 7.1 ‰ respectively compared to those of the Bushveld 'Granitic' magmas (granite & granitic will be refering to Bushveld granite & granophyre units in this section) that have δD and $\delta^{18}O$ values of ~ –85 ‰ and 6.2 ‰ respectively. The RLS has higher average $\delta^{18}O$ values (~ 1 ‰) (Fig. 55) than the Bushveld Granite units. The higher overall $\delta^{18}O$ values for the RLS are thought to be due to large amounts of crustal contamination of low to mid-crustal granitoids resulting in the elevated $\delta^{18}O$ values (Maier *et al*., 2000) but this process could not have been responsible for the lower $\delta^{18}O$ values of the granite units.

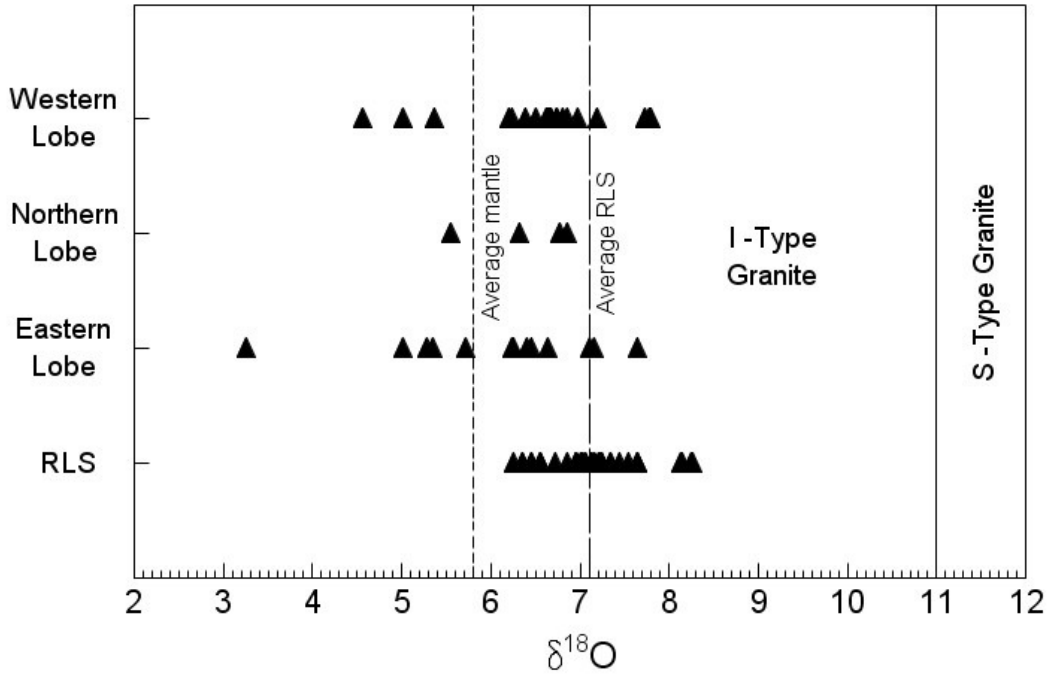

Fig. 55: Graph showing the range in $\delta^{18}O$ values of quartz for the Bushveld Complex granites and granophyres for each lobe vs. the $\delta^{18}O$ values for all minerals from the RLS (Harris *et al*., 2005) with the average mantle (Sharpe, 2007) and RLS (Harris *et al*., 2005) $\delta^{18}O$ values marked (dashed lines). The boundary between I and S–Type granites after Sharpe, (2007). All values plotted are magmatic $\delta^{18}O$ values.

The felsic units of the Bushveld Complex show a larger spread in ε_{Nd} values than the mafic/ultramafic RLS (Fig. 56) with the average ε_{Nd} value for the RLS noticeably lower(~ –6.4) than that of the felsic units average ε_{Nd} value (~ –3.8). The granitic units isotope data reflects a process involving less crustal contamination as indicated by the ε_{Nd} values involving a different source (indicated by the zircon and quartz $\delta^{18}O$ data) to that of the RLS.

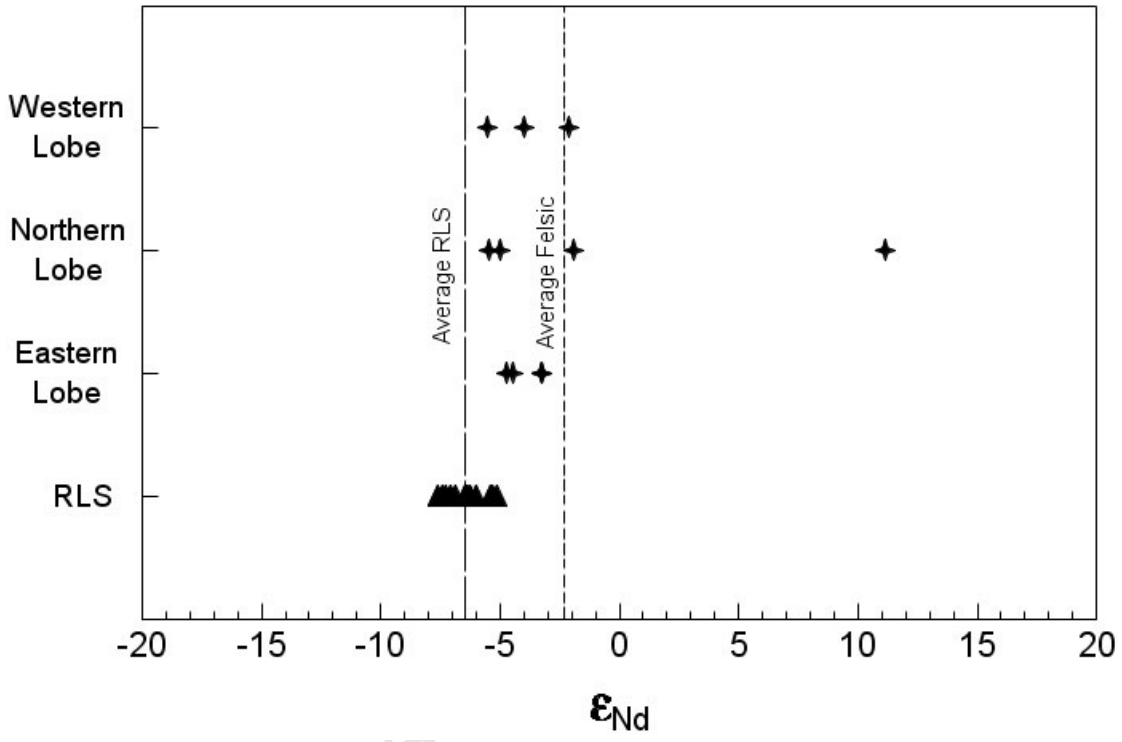

Fig. 56: Graph showing the range in ε_{Nd} values of the Bushveld Complex felsic units vs the ε_{Nd} values of the RLS (Harris *et al*., 2005). Average RLS and Bushveld felsic ε_{Nd} values also shown.

6.5 Comparison with Felsic Rocks in other LIPs

The following section will compare the $\delta^{18}O$ values of felsic units in other LIPs from around the world, where petrogenesis is well constrained, to that of the Bushveld Complex's granite and granophyre units to ascertain if these Bushveld units have $\delta^{18}O$ values typical of LIPs worldwide, indicating similar petrogenesis, or do they indicate significant differences, suggesting a different petrogenetic history.

6.5.1 Karoo, Parana/Etendeka and Chon Aike LIPs

Recent studies by Miller & Harris, (2007), Cochran (Hons Thesis, 2008) and Harris *et al.,* 2009 indicate that the Karoo LIP shares the unusual oxygen isotope characteristics of the Bushveld LIP. The Lebombo Rhyolites have a lower, nearer mantle, oxygen isotope signature (Fig. 53) compared to the ultramafic/mafic Karoo picrites, but it must be noted that the Parana/Etendeka magmatism was off-craton compared to the other examples. The $\delta^{18}O$ values show the felsic units to be seemingly less contaminated than the precursor ultramafic/mafic units with a range in $\delta^{18}O$ values between that fall mostly below the RLS average and just above the average mantle $\delta^{18}O$ value (Fig. 53).

Average $\delta^{18}O$ values for olivine in the ultramafic/mafic Tuli Picrites units were found to be ~ 6.54 ‰ ± 0.12 ‰ , using the $\delta^{18}O$ fractionation factor of ~ 0.5 ‰ between olivine and the magma, the average $\delta^{18}O$ value for the magma rises to ~ 7 ‰, very similar to the values obtained for the RLS. $\delta^{18}O$ values of quartz in the rhyolites average ~ 6.83 ‰ ± 0.42 ‰ (n = 20) (Miller & Harris, 2007), which are lower than the mafic units but within the $\delta^{18}O$ range for the Bushveld granite and granophyre units (Fig. 57). This $\delta^{18}O$ range is lower than the $\delta^{18}O$ value ranges of A-Type Granites from Namibia and Turkey (Fig. 57). Fractionation of $\delta^{18}O$ values between quartz and magma is ~ 0.6 ‰ (Matthews *et al*., 1994; Zhao & Zheng, 2003), resulting in the average $\delta^{18}O_{magma}$ of 6.23 ‰ ± 0.42 ‰ (n = 20) (Miller & Harris, 2007).

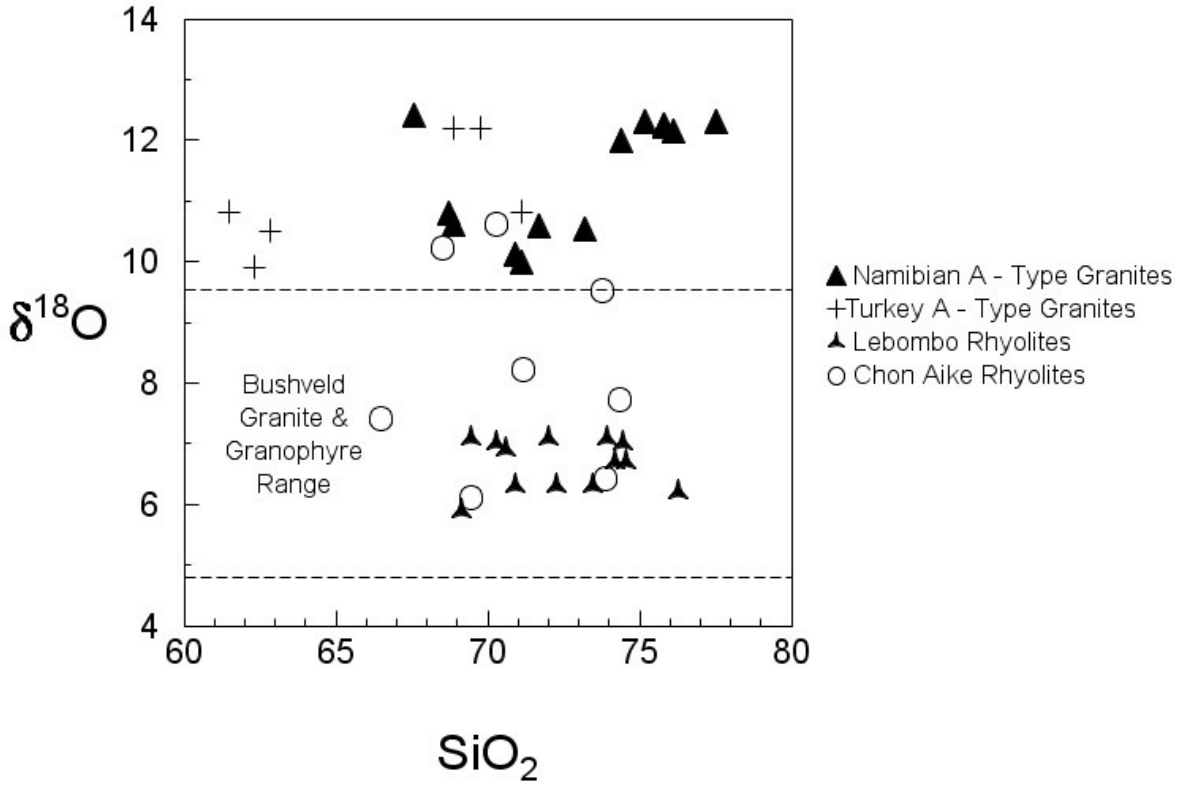

Fig. 57: Plot of silica vs. $\delta^{18}O$ values of the Lebombo & Chon Aike Rhyolites, Namibian A–Type Granites and the A–Type Granites from Turkey. The range in $\delta^{18}O$ values for the Bushveld granite & granophyre samples also drawn (dashed lines).

Source: LIPs (Lebombo Rhyolites (Miller & Harris, 2007) & Chon Aike Rhyolites (Riley *et al*., 2001)), Namibian A–Type Granites (Harris, 1995; &Trumbull *et al*., 2004), A–Type Granite from Turkey (Boztuğ *et al*., 2007).

The ~ 135 Ma Parana/Etendeka LIP has average $\delta^{18}O$ values for picrites of 5.33 ‰ ± 0.37 ‰ (Cochrane R, Hons. Thesis, 2008) and are consistent with the average mantle $\delta^{18}O$ value of ~ 5.8 ‰ but differ by ~ 1.2 ‰ from the Karoo and Bushveld LIPs. Two samples from the associated Okenyenya Complex show $\delta^{18}O$ values of 5.19 ‰ ± 0.12 ‰ (Cochrane R, Hons. Thesis, 2008) for olivine. The associated Etendeka felsic units have relatively high whole rock $\delta^{18}O$ values averaging 13.71 ‰ ± 2.07 (n = 13) (Harris *et al.* 1989) and do not reflect a low $\delta^{18}O$ source.

The close geographical and temporal relationship between the Karoo and Parana/Etendeka LIPs is not evident when studying their markedly different oxygen isotope characteristics, with the Karoo LIP seemingly having more in common with the Neo-Proterozoic Bushveld LIP. These three LIPs appear to have formed from processes operating in the same region of mantle and crust due to mantle plume activity below the continent but $\delta^{18}O$ analysis disputes the isotopic similarity of the mantle and or crust or indeed mantle plume characteristics below Southern Africa.

The Jurassic Chon Aike LIP is predominantly felsic (rhyolite) (Pankhurst *et al.*, 1998) covering a large portion of the Patagonian region of South America and North-Western Antarctica. $\delta^{18}O$ analysis of quartz from the Mapple Formation in Antarctica (Riley *et al.*, 2001) gave average values of 8.26 ‰ ± 1.69 (n = 8), with a range of 6.1 ‰ to 10.6 ‰ fallng into the Karoo/Bushveld and A-Type granite fields (Fig. 57). Riley *et al.*, (2001) also identified three distinct isotopic groups within the Mapple Formation and determined these groups were due to the three different eruptions of lava during the Jurassic, supporting the earlier distinctions made by Pankhurst *et al.*, (2000). The large scale lava formation was due to the influence of mantle plumes partially melting underplated mafic material in the lower crust followed by AFC processes to become the silicic magma that was erupted at surface to form the Chon Aike LIP (Riley *et al.*, 2001).

6.6 Comparison with A-Type Granites

Anorogenic granites typically feature hypersolvus to subsolvus alkali feldspar textures, bulk-rock compositions yielding ferroan, alkali-calcic to alkaline affinities and high LILE + HFSE abundances and anomalies due to high degrees of mineral fractionation (Bonin, 2006). A-Type magmas generally contain dissolved OH-F bearing fluids, crystallised under reduced and oxidized conditions and are generally associated with intra-plate tectonic settings where cratons are stabilized enough to move as a single unit (Bonin, 2006).

6.6.1 A – Type Granites from Brazil, Namibia, Turkey and Eastern China

The ~ 1.88 Ga (Dall'Agnol *et al*., 1999c) granitic plutons in northern Brazil have been divided into the Serra dos Carajás Granite Suite, the Jamon Granite Suite and the Velho Guilherme Granite Suite (Oliveira *et al*., 2008). These granitic suites were emplaced within the ~ 3 Ga Amazonian Craton with an extensional regime and magmatic underplating the cause of the melting (Dall'Agnol *et al*., 2005). The granitic plutons form the felsic component of a bimodal mafic/felsic magmatic system that grades into the more mafic compositions at the margins or core (Oliveira *et al*., 2008). Oxygen isotope data has been gathered from the three suites (Dall'Agnol *et al*., 2005 and references therein.) with most samples representing the whole rock composition but a number of quartz samples were also analysed for their oxygen isotope signature. The average values for quartz $\delta^{18}O$ from the three suites is 8.08 ‰ ± 0.7 (1σ, n = 9) (Dall'Agnol *et al*., 2005 and references therein). ranging from 7.06 ‰ to 9.00 ‰

The rocks of the central western region of Namibia record the breakup of Gondwana as the Parana/Etendeka LIP and associated small volume felsic bodies. The Brandberg, Erongo, Pareis, Cape Cross and Grosse Spitzkoppe plutons represent the largest of the granitic bodies found in the area and are associated with the rifting of Gondwana ~ 135 Ma. The $\delta^{18}O$ signature of five granitic A-Type plutons from Damaraland Namibia were analysed by Harris, (1995) and Trumbull *et al*., (2003). The average $\delta^{18}O$ values for the five plutons are relatively high (Fig. 58) at 10.52 ‰ ± 0.25 (n = 5), 12.24 ‰ ± 0.14 (n = 5), 9.98 ‰ (n = 1) and 12.16 ‰ ± 0.27 (n = 6) respectively, with $\delta^{18}O$ values ranging between 10.00 ‰ and 12.60 ‰ (Fig. 58). A combined $\delta^{18}O$ average of 11.23 ‰ anorogenic Namibian granites into S-Type granite field.

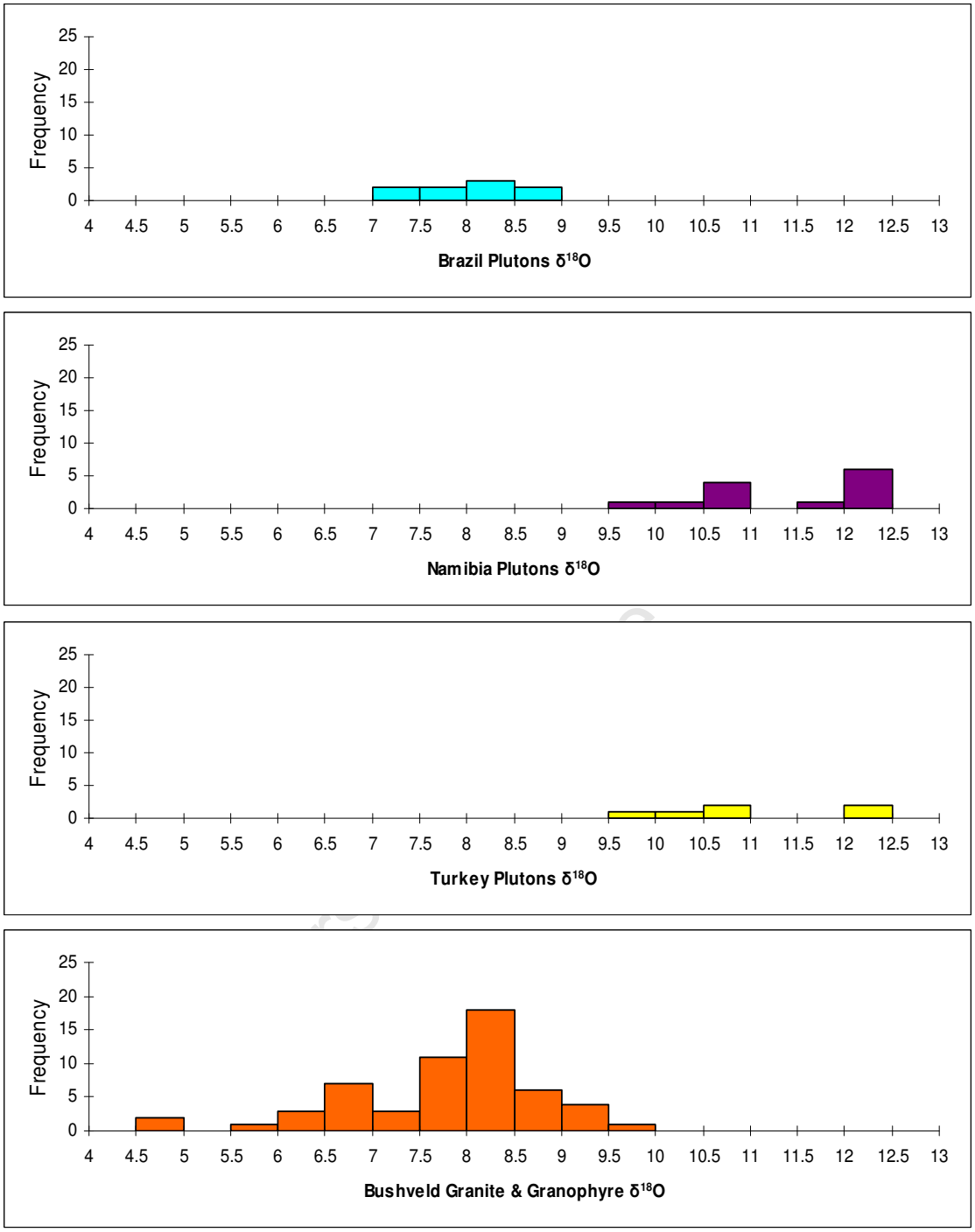

Fig. 58: Histograms depicting the range of $\delta^{18}O$ values of A-Type Granites compared to the Bushveld Complex granite and granophyre units.

Sources: Brazil Pluton data from Dall'Agnol *et al*., (2005) and references therein, Namibian Pluton data from Trumbull *et al*., (2003) and Turkey Pluton data from Boztuğ *et al*., (2007).

The Cenozoic Dumluca and Murmana plutons of South-Eastern Turkey are thought to be related to the Anatolian Collisional Arc (Boztuğ *et al*., 2007). The two plutons intrude into Palaeozoic ophiolites and sediments, consisting of mafic and felsic units. The felsic units range from granite to syenite to quartz monzo-diorite while the mafic units range from syenite to gabbro (Boztuğ *et al*., 2007). The average $\delta^{18}O$ values for the post collisional ~ 75 Ma Dumluca and Murmana A-Type felsic units in Turkey display relatively high $\delta^{18}O$ values (Fig. 58) of 10.50 ‰ ± 0.52 (1σ, n = 3) and 11.63 ‰ ± 0.98 (1σ, n = 3) respectively compared to the Karoo and Bushveld LIP felsic units, with a combined average of 11.07 ‰ ± 0.94 (n = 6). A significant amount of crustal assimilation/contamination at depth and shallower levels is thought to be the cause of the high $\delta^{18}O$ values (Boztuğ *et al*., 2007), ranging between 9.90 ‰ and 12.20 ‰ (Fig. 58) more indicative of S-Type granites around the world.

A recent study by Wei *et al*., (2008) on the A-Type granites of south Eastern-China provides oxygen isotope data for a comprehensive analysis of these Mesozoic igneous bodies. Comprising 5 plutons, the dataset has a combined average $\delta^{18}O$ value for quartz of 6.87 ‰ ± 1.53 (n = 63). The Nianzishan, Shanhaiguan, Laoshan, Suzhou and Kuiqi plutons range in age from 123 Ma to 93 Ma and intrude country rock of varying composition, ranging from Archaean Gneisses to Devonian Sandstones (Wei *et al*., 2000 & 2008). The oxygen isotope averages for the five plutons are markedly different with the Nianzishan Pluton quartz averaging 4.55 ‰ ± 2.28 (n = 12), showing quartz zonation/overgrowth with up to a 2 ‰ difference between zones (Wei *et al*., 2000 & 2008). The Shanhaiguan pluton quartz $\delta^{18}O$ values have an average value of 6.93 ‰ ± 0.40 (n = 7), the Laoshan pluton quartz averages 7.90 ‰ ± 0.16 (n = 8) with the Suzhou and Kuiqi plutons having average $\delta^{18}O$ values of 7.45 ‰ ± 0.33 (n = 30) and 7.14 ‰ ± 0.16 (n = 6) respectively. The values for quartz from the various plutons are fairly homogeneous, showing very little deviation among sample values, with the exception of the Nianzishan pluton that shows evidence of hydrothermal alteration. The combination of lower than mantle zircon and near mantle quartz $\delta^{18}O$ values during crystallisation eliminate post emplacement alteration and magmatic differentiation as being the cause of the low $\delta^{18}O$ values. The A-Type granites of Eastern-China are thought to be formed from a low $\delta^{18}O$ source, caused by melting of previously $\delta^{18}O$ depleted fragment/s (Wei *et al*., 2008) similar (Fig. 59) to the process envisaged for the formation of the Bushveld Complex granophyres and granites.

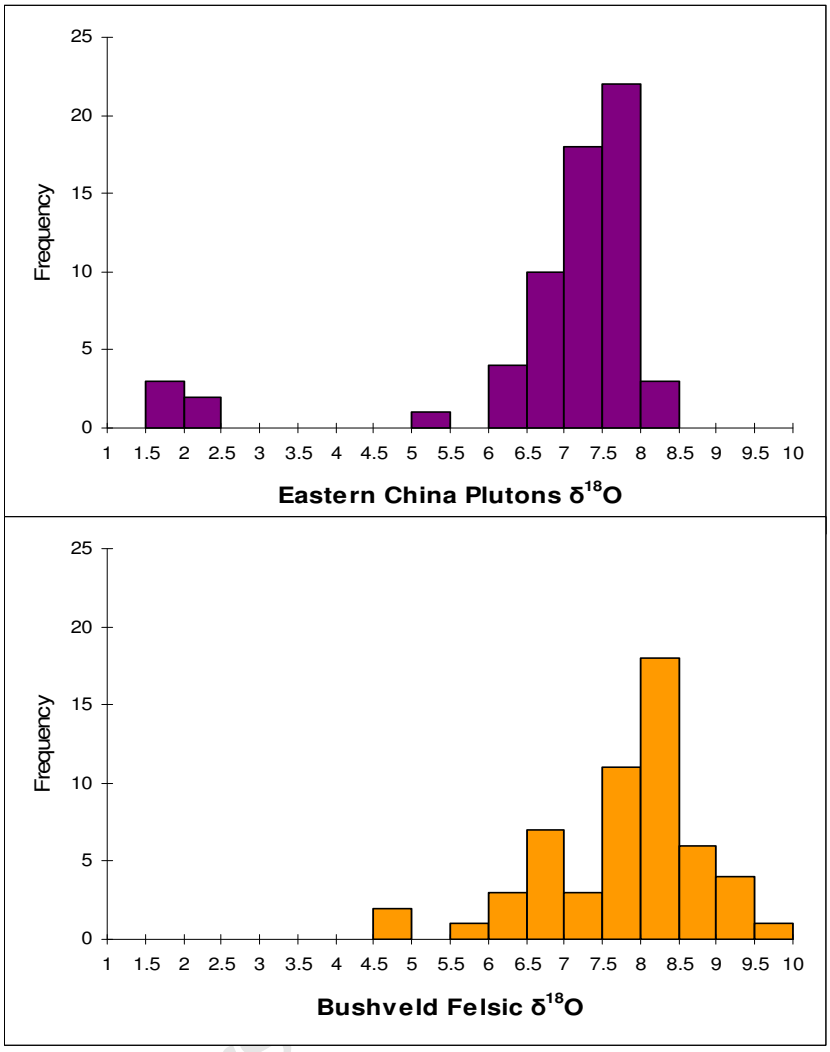

Fig. 59: Histogram of Bushveld granite and granophyre quartz $\delta^{18}O$ values compared to $\delta^{18}O$ quartz values from the A-Type granites of Eastern-China. Source: Eastern-China Pluton $\delta^{18}O$ data from Wei *et al.*, (2008).

While $\delta^{18}O$ values are not the definitive guide to A-Type classification, they do provide definitive evidence for the presence and formation of low $\delta^{18}O$ sources (< 5.8 ‰), and although A-Type granites do generally record low $\delta^{18}O$ values they do not all imply a low $\delta^{18}O$ source. The anorogenic and anhydrous nature of many A-Type magmas lend themselves to the preservation of magmatic or source $\delta^{18}O$ values, anomalous or not. The Bushveld Complex $\delta^{18}O$ values record near mantle $\delta^{18}O$ values and little evidence of alteration, with the $\delta^{18}O$ values on the low end of A-Type granite $\delta^{18}O$ values worldwide. The geological processes that produce A-Type granites are thought to be similar but the broad A-Type field may reflect the unknown quantities of mantle/crustal heterogeneity and the characteristics of individual mantle plumes through time.

6.7 Are the Bushveld Felsic Rocks Formed from Low $\delta^{18}O$ Magmas?

Low $\delta^{18}O$ magmas are classified as magmas that have lower $\delta^{18}O$ values than typical mantle $\delta^{18}O$ values of ~ 5.8‰ and are thought to be formed by the following processes:

1. Infiltration of heated low $\delta^{18}O$ fluid/s and subsequent interaction and $\delta^{18}O$ depletion under subsolidus conditions of an emplaced body to produce low $\delta^{18}O$ rocks that are remelted either partially or totally to produce a low $\delta^{18}O$ magma (Balsley & Gregory, 1998; Harris & Ashwal, 2002; Wei *et al*., 2008; Bindeman *et al*., 2008).

2. The $\delta^{18}O$ depletion of an isotopically normal magma by interaction with a low $\delta^{18}O$ fluid within the magma chamber (Friedman *et al*., 1974; Hildreth *et al*., 1984).

3. Assimilation of $\delta^{18}O$ depleted wall rock into the magma chamber. (Taylor, 1980 & 1986).

4. A low $\delta^{18}O$ magma source not related to the remelting of an existing $\delta^{18}O$ depleted body within the crust. i.e. A low $\delta^{18}O$ mantle source.

The $\delta^{18}O$ values measured for the Bushveld Complex granite and granophyre units cluster very near average mantle $\delta^{18}O$ values, which is significantly lower than the RLS. The $\delta^{18}O$ values of the Bushveld Complex granite and granophyre units that we observe today have undergone degassing, post emplacement alteration and probably a certain amount of contamination/assimilation processes that obscure the original magmatic $\delta^{18}O$ values, with the near mantle $\delta^{18}O$ values observed today possibly being higher than the original low $\delta^{18}O$ magma values. The $\delta^{18}O$ values of the Bushveld Complex granite and granophyre units zircon and quartz $\delta^{18}O$ data indicate an original source with mantle or below mantle $\delta^{18}O$ values.

The isotope data of the Bushveld granites and granophyres are interpreted to indicate that a magmatic source with either mantle or RLS $\delta^{18}O$ values interacted with magma or altered material of different $\delta^{18}O$ composition to produce a hybrid magma of felsic composition with $\delta^{18}O$ values that stayed near mantle values through intrusion and movement through the crust, emplacement and subsequent alteration processes. Oxygen isotope fractionation during fractional crystallisation of magma to more silica rich compositions typically elevates $\delta^{18}O$ values between 0.6 ‰ and 1.0 ‰ suggesting source magma $\delta^{18}O$ values for the Bushveld granites and granophyres of < 5.8 ‰. Assimilation/contamination and typical (non highly negative meteoric) hydrothermal alteration processes, having all affected the Bushveld Complex granites and granophyres, also generally elevate $\delta^{18}O$ values, indicating that the retention of low $\delta^{18}O$ values despite these processes required low $\delta^{18}O$ values (< 5.8 ‰) at some point to offset the $\delta^{18}O$ elevation trends.

If the magma responsible for the assimilation was of RLS composition (7.1 ‰) assimilation of material of mantle or above composition would not form a hybrid magma of Bushveld Complex Felsic units $\delta^{18}O$ composition. Without invoking lower than mantle $\delta^{18}O$ values the hybrid magma would have to consist of > 80 % $\delta^{18}O$ mantle composition magma mixed with < 20 % RLS $\delta^{18}O$ composition magma but this combination would not produce a granitic source. A massive injection of mantle $\delta^{18}O$ composition magma may have occurred and assimilated RLS magmas but the hybrid magma would be of mafic/ultramafic composition and require large amounts of fractional crystallisation to evolve to Bushveld Felsic unit composition which typically raises $\delta^{18}O$ values. There is no possible combination of non low $\delta^{18}O$ magmas that would produce a Bushveld felsic magma chemical composition with the observed near mantle $\delta^{18}O$ values. The $\delta^{18}O$ values of the Bushveld granites and granophyres require:

1) Derivation by partial melting of RLS (or RLS like) source which was then contaminated by low $\delta^{18}O$ material.

2) The source (partial melt of RLS or similar composition) became hydrothermally altered before partial melting, lowering $\delta^{18}O$.

3) A different source material from those described above which cannot be mantle derived in a closed system as the ε_{Nd} values are too low.

6.8 Comparison with Low $\delta^{18}O$ Felsic Magmas

A number of low $\delta^{18}O$ provinces or regions have been identified around the world and their petrogenesis fairly well constrained by researchers. Comparing the Bushveld Complex's granite and granophyre oxygen isotope data with that from other low $\delta^{18}O$ regions (Fig. 60) may help to further constrain the petrogenetic history of the Bushveld Complex.

The degree of contamination/alteration to produce low $\delta^{18}O$ magmas is assumed to be very high as the erupted material would presumably come into contact with and assimilate material in the lower to upper crust that generally has higher than mantle oxygen isotope values. The hydrothermal fluids interacting with an igneous body would have to have very low or negative $\delta^{18}O$ values to change the oxygen isotope signature to the low values observed in such areas as the Seychelles, Iceland, Yellowstone and the Snake River Plain. The usually pervasive contamination/alteration indicates high temperatures, material previously altered in $\delta^{18}O$ through hydrothermal alteration and or considerable fluid volume with sufficiently low $\delta^{18}O$ values and time period over which to operate to further lower the $\delta^{18}O$ values of large volumes of igneous rock. The original cause of the alteration is thought to be the circulation of hydrothermal fluids through the igneous body while it is cooling, with the more negative $\delta^{18}O$ value of the hydrothermal fluids originating from the local low $\delta^{18}O$ meteoric waters.

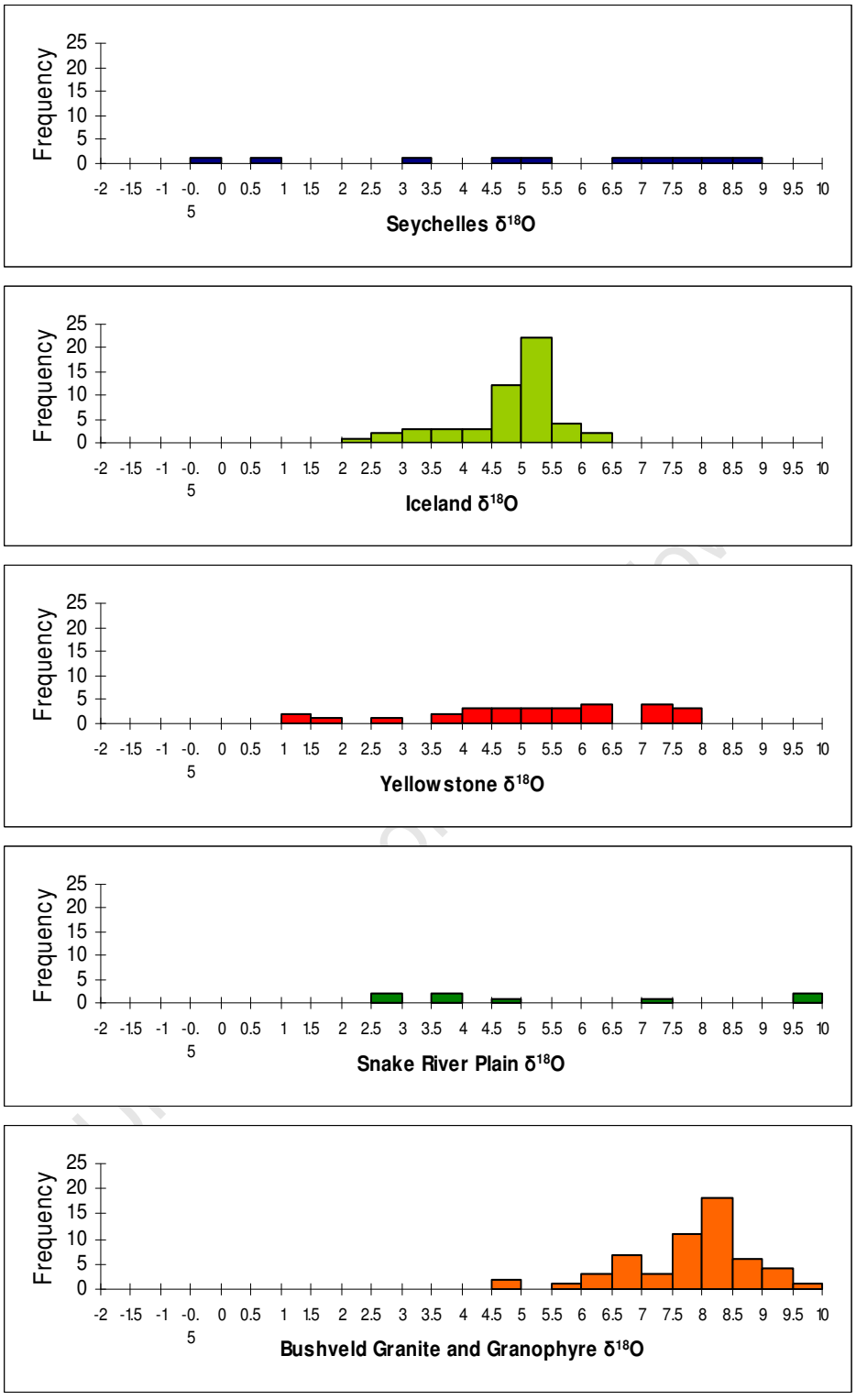

Fig. 60: Quartz $\delta^{18}O$ values for the Seychelles, Iceland, Yellowstone and the Snake River Plain vs Bushveld Complex granite and granophyre units. Sources: $\delta^{18}O$ data from The Seychelles (Harris & Ashwal, 2002); Iceland (Óskarsson & Steinthórsson, 1993); Yellowstone (Bindeman & Valley, 2001) & the Snake River Plain (Boroughs *et al.*, 2005).

6.8.1 Seychelles, Iceland, Yellowstone and Snake River Plain Low ^{18}O Magmas

The Seychelles are situated in the Indian Ocean ~ 1000 km east of the African mainland and ~ 380 km NE of the northern tip of Madagascar and are made up of a number of small islands clustered around the largest island of Mahé. The Seychelles geology is unusual in that they consist of mainly 750 Ma granites, which are recognised as fragments of the African continent, formed during the breakup of Gondwana and was the first discovered evidence of a low $\delta^{18}O$ magma source (Taylor, 1974). Two types of granite have been distinguished based on chemical and isotopic compositions, the Mahé and Praslin groups (Ashwal *et al*., 2002). A study by Harris and Ashwal, (2002) analysed the $\delta^{18}O$ values of these granites (Fig. 60) to provide evidence for a low $\delta^{18}O$ source and alteration process. The $\delta^{18}O$ values for the quartz in the Mahé and Praslin group granites are 6.68 ‰ ± 1.85 (n = 4) and 4.45 ‰ ± 3.76 (n = 6) respectively with the combined average $\delta^{18}O$ value of 5.34 ‰ ± 3.21 (n = 10). The relatively low $\delta^{18}O$ values for quartz and large standard deviations, especially for the Praslin group granites indicate the effects of fluid alteration on the Seychelles Granite. As no evidence for post emplacement hydrothermal alteration was discovered, a previously altered low $\delta^{18}O$ granitic source was deemed to be responsible for the low $\delta^{18}O$ values from the Seychelles (Harris & Ashwal, 2002).

The presence of low $\delta^{18}O$ magmas from Iceland has been known since the early 1970's (Muehlenbachs *et al*., 1974) and has since been investigated by Hattori and Muehlenbachs, (1982), Condomines *et al*., (1983), Hémond *et al*., (1988) and Hémond *et al*., (1993) among others. The low $\delta^{18}O$ magmas are emplaced alongside high $\delta^{18}O$ magmas and both seem to be erupting from the mid ocean ridge that Iceland straddles. While the presence of low and high $\delta^{18}O$ magmas in very close proximity is uncommon, their apparently shared mid ocean ridge source is very rare. The low $\delta^{18}O$ magmas from Iceland are thought to be as a result of the partial melting of a previously altered source that is now being recycled from the upper mantle. Whole rock $\delta^{18}O$ values for Iceland felsic units are variable (Fig. 60) with many units showing the effects of post emplacement hydrothermal alteration. The generally low $\delta^{18}O$ values for basalts (2.05 ‰ to 6.3 ‰) (Óskarsson & Steinthórsson, 1993) and whole rock for silicic and intermediate glasses (1.4 ‰ to 6.1 ‰) (Condomines *et al*., 1983) indicate melting of a previously altered fragment of oceanic or continental crust.

Low $\delta^{18}O$ magmas are a feature of the Yellowstone and Snake River volcanic fields and have been studied by various workers (Hildreth *et al*., 1984; Hildreth *et al.,* 1991; Bindeman *et al*., 2001; Boroughs *et al*., 2005) with the aim of determining the processes involved in the formation of the extensive low $\delta^{18}O$ volcanic lavas in the region. The previous studies of the Yellowstone Rhyolites have determined that caldera collapse of previous Yellowstone volcanoes and subsequent intense hydrothermal interaction within the collapsed region was responsible for lowering the oxygen isotope signature. The altered material was then buried and partially or totally remelted and assimilated a short while later during a subsequent stage of volcanic activity over the Yellowstone hotspot and erupted as extensive low $\delta^{18}O$ felsic lavas. The Snake River Rhyolites have more negative $\delta^{18}O$ values than those found at Yellowstone with the greater depletion in $\delta^{18}O$ due to the re-melting of previously depleted $\delta^{18}O$ crustal material, not associated with volcanism (depleted caldera blocks), 30 to 40 Ma before volcanic activity in the region (Boroughs *et al*., 2005). The quartz $\delta^{18}O$ values of the Yellowstone volcanic units studied by Bindeman & Valley, (2001) have a combined average of 5.27 ‰ ± 1.92 (n = 163) with some lava flows and tuffs showing much greater degrees of hydrothermal alteration than others with $\delta^{18}O$ values ranging from average values of 1.01 ‰ to 7.89 ‰ (Fig. 61). The Snake River tuffs and lavas have average $\delta^{18}O$ quartz values of 5.6 ‰ ± 2.88 (n = 8), ranging from 2.6 ‰ to 9.6 ‰ (Fig. 60).

Studies by Balsley and Gregory, (1998) have concluded that the amount of alteration of isotopic values is possible due to the anhydrous nature of the magma which can, due to its high liquidus temperature, interact with and assimilate previously altered material relatively easily and not reach water saturation. Water saturation results in quenching of the assimilation and fractional crystallisation (AFC) process and or eruption of the magma (Balsley & Gregory, 1998), thus the preservation of low $\delta^{18}O$ values may be related to the water content of the parental magma and assimilated material, with saturated magmas, not being able to melt/assimilate sufficient material to significantly lower the $\delta^{18}O$ signature.

The data from the low $\delta^{18}O$ units and regions around the world suggest that previously altered igneous bodies were re-melted by high temperature and assimilated by anhydrous sources, which then produced low $\delta^{18}O$ magmas reflecting the isotopic composition of the combined magmas. The isotopic composition would thus show $\delta^{18}O$ depletion relative to the original near - mantle value of the anhydrous high temperature magma source which may not truly indicate the true isotopic signature of the altered material. The ranges in $\delta^{18}O$ values from the low $\delta^{18}O$ regions suggests that the degree of alteration is crucial to the preservation of low $\delta^{18}O$ source values, with the presence of low $\delta^{18}O$ sources probably greatly under estimated as only relatively young, un-metamorphosed bodies with greatly lowered $\delta^{18}O$ values seem to preserve sufficiently low $\delta^{18}O$ values for definitive source characterization. The low $\delta^{18}O$ values for the Yellowstone and Snake River tuffs are interpreted to be the result of $\delta^{18}O$ depletion through hydrothermal alteration with low $\delta^{18}O$ fluid, taking place over shorter (Yellowstone volcanism) and longer (Snake River) time periods.

6.9 Origin of the Bushveld Felsic Magmas

$\delta^{18}O$ values for felsic magmas ~ 5.8 ‰ are unusual. The relatively high $\delta^{18}O$ values for the mafic RLS suggest crustal contamination/assimilation of unaltered crustal material and no evidence of interaction with or formation from a low $\delta^{18}O$ source. The granite and granophyre units of the Bushveld Complex have isotope characteristics that preclude certain petrogenetic processes; a mantle plume may have provided the heat necessary to partially melt material that could have formed the granites and granophyres, but a magma of mantle isotope composition could not have been the parental magma or even the major component in a hybrid magma that may have formed the granite and granophyre units. A hybrid magma consisting of a mixture of a mafic component and a felsic or previously altered mafic component can best explain the observed isotope values. The mafic component was most likely a partial melt of RLS that melted and mixed with a more felsic component or depleted RLS that melted and evolved to more felsic compositions.

The contamination of the RLS parental magma at depth makes it unlikely but possible that a large volume of parental RLS magma bypassed this process and took a different path to shallower depths, but the $\delta^{18}O$ values of the granite and granophyre units are too low to have formed from a RLS parental magma alone, without evolving and or assimilating the surrounding crustal/underplated rock.

Assimilation of a $\delta^{18}O$ depleted fragment into a magma of mantle or RLS composition, would not require a separate low $\delta^{18}O$ mantle source or rely on impossible scenarios of a mantle source that suffered no contamination/assimilation of any material with $\delta^{18}O$ values > 6 ‰ at mid-shallow crustal levels and evolved to a felsic composition without oxygen isotope fractionation. The process of a source magma moving upward to shallower crustal levels and partially melting a region or fragment of low $\delta^{18}O$ crust has been identified in Yellowstone (Hildreth *et al*., 1991; Bindeman & Valley, 2009) and Iceland (Muehlenbachs *et al*., 1973; Hémond *et al*., 1993). Melting and assimilating $\delta^{18}O$ depleted crustal or underplated material would mean a great abundance of source magma, similar enough in density to facilitate mixing with the $\delta^{18}O$ depleted material that is required to homogenize the magma to low $\delta^{18}O$ values. The hybrid low $\delta^{18}O$ melt could then be contaminated by the RLS and or crustal material and evolve to more felsic compositions and still not reach parity with observed RLS $\delta^{18}O$ values.

The radiogenic Sr data indicates that the Bushveld Complex felsic units were affected after emplacement, by fluids, (constrained by oxygen isotope values) of possible magmatic origin as the extremely large range in $^{\varepsilon}_{Sr}$ values record. The ε_{Nd} values for the Bushveld Complex felsic units represent a degree of crustal contamination but not to the same degree of the previously erupted RLS (Figs. 54 & 56), this is interpreted to indicate the assimilation of a smaller volume of relatively greater $\delta^{18}O$ depleted crustal material or a larger volume of less depleted underplated RLS. The Rooiberg Felsite Suite has variable radiogenic isotope values and a crustal $\delta^{18}O$ value of 7.3 ‰ (1 zircon analysis) which suggest alteration and parental magma of crustal origin not RLS or a partial melt thereof.

The Bushveld Complex's granite and granophyre $\delta^{18}O$ values are not as low as those of the depleted $\delta^{18}O$ regions of the world but are lower than typical A-Type granites and significantly lower than non A-Type granitic bodies. This may indicate the further contamination of the Bushveld felsic magma and or different processes of $\delta^{18}O$ depletion and preservation compared to other isotopically and geochemically similar units. The formation of low $\delta^{18}O$ provinces, by melting and assimilating varying quantities of crustal or underplated mafic/ultramafic material, having a large range of $\delta^{18}O$ values, could produce a range of average $\delta^{18}O$ values for depleted source magmas.

While the Bushveld Complex's $\delta^{18}O$ average value is by definition not low enough to classify it as a low $\delta^{18}O$ province, the isotope evidence suggests that it must have been formed from a low $\delta^{18}O$ source. A $\delta^{18}O$-depleted continental crust or underplated RLS source, partially melted and assimilated by an anhydrous magma of RLS or RLS partial melt composition, is proposed to have formed the low $\delta^{18}O$ hybrid source magma to the Bushveld granophyres and granites. This low $\delta^{18}O$ hybrid source magma evolved to more felsic compositions with possible further contamination/assimilation during emplacement to form the elevated, near mantle, $\delta^{18}O$ values of the Bushveld Complex's granites and granophyres.

The Bushveld Complex may represent the oldest and largest exposure of 'low' $\delta^{18}O$ magma yet discovered, although the preserved $\delta^{18}O$ values are not as low as other low $\delta^{18}O$ regions around the world. Radiogenic (Nd) isotope data indicates that the low $\delta^{18}O$ source magma could not have been of purely mantle origin but required a certain amount of crustal input to achieve the observed values. The Bushveld Complex granites and granophyres show evidence of crustal heterogeneity at ~ 2 Ga revealed by heat input from a theorised plume that was able to melt or partially melt a greater proportion of the overlying or nearby material within the crust than through general magma generation processes.

7 CONCLUSIONS

1) Quartz $\delta^{18}O$ values range from 4.6 ‰ to 10.8 ‰, zircon $\delta^{18}O$ values range from 2.5 ‰ to 7.3 ‰ and alkali feldspar $\delta^{18}O$ values range from 7.4 ‰ to 10.2 ‰. Amphibole and Biotite have $\delta^{18}O$ values ranging from 2.1 ‰ to 6.0 ‰ and 1.2 ‰ to 9.1 ‰ respectively. The $\delta - \delta$ plots indicate that quartz and zircon values are in oxygen-isotope equilibrium at magmatic temperatures, whereas quartz and the other analysed minerals in the Bushveld granites and granophyres show varying degrees of oxygen-isotope disequilibrium.

2) Alkali feldspar $\delta^{18}O$ values from the Bushveld Complex granite and granophyre units are generally higher than those of quartz from the same samples. This data suggests that relatively low temperature hydrothermal alteration has increased the alkali feldspar $\delta^{18}O$ values.

3) No evidence was found for oxygen-isotope zoning in quartz from the Bushveld granites and granophyres. This indicates that alteration did not affect quartz oxygen-isotope ratios after emplacement, and that they can be used to reliably estimate parental magma $\delta^{18}O$ values.

4) It was not possible to constrain the $\delta^{18}O$ values of the Rooiberg Felsite magma(s) as no minerals apart from a single zircon aliquot could be separated from the fine-grained felsites. The single zircon separate from the Rooiberg Felsite was analysed and has a $\delta^{18}O$ value of 7.23 ‰. This value is ~ 2 ‰ higher than the zircon $\delta^{18}O$ values found for in the granites and granophyres, which suggests crystallization from a magma having a significantly higher $\delta^{18}O$ value. It may represent an inherited zircon from one of the sedimentary units found within the Rooiberg Felsite.

5) Magma degassing and low temperature post emplacement hydrothermal alteration of the granite and granophyre units can explain the δD values of the hydrous phases (hornblende & biotite). These processes did not affect the $\delta^{18}O$ values of zircon and quartz, unlike those of hornblende, biotite and feldspar.

6) The range for $\delta^{18}O$ magma values for the Bushveld Complex granite and granophyre is 5.8 ‰ to 6.2 ‰ averaging 6.0 ‰ (n = 63), which is lower than the average $\delta^{18}O$ value of 7.1 ‰ for the RLS (Harris *et al.*, 2005).

7) The initial Sr-isotope ratios range from – 1.99 to 0.86 and are clearly affected by post emplacement hydrothermal alteration. The initial Nd-isotopes can be more reliably related to magmatic values and are best explained as being due to a substantial crustal component, although less than apparently experienced by the RLS (Maier *et al.*, 2000).

8) The Bushveld granites and granophyres have $\delta^{18}O$ values at the low end of the range shown by felsic units in other LIPs (Karoo, Parana/Etendeka and Chon Aike).

9) Among so-called A-Type granites and rhyolites, the Bushveld granite and granophyre $\delta^{18}O$ values are among the lowest recorded. Only Eastern China, the Seychelles, Iceland, Yellowstone and the Snake River Plain have lower $\delta^{18}O$ values. These felsic rocks are considered to be low-$\delta^{18}O$ magmas (Taylor & Sheppard, 1986).

10) The relationship between the felsic units of the Bushveld Complex and the RLS is probably one of similar source with a more evolved RLS composition magma having near mantle $\delta^{18}O$ values, providing the heat to melt and mix with previously altered crustal or altered RLS material. The pulsed nature of the RLS and its mafic/ultramafic mineralogy suggest an anomalous heat source (perhaps a mantle plume) driving the process with crustal weaknesses to exploit within the craton to allow the necessary pressure gradient. Two mechanisms for the production of the observed low $\delta^{18}O$ values compared to the RLS are as follows. The first option is that the felsic magma was not contaminated by crustal material to the same degree that the RLS magma was, resulting in more mantle-like $\delta^{18}O$ values. The second mechanism is that the felsic magmas are derived from a similar source to the RLS whose $\delta^{18}O$ values had been lowered by hydrothermal exchange at high temperatures. It is also possible that this source was hydrothermally altered RLS, though such material has not yet been recognised.

Recommendations:

The oxygen isotope data represented in this thesis underlines the need for an inclusive study of all Bushveld Complex units. The oxygen isotope data hints at discrepancies between the felsic and mafic/ultramafic units and possibly, on a larger scale with the Southern African LIPs being similar compared to international examples. Future studies on the Bushveld Complex could examine any new or produce new geophysical data from various regions and within the Bushveld Complex to resolve possible source regions. The lack of reliable data for the Rooiberg Felsites poses a problem when trying to resolve Bushveld Complex systematics and needs to be investigated, if possible. Finally, quantification of the data and possibly modelling outcomes would provide valuable support for any conclusions reached.

References

Ashwal, L.D., Demaiffe, D. and Torsvik, T.H. 2002. Petrogenesis of Neoproterozoic granitoids and related rocks from the Seychelles: the case for an Andean arc origin. *J. Petrol.,* **43**, 45 – 83.

Balsley, S.D. and Gregory, R.T. 1998. Low - ^{18}O silicic magmas: why are they so rare? *Earth and Planetary Science Letters*. **162,** 123 – 136.

Barnes, S – J., Maier, W.D. and Ashwal, L.D. 2004. Platinum – group element distribution in the Main Zone and Upper Zone of the Bushveld Complex, South Africa*, Chemical Geology*, **208**, 293 – 317.

Bindeman, I.N. and Valley, J.W. 2001. Low – $\delta^{18}O$ Rhyolites from Yellowstone: Magmatic Evolution Based on Analyses of Zircons and Individual Phenocrysts. *Journal of Petrology*. **42**, 1491 –1517.

Bindeman, I.N., Fu, B., Kita, N.T. and Valley, J.W. 2008. Origin and evolution of silicic magmatism at Yellowstone based on ion microprobe analysis of isotopically zoned zircons. *Journal of Petrology,* **49**, 163 – 193.

Bonin, B. 2006. A-type granites and related rocks: Evolution of a concept, problems and prospects. *Lithos,* **97,** 1 – 29.

Boroughs, S., Wolff, J., Bonnichsen, B., Godchaux, M. and Larson, P. 2005. Large – volume low – $\delta^{18}O$ rhyolites of the central Snake River Plain, Idaho, USA. *Geology*, **33,** 821 – 824.

Boztuğ, D., Harlavan, Y., Arehart, G.B., Satır, M. and Avcı, N. 2007. K – Ar age, whole-rock and isotope geochemistry of A – type granitoids in the Divriği – Sivas region, eastern – central Anatolia, Turkey. *Lithos*. **97**, 193 – 218.

Bryan, S.E., Riley, T.R., Jerram, D.A., Leat, P.T. and Stephens, C.J. 2002. Silicic volcanism: an under – valued component of large igneous provinces and volcanic rifted margins. In: Menzies, M.A., Klemperer, S.L., Ebinger, C.J. and Baker, J. Eds, *Magmatic Rifted Margins, Geological Society of America Special Paper*, **362**, 99 – 118.

Bryan, S.E. and Ernst, R.E. 2008. Revised definition of Large igneous Provinces (LIPs). *Earth – Science Reviews*, **86,** 175 – 202.

Buchanan, D.L. 1975. The petrography of the Bushveld Complex intersected by boreholes in the Bethal area. *Transactions of the Geological Society of South Africa.* **78**, 335 – 348.

Buchanan, P.C., Koeberl, C. and Reimold, W.U. 1999. Petrogenesis of the Dullstroom Formation, Bushveld Magmatic Province, South Africa. *Contrib. Mineral. Petrol.* **137**, 133 – 146.

Buchanan, P.C., Reimold, W.U., Koeberl, C. and Kruger, F.J. 2002. Geochemistry of intermediate to siliceous volcanic rocks of the Rooiberg Group, Bushveld Magmatic Province, South Africa. *Contrib. Mineral. Petrol.* **144**, 131 – 143.

Buchanan, P.C., Reimold, W.U., Koeberl, C. and Kruger, F.J. 2004. Rb – Sr and Sm – Nd isotopic compositions of the Rooiberg Group, South Africa: early Bushveld-related volcanism. *Lithos.* **29**, 373 – 388.

Buick, I. S., Maas, R. and Gibson, R. 2001. Precise U-Pb titanite age constraints on the emplacement of the Bushveld Complex, South Africa. *Journal of the Geological Society.* **158,** 3 – 6.

Cawthorne, R.G., Davies, G., Clubly-Armstrong, A. and McCarthy, T.S. 1981. Sills associated with the Bushveld Complex, South Africa: an estimate of the parental magma composition. *Lithos*. **14**, 1 – 15.

Cawthorn, R.G. 1998. Geometrical relations between the Transvaal Supergroup, the Rooiberg Group, and the mafic rocks of the Bushveld Complex. *South African Journal of Geology.* **101,** 275 – 280.

Cawthorn, R.G., Cooper, G.R.J. and Webb, S.J. 1998. Connectivity between the western and eastern limbs of the Bushveld Complex. *South African Journal of Geology.* **101**, 291 – 298.

Cawthorn, R.G., Eales, H.V., Walraven, F., Uken, R. and Watkeys, M.K. 2006. The Bushveld Complex. In: Johnson, M.R., Anhausser, C.R. And Thomas, R.J. (Eds.). The geology of South Africa. Geological Society of South Africa, Johannesburg/Council for Geoscience, Pretoria, 261 – 281.

Chappell, B.W. and White, A.J.R. 1974. Two contrasting granite types. *Pacific Geology,* **8**, 173 – 174.

Chenet, A-L., Quidelleur, X., Fluteau, F., Courtillot, V. and Bajpa, S. 2007. 40K – 40Ar dating of the Main Deccan large igneous province: Further evidence of KTB age and short duration. *Earth and Planetary Science Letters*. **263,** 1 – 15.

Chiba, H., Chacko, T., Clayton, R.N. and Goldsmith, J.R. 1989. Oxygen isotope fractionations involving diopside, forsterite, magnetite, and calcite. *Geochim. Cosmochim. Acta*, **53**, 2985 – 2995.

Clarke, B., Uken, R. and Reinhardt, J. 2009. Structural and compositional constraints on the emplacement of the Bushveld Complex, South Africa. *Lithos.* **111**, 21 – 36.

Clayton, R.N, Goldsmith, J.R and Mayeda, T.K. 1989. Oxygen isotope fractionation in quartz, albite, anorthite and calcite. *Geochimica et Cosmochimica Acta.* **53***,* 725 – 733.

Cochran, R. 2008. Oxygen Composition of Tuli, Dronning Maud Land and Etendeka Picrites: Relative Roles of Crust and Mantle in Petrogenesis. unpubl. Hons. Thesis. 51p.

Coertze, F.J., Burger, A.J., Walraven, F., Marlow, A.G. and MacCaskie, D.R. 1978. Field relations and age determinations in the Bushveld Complex: *Trans. Geol. Soc. S. Afr*., **81**, 1 – 11.

Collins, W.J., Beams, S.D., White, A.J.R. and Chappell, B.W. 1982. Nature and origin of A-type granites with particular reference to south – eastern Australia. *Contributions to Mineralogy and Petrology*, **80**, 189 – 200.

Condomines, M., Grönvold, K., Hooker, P.J., Muehlenbachs, K., O'Nions, R.K., Óskarsson, N. and Oxburgh, E.R. 1983. Helium, oxygen, strontium and neodymium isotopic relationships in Icelandic volcanics. *Earth Planet. Sci. Lett*., **66**, 125 – 136.

Coplen, T. B., Kendall, C. and Hopple, J. 1983. Comparison of stable isotope reference samples. *Nature*, **302**, 236 – 238.

Council of Geosciences. 1978 1:250,000 geologic maps (2528 Pretoria and 2428 Nylstroom sheets). Pretoria, South Africa.

Courtillot, V.E. 1990. What caused the mass extinction? A volcanic eruption. *Sci. Am*. **263**, 53 – 60.

Courtillot, V.E. 1994. Mass extinctions in the last 300 million years: one impact and seven flood basalts*, Isr. J. Earth Sci.*, **43**, 255 – 266.

Crocker, I.T., Eales, H.V. and Ehlers, D.L. 2001. The fluorite, cassiterite and sulphide deposits associated with the acid rocks of the Bushveld Complex, *Council for Geoscience – Memoir*, **90**, 115p.

Dall'Agnol, R., Rämö , O.T., Magalhães, M.S., Macambira, M.J.B. 1999c. Petrology of the anorogenic, oxidised Jamon and Musa granites, Amazonian craton: implications for the genesis of Proterozoic A-type granites. *Lithos.* **46**, 431 – 462.

Dall'Agnol, R., Teixeira, N.P., Rämö, O.T., Moura, C.A.V., Macambira, M.J.B. and Oliveira, D.C. 2005. Petrogenesis of the Paleoproterozoic, rapakivi, A-type granites of the Archean Caraja´s Metallogenic Province, Brazil. *Lithos.* **80**, 101 – 129.

de Wit, M.J., de Ronde, C.E.J.,Tredoux, M., Roering, C., Hart, R.J., Armstrong, R.A., Green, R.W.E., Peberdy, E. and Hart, R.A. 1992. Formation of an Archaean continent. *Nature.* **357**, 553 – 562.

Eales, H. V. and Cawthorn, R. G. 1996. The Bushveld Complex. In: Cawthorn, R. G. (ed.) Layered Intrusions. Amsterdam: Elsevier, pp. 181 – 229.

Elston, W.E. 1992. Does the Bushveld-Vredefort system (South Africa) record the largest known terrestrial impact catastrophy? International Conference on Large Meteorite Impacts and Planetary Evolution, *Lunar Planetary Institute Contribution,* **790,** 23 - 24.

Ernst, R.E., Buchan, K.L. 2001. Large mafic magmatic events through time and links to mantle – plume heads. In: Ernst, R.E., Buchan, K.L. (Eds.), Mantle Plumes: Their Identification Through Time. *Geological Society of America Special Paper*. **352**, 483 – 575.

Ernst, R.E. and Buchan, K.L., 2004. Large Igneous Provinces (LIPs) in Canada and adjacent regions: 3 Ga to present. *Geoscience Canada* . **31**, 103 – 126.

Ernst, R.E., Buchan, K.L., Campbell, I.H. 2005. Frontiers in Large Igneous Province research. *Lithos*. **79**, 271 – 297.

Friedman, I., Lipman, P.W., Obradovich, J.D., Gleason, J.D., and Christiansen, R.L. 1974. Meteoric water in magmas. *Science*, **184**, 1069 – 1072.

Geological Survey of, South Africa. 1981. 2526 Rustenburg 1:250 000 Geological Map Series.

Gibson, R. L. and Stevens, G. 1998. Regional metamorphism due to anorogenic intracratonic magmatism. What drives Metamorphism and metamorphic Reactions? P. J. O. B. Treloar, P.J. London, Geological Society of London**:** 121 – 135.

Gregory, R.T. and Criss, R.E. 1986. Isotopic exchange in open and closed systems. In: Stable Isotopes in High Temperature Geological Processes. Valley *et al*. Eds., *Rev. Mineral*., **16**, 91 – 127.

Hall, A.L. 1932. The Bushveld Igneous Complex of the central Transvaal. *Geological Survey of South Africa Memoir.* **28**. 560 pp.

Harmer, R.E. and Eglington, B.M. 1990. A review of the statistical principles of geochronometry; towards a more consistent approach for reporting geochronological data. *South African Journal of Geology*, **93**, 845 – 856.

Harmer, R.E. 2000. New precise dates on the acid phase of the Bushveld and their implications. Abstract. Workshop on theBushveld Complex, Burgersfort. South Africa.

Harmer, R.E. & Sharpe, M.R. 1985. Field relations and strontium isotope systematics of the marginal rocks of the eastern Bushveld Complex. *Econ. Geol.* **80**, 813 – 837.

Harmer, R..E. and Armstrong, R..A. 2000. Duration of Bushveld Complex (sensu lato) magmatism: Constraints from new SHRIMP zircon chronology: National Research Foundation, Bushveld Complex Workshop, Gethlane Lodge, South Africa, Abstracts, p. 11 – 12.

Harris, C. 1995. Oxygen isotope geochemistry of the Mesozoic anorogenic complexes of Damaraland, northwest Namibia: evidence for crustal contamination and its effect on silica saturation. *Contrib. Mineral. Petrol.* **122**, 308 – 321.

Harris, C., Smith, S.H., Milner, S.C., Erlank, A.J., Duncan, A.R., Marsh, J.S. and Ikin, N.P. 1989. Oxygen isotope geochemistry of the Mesozoic volcanics of the Etendeka Formation Namibia. *Contrib. Mineral. Petrol*., **102**, 454 – 461.

Harris, C., Faure, K., Diamond, R.E. and Scheepers, R. 1997. Oxygen and hydrogen isotope geochemistry of S – and I – type granitoids: the Cape Granite suite, South Africa. *Chemical Geology,* **143**, 95 –114.

Harris, C., Smith, H.S. and le Roex, A.P. 2000. Oxygen isotope composition of phenocrysts from Tristan da Cunha and Gough Island lavas: variation with fractional crystallization and evidence for assimilation. *Contrib. Mineral. Petrol*., **138**, 164 – 175.

Harris, C. and Ashwal, L.D. 2002. The origin of low $\delta^{18}O$ granites and related rocks from the Seychelles. *Contrib Mineral Petrol*. **143**, 366 – 376.

Harris C., Pronost, J.J.M., Ashwal, L.D. And Cawthorn, R.G. 2005. Oxygen and Hydrogen Isotope Stratigraphy of the Rustenburg Layered Suite, Bushveld Complex: Constraints on Crustal Contamination. *Journal of Petrology*. **46**, 579 – 601.

Harris, C. and Grantham, G.H. 2009. Geology and petrogenesis of the Straumsvola nepheline syenite complex, Dronning Maud Land, Antarctica. Penrose conference abstract, 9-13 September, Twin Falls, Idaho, USA.

Hatton, C.J., 1995. Mantle plume origin for the Bushveld Complex and Ventersdorp magmatic province. *Journal of African Earth Sciences.* **21**, 571 – 577.

Hatton, C. J. and Schweitzer, J.K. 1995. Evidence for synchronous extrusive and intrusive Bushveld magmatism. *Journal of African Earth Sciences.* **21,** 579 – 594.

Hattori, K., Muehlenbachs, K. 1982. Oxygen isotope ratios of the Icelandic crust. *J. Geophys. Res.*, **87**, 6559 – 6565.

Hémond, C., Condomines, M., Fourcade, S., Allègre, C., Óskarsson, N. and Javoy, M. 1988. Thorium, strontium and oxygen isotopic geochemistry in recent tholeiites from Iceland: crustal influence on mantle-derived magmas. *Earth Planet. Sci. Lett.*, **87**, 273 – 285.

Hémond, C., Arndt, N.T., Lichtenstein, U., Hofmann, A.W., Óskarsson, N. and Steinthórsson, S. 1993. The heterogeneous Iceland plume: Nd–Sr–O isotopes and trace element constraints. *J. Geophys. Res*., **98**, 15833 – 15850.

Hildreth,W., Christiansen, R.L., and O'Neil, J.R. 1984. Catastrophic isotopic modification of rhyolitic magma at times of caldera subsidence,Yellowstone Plateau Volcanic Field. *Journal of Geophysical Research*, **89**, 8339 – 8369.

Hildreth,W., Halliday, A.N., and Christiansen, R.L. 1991. Isotopic and chemical evidence concerning the genesis and contamination of basaltic and rhyolitic magmas beneath the Yellowstone Plateau Volcanic Field. *Journal of Petrology*, **32**, 63 – 138.

Hoefs, J. 1987. Stable Isotope Geochemistry, 3rd ed. Springer - Verlag, Heidelberg. 241 pp.

Kellogg, E.S., Harlan, S.S., Mehnert, H.H., Snee, L.W., Pierce, K.L., Hackett, W.R. and Rodgers, D.W. 1994. Major 10.2-Ma rhyolitic volcanism in the eastern Snake River Plain, Idaho - isotopic age and stratigraphic setting of the Arbon Valley Tuff Member of the Starlight Formation. U.S. G.P.O. (Washington, DC and Denver, CO) 18 pp.

King, E.M., Valley, J.W., Davis, D.W. and Kowallis, B.J. 2001a. Empirical determination of oxygen isotope fractionation factors for titanite with respect to zircon and quartz. *Geochimica et Cosmochimica Acta*, **65**, 3165 – 3175.

Kinnaird, J.A. 2005. The Bushveld Large Igneous Province. www.largeigneousprovinces.org/LOM.html

Kleemann, G. J. 1987. The geochemistry and petrology of the roof rocks of the Bushveld Complex, east of Groblersdal: *Bulletin Geological Survey South Africa*, **81**, 87 p.

Kleemann, G. J. and Twist, D. 1989. The compositionally zoned sheet-like granite pluton of the Bushveld Complex: Evidence bearing on the nature of A-type magmatism. *Journal of Petrology.* **30**, 1383 – 1414.

Kruger, F.J. and Marsh, J.S. 1982. Significance of $^{87}Sr/^{86}Sr$ ratios in the Merensky cyclic unit of the Bushveld Complex. *Nature*. **298**, 53 – 55.

Kruger, F.J. 2005. Filling the Bushveld Complex magma chamber: lateral expansion, roof and floor interaction, magmatic unconformities, and the formation of giant chromitite, PGE and Ti-V-magnetitite deposits. *Mineralium Deposita*. **40,** 451 – 472.

Le Maitre, R.W., Bateman, P., Dudek, K., Keller, J., Lameyre Le Bas, M.J., Sabine, P.A., Schmid, R., Sorenson, H., Streckeison, A., Woolley, A.R. and Zanettin, B. 1989. Classification of igneous rocks and glossary of terms. Blackwell, Oxford.

Le Roex, A.P., Bell, D.R. and Davis, P. 2003. Petrogenesis of Group I Kimberlites from Kimberley, South Africa: Evidence from Bulk-rock Geochemistry. *Journal of Petrology*, **44,** 2261 – 2286.

Loiselle, M.C. and Wones, D.R. 1979. Characteristics and origin of anorogenic granites. *Geological Society of America. Abstract. Programme*, **11**, 468.

Luth, W.C., Jahns, R.H. and Tuttle, O.F. 1964. The granite system at pressures of 4 to 10 kilobars. *J. Geophys. Res.*, **69**, 759 – 773.

Maier, W.D., Arndt, N.T. and Curl, E.A. 2000. Progressive crustal contamination of the Bushveld Complex: evidence from Nd isotopic analyses of the cumulate rocks. *Contrib. Mineral. Petrol.* **140**, 316 – 327.

Marlow, A.G. 1976. The geology of the Bushveld Complex on the Skhukune Plateau, eastern Transvaal: M.Sc. thesis, Univ. Pretoria, 105p. (unpubl.).

Martin, R.F. and Bonin, B. 1976. Water and magma genesis: the association hypersolvus granite–subsolvus granite. *Canadian Mineralogist,* **14**, 228 – 237.

Mattey, D., Lowry, D. and Macpherson, C. 1994. Oxygen isotope composition of mantle peridotites. *Earth and Planetary Science Letters,* **128**, 231 – 241.

Matthews, A., Palin, J.M., Epstein, S. and Stolper, E.M. 1994. Experimental study of $^{18}O/^{16}O$ partitioning between crystalline albite, albitic glass, and CO_2 gas. *Geochim. Cosmochim. Acta,* **58**, 5255 – 5266.

Miková, and Denková, .2007. Modified chromatographic separation scheme for Sr and Nd isotope analysis in geological silicate samples. *Journal of Geosciences*, **52**, 221 – 226.

Miller, J.A. and Harris, C. 2007. Petrogenesis of the Swaziland and Northern Natal rhyolites of the Lebombo rifted margin, South East Africa. *Journal of Petrology.* **48**, 185 – 218.

Moore, R.O. 1986. A study of the kimberlites, diamonds and associated rocks and minerals from the Monastery Mine, South Africa. Ph.D. thesis. University of Cape Town, South Africa.

Muehlenbachs, K., Anderson, A.T. and Sigvaldason, G.E. 1974. Low-O^{18} basalts from Iceland. *Geochim. Cosmochim. Acta*, **38**, 577 – 588.

Munteanu, M., Wilson, A., Yao, Y., Harris, C., Chunnett, G and Luo, Y. 2010. The Tongde dioritic pluton (Sichuan, SW China) and its geotectonic setting: Regional implications of a local-scale study. *Gondwana Research*, (*article in press*.).

Oliveira, D. C., Dall'Agnol, R., Silva, J. B. C. and Almeida, J. A. C. 2008. Gravimetric, radiometric, and magnetic susceptibility study of the Paleoproterozoic Redenção and Bannach plutons, eastern Amazonian Craton, Brazil: Implications for architecture and zoning of A-type granites. *Journal of South American Earth Sciences.* **25,** 100 – 115.

Óskarsson, N. and Steinthórsson, S. 1993. The Heterogeneous Iceland Plume: Nd – Sr – O Isotopes and Trace Element Constraints. *J. Geophys. Res*., **98**, 15833 – 15850.

Pankhurst, R.J., Leat, P.T., Sruoga, P., Rapela, C.W., Márquez, M., Storey, B.C. and Riley, T.R. 1998. The Chon Aike silicic igneous province of Patagonia and related rocks in Antarctica: a silicic large igneous province. *J. Volc. Geotherm. Res*., **81**, 113 – 136.

Pankhurst, R.J., Riley, T.R., Fanning, C.M. and Kelley, S.R. 2000. Episodic silicic volcanism in Patagonia and the Antarctic Peninsula: chronology of magmatism associated with the break – up of Gondwana. *J. Petrol*., **41**, 605 – 625.

Pupin, J.P. 1980. Zircon and granite petrology. *Contributions to Mineralogy and Petrology,* **73**, 207 – 220.

Rampino, M.R. and Stothers, R.B. 1988. Flood basalt volcanism during the past 250 million years. *Science*, **241**, 663 – 668.

Reid, D. L., Cawthorn, R. G., Kruger, F. J. and Tredoux, M. 1993. Isotope and trace-element patterns below the Merensky Reef, Bushveld Complex, South Africa: evidence for fluids? *Chemical Geology (Isotope Geosciences Section).* **106**, 171 – 186.

Riley, T.R., Leat, P.T., Pankhurst, R.J. and Harris, C. 2001. Origins of Large Volume Rhyolitic Volcanism in the Antarctic Peninsula and Patagonia by Crustal Melting. *J. Petrol*., **42**, 1043 – 1065.

Rosenbaum, J.M. and Mattey, D.,1995. Equilibrium garnet – calcite oxygen isotope fractionation*. Geochim. Cosmochim. Acta*, **59**, 2839 – 2842.

SACS (South African Committee for Stratigraphy). 1980. Handbook of the Geological Survey of South Africa, vol. 8. Geological Society of South Africa, Pretoria, p. 690.

Schiffries, C. M. and Rye, D. M. 1989. Stable isotopic systematics of the Bushveld Complex: I. Constraints of magmatic processes in layered intrusions. *American Journal of Science.* **289**, 841 – 873.

Schweitzer, J.K. and Hatton, C.J. 1995. Chemical alteration within the volcanic roof rocks of the Bushveld Complex. *Econ. Geol*. **90**, 2218 – 2231.

Schweitzer, J.K., Hatton, C.J. and de Waal, S.A. 1995. Regional lithochemical stratigraphy of the Rooiberg Group, upper Transvaal Supergroup: a proposed new subdivision. *S. Afr. J. Geol*. **98**, 245 –255.

Schweitzer, J.K., Hatton, C.J. and De waal, S.A. 1997. Link between the granitic and volcanic rocks of the Bushveld Complex, South Africa. *Joumal of African Earth Sciences*. **24**, No. 1/2, 95 – 104.

Sharpe, M.R. 1985. Strontium isotope evidence for preserved density stratification in the Main Zone of the Bushveld Complex. *Nature*. **316**, 119 – 126.

Sharp Z.D. 2007 Principles of stable isotope geochemistry. Pearson Education, Upper Saddle River, NJ, USA. 343 pp.

Spicuzza, M.J., Valley, J.W., Kohn, M.J., Girard, J.P., and Fouillac, A.M. 1998a. The rapid heating, defocused beam technique: A CO_2-laser-based method for highly precise and accurate determination of $\delta^{18}O$ values of quartz. *Chemical Geology*, **144**, 195 – 203.

Spicuzza, M.J., Valley, J.W., and McConnell, V.S. 1998b. Oxygen isotope analysis of whole rocks via laser fluorination: An airlock approach. *Geological Society of America Abstracts with Programs*, **30**, no. 7, p. A80.

Suzuoki, T. and Epstein, S. 1976. Hydrogen isotope fractionation between OH – bearing minerals and water. *Geochim. et. Cosmochim*. Acta, **40**, 1229 – 1240.

Tanaka, T., Togashi, S., Kamioka, H., Amakawa, H., Kagami, H., Hamamoto, T., Yuhara, M., Orihashi, Y., Yoneda, S., Shimizu, H., Kunimaru, T., Takahashi, K., Yanagi, T., Nakano, T., Fujimaki, H., Shinjo, R., Asahara, Y., Tanimizu, M. and Dragusanu, C. 2000. JNdi-1: a neodymium isotopic reference in consistency with LaJolla neodymium*. Chemical Geology Short Communication*., **168**, 279 – 281.

Taylor, H.P. 1968. The oxygen isotope geochemistry of magmatic rocks. *Contrib. Mineral. Petrol*., **19**, 1 – 21.

Taylor, H.P. 1974. The application of oxygen and hydrogen isotope studies to problems of hydrothermal alteration and ore deposition. *Econ. Geol*., **69**, 843 – 883.

Taylor, H.P. 1980. The effects of assimilation of country rocks by magmas on $^{18}O/^{16}O$ and $^{87}Sr/^{86}Sr$ systematics in igneous rocks. *Earth and Planetary Science Letters*, **47**, 243 – 254.

Taylor, H.P. and Sheppard, S.M.F. 1986. Magmatic rocks: I. Processes of isotopic fractionation and isotope systematics. *Rev. Miner*., **16**, 227 – 271.

Trumbull, R.B., Harris, C., Frindt, S. and Wigand, M. 2003. Oxygen and neodymium isotope evidence for source diversity in Cretaceous anorogenic granites from Namibia and implications for A-type granite genesis. *Lithos.* **73,** 21 – 40.

Twist, D. 1985. Geochemical evolution of the Rooiberg silicic lavas in the Loskop Dam area; Southeastern Bushveld. *Econ. Geol*., **80**, 1153 – 1165.

Twist, D. and French, B.M. 1983. Voluminous acid volcanism in the Bushveld Complex: a review of the Rooiberg Felsite. *Bull. Volc*., **46**, 225 – 242.

Twist, D. and Harmer, R.E.J. 1987. Geochemistry of contrasting siliceous magmatic suites in the Bushveld Complex: genetic aspects and implications for discrimination diagrams. *Journal of Volcanology and Geothermal Research,* **32**, 83 – 98.

Valley, J.W., Kitchen, N.,Kohn, M.J., Niendorf, C.R., and Spicuzza, M.J. 1995. UWG-2, a garnet standard for oxygen isotope ratio: Strategies for high precision and accuracy with laser heating. *Geochimica et Cosmochimica Acta*, **59**, 5223 – 5231.

Valley, J.W., Kinny, P.D., Schulze, D.J. and Spicuzza, M.J. 1998. Zircon megacrysts from kimberlite: oxygen isotope variability among mantle melts. *Contrib. Mineral. Petrol.* **133,** 1 – 11.

Valley, J.W., Bindeman, I.N. and PECK, W.H. 2003. Empirical calibration of oxygen isotope fractionation in zircon. *Geochimica et Cosmochimica Acta*, **67**, 3257 – 3266.

Vennemann, T. W. and O'Neil, J. R. 1993. A simple and inexpensive method of hydrogen isotope and water analyses of minerals and rocks based on zinc reagent. *Chemical Geology (Isotope Geosciences Section).* **103**, 227 – 234.

Wager, L.A. & Brown, G.M. 1967. Layered Igneous Rocks. Oliver and Boyd, Edinburgh and London, 588 p.

Walraven, F. 1985. Genetic aspects of the granophyric rocks of the Bushveld Complex. *Economic Geology.* **80**, 1166 – 1180.

Walraven, F. 1987. Textural, geochemical and genetic aspects of the granophyric rocks of the Bushveld Complex. Memoir **72**, Geological Survey South Africa, 145 pp.

Walraven, F. 1988. Notes on the age and genetic relationships of the Makhutso Granite, Bushveld Complex, South Africa. *Chem. Geol*., **72**, 17 – 28.

Walraven F. 1997. Geochronology of the Rooiberg Group, Transvaal Supergroup, South Africa. EGRI Information Circular **316**, University of the Witwatersrand, 21p.

Walraven, F. and Hattingh E. 1993. Geochronology of the Nebo Granite, Bushveld Complex. *South African Journal of Geology*. **96**, 31 – 41.

Wei, C-S., Zheng, Y-F. and Zhao, Z-F. 2000. Hydrogen and oxygen isotope geochemistry of A-type granites in the continental margins of eastern China. *Tectonophysics*. **328**, 205 – 227.

Wei, C-S., Zhao, Z-F and Spicuzza, M.J. 2008. Zircon oxygen isotopic constraint on the sources of late Mesozoic A-type granites in eastern China. *Chemical Geology.* **250,** 1 – 15.

Wignall, P.B. 2001. Large igneous provinces and mass extinctions, *Earth – Science Reviews*, **53**, 1 – 33.

Willmore, C.C., Boudreau, A.E., Spivack, A. and Kruger, F.J. 2002. Halogens of the Bushveld Complex, South Africa: δ^{37}Cl and Cl/F evidence for hydration melting of the source region in a back-arc setting. *Chemical Geology*, **182**, 503 – 511.

Wu, F-Y., Sun, D-Y., Li, H., Jahn, B-M and Wilde., S. 2002. A-type granites in northeastern China: age and geochemical constraints on their petrogenesis**.** *Chemical Geology.* **187**, 143 – 173. Nd table

Zhao, Z-F. and Zheng, Y-F. 2003.Calculation of oxygen isotope fractionation in magmatic rocks. *Chemical Geology,* **193**, 59 – 80.

Zheng, Y-F. 1993a. Calculation of oxygen isotope fractionation in anhydrous silicate minerals. *Geochim. Cosmochim. Acta.* **57**, 1079 – 1091.

Zheng, Y-F. 1993b. Calculation of oxygen isotope fractionation in hydroxyl-bearing silicates. *Earth and Planetary Science Letters*. **120**, 247 – 263.